DELFT UNIVERSITY OF TECHNOLOGY
Faculty of Civil Engineering and Geoscience
Department of Geoscience and Engineering

Joint Master in Applied Geophysics

Seismic signatures of 2D fracture networks

Angela Stallone
August 2012

TU Delft IDEA League

Contents

CHAPTER 1

Abstract

Fractures and faults play an important role in controlling the flow and transport properties in a reservoir and that is the main reason for which their characterization is very important in hydrocarbon exploration. In addition to this, the possibility of characterizing fractures can represent a great advantage in other fields, like geothermal exploration, hydrofracturing applications or volcanic risk evaluation. Seismic simulation by finite-difference modeling has been implemented as a tool to characterize fracture networks by testing their seismic signatures. The medium in which fractures are placed is represented by a squared model with the sides measuring 5000m; two receivers arrays, each including 1000 receivers, have been implemented: the first at the top of the model (to record the reflected wavefield), the second at a depth of 4000m (to record the transmitted wavefield). Fractures are randomly positioned in the center of the model, between 1250m and 3750m. In the case of a layered medium, only the middle layer, 1500m thick, contains random fractures.

The sensitivity of seismic wave propagation to fractures has been analyzed by testing the influence of different fracture features: length, orientation, density (number of fractures). Even a single fracture affects the incident seismic signal, producing diffracted/scattered and transmitted waves. Moreover, its orientation significantly affects the reflected wavefield in the time domain in terms of amplitude and complexity of the response and in the frequency domain as well, where peak amplitude and peak frequency change depending on the fractures orientation. More than the orientation, the fracture length strongly affects the seismic signal in time and frequency domains.

Considering a network of fractures, the imprint of the fracture orientation on the reflected wavefield is significant only in the frequency-wavenumber domain; on the other hand, it is much stronger for the transmitted wavefield in the frequency domain, where the peak amplitude and the peak frequency undergo high variation: in particular, the horizontal fractures produce the strongest frequencies attenuation and the lowest peak frequency. The fracture length variation produces the most interesting signature in the time domain for the reflected wavefield (an increase in the fracture length produces longer coda waves) and in the frequency domain for the transmitted field: in particular, the longest fractures produce the strongest frequencies attenuation and the lowest peak frequency. Significant is the signature

of the fracture density, but it is particularly strong on the transmitted wavefield in the frequency domain: in particular, the highest number of fractures produce the same effect of the horizontal and longest fractures (strongest frequencies attenuation and lowest peak frequency). Eventually, the introduction of a fractured layer yields strong change in the incident signal, which is highly attenuated and disrupted.

The results of the present work can have implications in all the fields where the detection and the characterization of fractures in the subsurface is vital, such as the geothermal exploration or the hydraulic fracturing applications. Despite of the complexity of a fractured systems, some recurrent trends and characteristic responses have been determined. However, it should kept in mind that fracture features are strictly related (they influence each other) and that different features can yield similar responses: this means that fracture characteristics can not be straightforward inferred from their seismic signatures.

CHAPTER 2

Acknowledgment

I would like to thank my two supervisors, Professor Auke Barnhoorn and Dr Ir Jan Thorbecke, for all their support and help. I have really appreciated their friendly and patient approach; I can say that the positive energy *propagating* between me and them has been one of the reasons that have made this thesis possible. I also want to thank Professor Wapenaar and Professor Ghose for their help: my doubts have been strongly *attenuated* after having discussed with them. Now that I have reached the *peak* of my educational *path*, I have to express all my gratitude to my parents: without them, it would not have been possible for me to attend this Joint Master around the Europe. A sincere thank to my sweet brother Domenico, who has always supported me, especially in the most difficult moments. Eventually, I have to thank my colleague, best friend and boyfriend Giovanni: despite of all the *perturbations*, I have reached the end of this wonderful travel and this would not have been possible without him.

CHAPTER 3

Introduction

Fractures are a common feature in the subsurface and their characterization has important practical applications. Fractures and faults play an important role in controlling the flow and transport properties in a reservoir. Rocks in a reservoir can be characterized by a high porosity, but low permeability; however, the presence of a fracture network can enhance the overall permeability, rendering the reservoir more profitable. On the other hand, fractures can also reduce hydrocarbon productivity by decreasing the reservoir permeability (if they are filled with clay or mineral veins, for example) or by causing leakage across the cap rock. This is the main reason for which naturally fractured reservoirs represent a major challenge in hydrocarbon exploration. In addition to this, the possibility of characterizing fractures can represent a great advantage in other fields, like geothermal exploration; more precisely, the EGS ("Enhanced Geothermal Systems") could benefit from this possibility, as these technologies pursue the enhancement of the reservoir permeability by artificially creating a fractures network. Eventually, parallel fractures can introduce anisotropy in fluids transport. Since fractures have a great influence on the elastic properties of the rocks, they affect the velocity of the seismic waves traveling through a fractured medium; anyhow, P-velocities decrease often by a negligible amount when the medium changes from non-fractured to a medium with aligned fractures; on the other hand, the effects on the S-velocities are much more significative (Xu and King, 1989; Hardage, June 2011). Fractures also yield seismic wave attenuation (Hudson,1981; Pyrak-Nolte et al., 1990) and scattering (Coates and Schoenberg, 1995; Haugen and Schoenberg, 2000).

This Master thesis has the aim of determining the seismic signatures of fractures and fracture networks in an idealized rock medium. In particular, the sensitivity of the seismic signal to different fracture features (length, orientation, fractures density) has been tested. The aim is to identify and characterize a fracture network in the subsurface through the seismic response, which could be helpful for several applications as mentioned in the beginning. In order to analyze the seismic wave propagation in fractured media, numerical modeling techniques are commonly employed, since they yield the most accurate solutions for complex models as well; moreover, they offer a much bigger range of test possibilities compared to the laboratory experiments, as they allow to play with numerous parameters and to reconstruct field

survey in a more realistic way. In this study the finite-difference method has been implemented to simulate wave propagation in media with discrete distributions of fractures with the software FDELMODC. The study starts with a simple 2D homogeneous model including a single fracture; the aim is to test the influence of the orientation and the length of the fracture on the seismic signature. The model has been made progressively more and more complicated, by including an increasing number of fractures. In order to make the simulation as reliable as possible, more realistic models have been implemented by including different discrete distributions of fractures. In this work fractures have been modeled as very thin layers full-filled of water (they have been assigned a density of $1 g/cm^3$) along which P-waves propagate with a velocity of 1690 m/s (P-wave velocity in salt water). The homogeneous background has been assigned a density of 2.65 g/cm^3 (sandstone density) and a P-wave of 5490 m/s[1].

The thesis starts with a theoretical overview of the wave propagation in the fractured media and the synthetic seismic modeling (Chapter 1 and 2). Then, the results are presented (Chapter 3 and 4). Finally, the discussion of the results (Chapter 5) and the conclusions (Chapter 6) close the thesis.

[1]This velocity value, which is quite high, has been selected in order to determine a high impedance contrast between the fractures and the surrounding medium. The aim is to maximize the fracture response.

CHAPTER 4

Seismic wave propagation

In this Chapter the acoustic wave equation is briefly introduced together with the equation of continuity and the equation of motion from which it is derived. Then, the seismic propagation in fractured media is analyzed more in detail, with particular emphasis to the reflection and transmission coefficients at a linear slip interface (fracture) and to the influence of the fracture features.

4.1. Acoustic wave equation

4.1.1. Equation of continuity and Equation of motion. A seismic wave is a mechanical disturbance that propagates through a medium without involving a net movement of material. There are two types of seismic waves: body waves and surface waves (the latter will not be described because they have not been considered in the present work). Body waves, that travel along the interior of the Earth, can be classified in *compressional waves* and *shear waves*: compressional waves (P-waves) are longitudinal, that is, the direction of propagation is parallel to the direction of particle displacement. Fluids and solids tend to oppose compression, therefore compressional waves can propagate through them. Shear waves are transverse, that is, the direction of propagation is perpendicular to the direction of particle displacement; shear waves can propagate through solids but not through fluids (their shear modulus is zero). In the following, the two-way acoustic wave equation in an ideal fluid has been derived following the approach used by Wapenaar and Berkhout (1989).

Assume an inhomogeneous non-viscous fluid medium with no shear strength. Localized deformations of the fluid will result in the propagation of an acoustic wave (a compressional wave) which is described by two equations:

- *Linearized equation of continuity*

$$\frac{1}{K(\bar{r})}\frac{\partial p(\bar{r},t)}{\partial t} + \nabla \cdot \bar{v}(\bar{r},t)\frac{\partial i_v(\bar{r},t)}{\partial t} \tag{4.1.1}$$

where $K(\bar{r})$ is the adiabatic compression modulus, p is the acoustic pressure, $\bar{v}$ is the particles velocity and i_v is the volume density of volume injection.

The equation of continuity is derived by applying the *law of conservation of mass* which states that the total amount of mass is conserved. As a second step,

linearization of the equation of continuity is performed by assuming small density and pressure changes are applied around steady reference conditions.

- *Linearized equation of motion*

$$\rho(\bar{r})\frac{\partial \bar{v}(\bar{r},t)}{\partial t} + \nabla p(\bar{r},t) = \bar{f}(\bar{r},t) \tag{4.1.2}$$

where $\rho(\bar{r})$ is the static mass density, $\nabla p(\bar{r},t)$ represents the spatial variation of the acoustic pressure and $\bar{f}(\bar{r},t)$ is the volume density of the external force.

The equation of motion is derived by applying the *law of the conservation of momentum*, which states that the total amount of momentum is conserved. The linearization is performed according to the assumptions described above.

4.1.2. Acoustic two way equation. Eq. (1) and (2) are combined by eliminating the velocity. This result in the Acoustic two-way equation:

$$\rho\nabla\cdot(\frac{1}{\rho}\nabla p) - \frac{\rho}{K}\frac{\partial^2 p}{\partial t^2} = -s(\bar{r},t) \tag{4.1.3}$$

with

$$s = \rho\frac{\partial^2 i_v}{\partial t^2} - \rho\nabla\cdot(\frac{1}{\rho}\bar{f}) \tag{4.1.4}$$

where s is the source function, which depends on i_v and f (that are related to the type of source).

4.2. Seismic wave propagation in a fractured medium

The effect of fractures on velocities and attenuation of the seismic waves has been largely discussed in the literature (Boadu and Long, 1996; Pyrak-Nolte et al., 1987; Hudson,1981; Pyrak-Nolte et al., 1990). However, it should be specified that P-velocities decrease by a often negligible amount when the medium changes from non-fractured to a medium with aligned fractures; on the other hand, the effects of a fractured medium on the S-velocities are much more significant (Xu and King, 1989; Hardage, June 2011). Moreover the preferential orientation of fractures makes the medium azimuthally anisotropic with respect to seismic wave propagation, but this effect has been proven to be more significant for S-waves (Hardage, June 2011). Having said that, the effect of a fractured medium on velocities and attenuation of the seismic waves can be more or less significant depending on several factors, as wavelength, fracture length and fracture spacing (Boadu and Long, 1996). Vlastos et al. (2003) have considered the effect of fracture length compared to wavelength, showing that for small fractures, scattering (Coates and Schoenberg, 1995; Haugen

and Schoenberg, 2000) is the most important feature in the wavefield; in addition to this, the fracture spacing plays an important role as well, as shown by Willis et al. (2004): if the fracture spacing is close in size to the seismic wavelength, then the fractures will scatter the seismic energy. On the other hand, when the length of the fractures is comparable to or larger than the wavelength, the interaction between seismic waves and fractures is more complicated since the fractures act as individual interfaces (Vlastos et al., 2003), giving rise to wave reflection, transmission and conversion; moreover head waves can be created (Gu et al., 1996) and diffractions from the tips (Vlastos et al., 2003, Appendix B); depending on the spacing among the several fractures, channel waves[1] can occur as well (Nihei et al., 1999; Yi et al., 1998). Note that in the following only reflected, transmitted and diffracted waves will be discussed. An example of the effect of the fracture length (compared to the wavelength) on the seismic wave propagation is clearly shown Fig.4.2.1 and 4.2.2 (Vlastos et al., 2003):

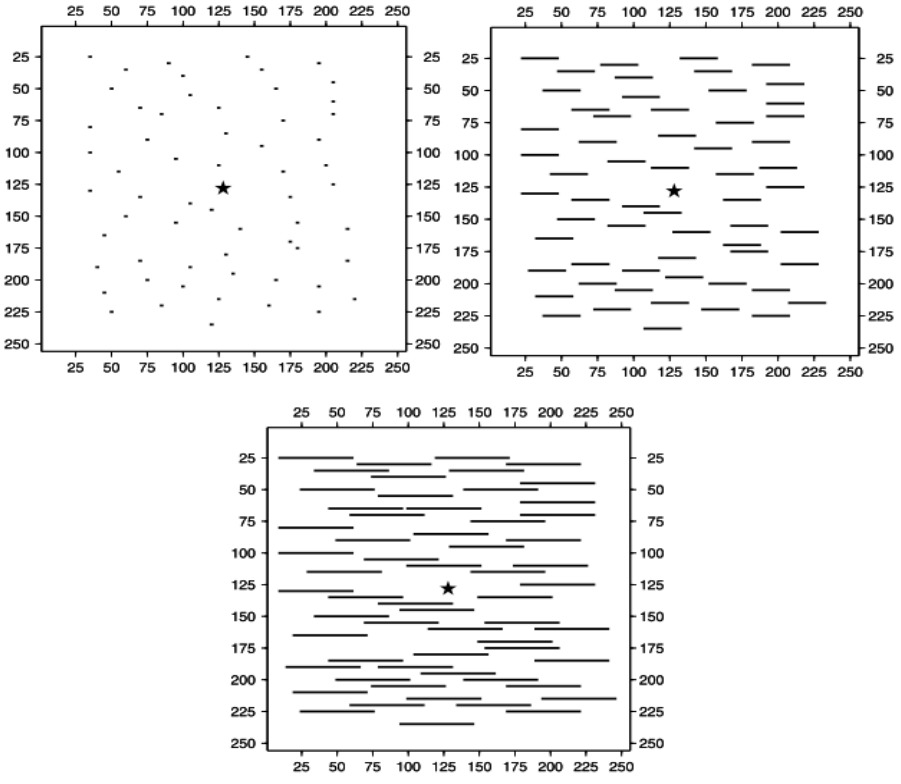

FIGURE 4.2.1. Schematic representations of the models with discrete distributions of fractures with an increasing length: 0.1λ, λ and 2λ (Vlastos et al., 2003).

[1]Seismic waves can get trapped between two fractures if these constitute a *wave guide*

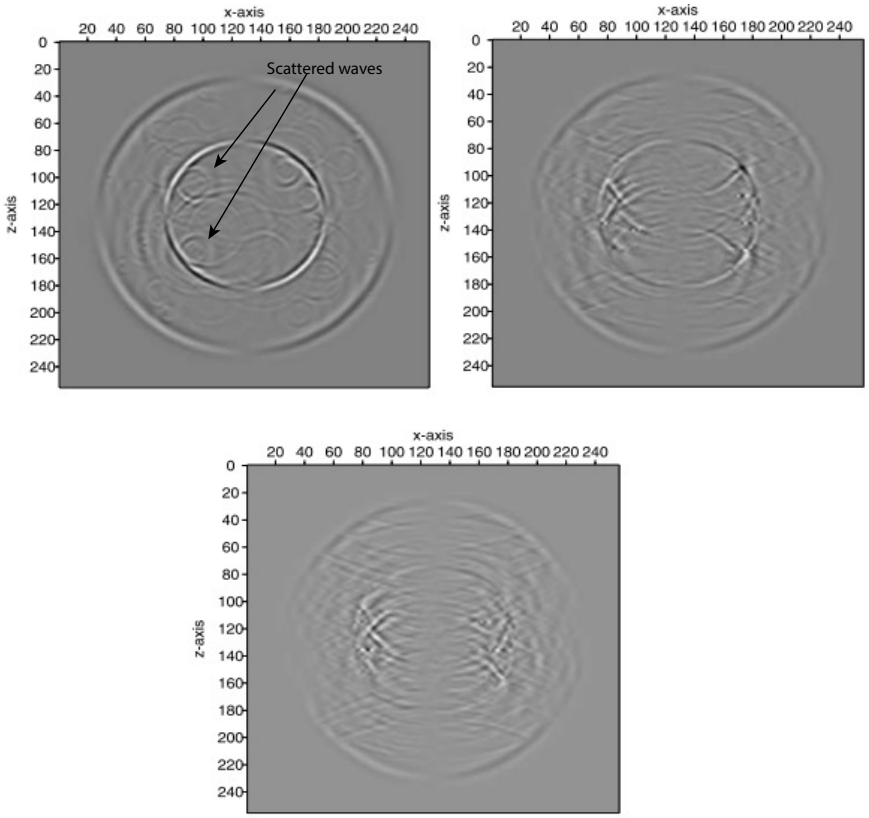

FIGURE 4.2.2. Snapshots corresponding to the models shown in the previous figures. Note the fractures acting as point scatterers in the first figure (when the wavelength is larger than the size of the fractures) and as individual interfaces in the other two models (when the size of the fractures is equal to or larger than the wavelength) (Vlastos et al., 2003).

Another important aspect in studying the seismic signature of the fractures consists in simulating the effect of different fractures features (shape, length, orientation, distribution density), in order to figure out their individual contributions to the wavefield change.

4.2.1. Reflection and transmission of plane waves at a linear slip interface. The effects of a fracture on seismic wave propagation can be analyzed by incorporating the "*linear slip boundary condition*" in the wave equation: in the *displacement–discontinuity model* (Schoenberg, 1980) a fault is modeled as an imperfectly bounded interface across which the traction is continuous, yet displacement is allowed to be discontinuous; this provides two boundary conditions for which stress must be continuous and the displacement discontinuity vector must be proportional to the stress on the fracture via the fracture compliance matrix (Schoenberg, 1980). The "linear slip boundary condition", inserted in the acoustic wave equation, yields

to the definition of the reflection and transmission coefficients for a plane-wave interacting with a fracture or a fault. Before introducing the reflection and transmission coefficients, it is necessary to describe the scattering effect.

Scattering of the seismic waves consists in the irregular and diffuse dispersion of energy caused by inhomogeneities (Sheriff, 1991), fractures in this case, yielding a decrease in amplitude with travel distance ("Scattering attenuation", Aki and Wu (1988)) and a frequency-dependance (dispersion). As already introduced, scattering is predominant when the fracture length and the fracture spacing is on the order of a wavelength or less. The scattered signal appears as a ringing coda-type signature ("*coda wave*", Aki (1969)) which is a non-coherent signal recorded after the first arrivals that has an envelope whose amplitude decreases with increasing lapse time. Note that the term "*coda wave*" is usually referred to the multiple scattering, which is experienced by a wave repeatedly scattered by multiple heterogeneities in the subsurface; this yields the decrease in amplitude with travel distance and the dispersion. In Fig. 4.2.3 it is shown an example of coda wave due to the presence of fractures:

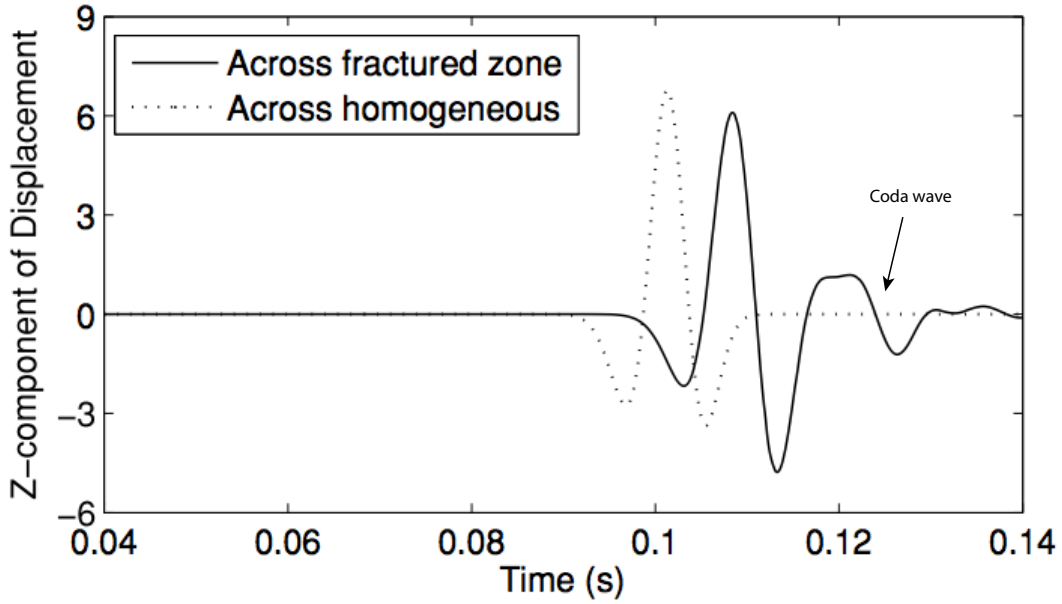

FIGURE 4.2.3. Comparison of the z-direction component of the displacement between the cases that the elastic plane wave propagates across a fractured zone and across the homogeneous background medium without fractures. The coda wave due to fractures is visible (solid line). It is also visible the time delay between the elastic wave propagating in the fractured medium and that propagating in the non-fractured one (Zhang and Gao, 2009).

The waveform of the scattered signal is approximately one-time derivative of the incident signal, as it can be deduced by the mathematical definition of the reflection and transmission coefficients for a plane wave at a linear slip interface (Coates and Schoenberg, 1995):

$$\underset{\sim}{T} = \left[\underset{\sim}{I} + \frac{iw}{2}(\underset{\sim}{X}^{-1}\underset{\sim}{Z}_T\underset{\sim}{Y} + \underset{\sim}{Y}^{-1}\underset{\sim}{Z}_N\underset{\sim}{X})\right]^{-1} \tag{4.2.1}$$

$$\underset{\sim}{R} = \frac{iw}{2}(\underset{\sim}{X}^{-1}\underset{\sim}{Z}_T\underset{\sim}{Y} - \underset{\sim}{Y}^{-1}\underset{\sim}{Z}_N\underset{\sim}{X}) \times \left[\underset{\sim}{I} + \frac{iw}{2}(\underset{\sim}{X}^{-1}\underset{\sim}{Z}_T\underset{\sim}{Y} + \underset{\sim}{Y}^{-1}\underset{\sim}{Z}_N\underset{\sim}{X})\right]^{-1} \tag{4.2.2}$$

where:

- $\underset{\sim}{X}$ and $\underset{\sim}{Y}$ are two "impedance matrices"[2] functions of horizontal slowness and material properties for the upper and lower medium (Schoenberg and Protazio 1992)[3].

- $\underset{\sim}{Z}_T$ and $\underset{\sim}{Z}_N$ are 3x3 matrices that contain all the tangential and normal components of the *fracture compliance matrix*, respectively. The fracture compliance matrix is the inverse of the stiffness matrix (effective elastic constants).

- w is the angular frequency

- I is the identity matrix

- i is the imaginary unit ($\sqrt{-1}$)

The above expressions for $\underset{\sim}{T}$ and $\underset{\sim}{R}$ show that the reflection and the transmission coefficients are frequency-dependent. The term iw corresponds to a time derivative in the time domain; on the basis of this, it is possible to demonstrate that at low frequencies the pulse shape of a scattered wave is close to the derivative of the incident signal (low frequency approximation: the seismic wavelength is much larger than the fracture length). As the frequency increases, the scattered-wave shapes are altered by the presence of higher derivatives of the incident-wave pulse shape (Haugen and Schoenberg, 2000). By multiplying the reflection/transmission coefficient with the downgoing wavefield (which is derived by the vertical component of the particle velocity that is measured at the surface) , it is possible to find an expression for the scattered wavefield.

When the length of the fractures is comparable to or larger than the wavelength (high frequency approximation) the fractures act more as individual interfaces (Fig.

[2]Note that or the 2D wave propagation, $\underset{\sim}{X}$ and $\underset{\sim}{Y}$ are 2x2 matrices.

[3]Schoenberg and Protazio describe the plane-wave reflection and transmission at interfaces between two anisotropic elastic media (both media have to be at least monoclinic, which means they have to have a horizontal symmetry plane); it is assumed that the fracture is embedded in an otherwise homogeneous medium. The reflectivity and transmissivity matrices are derived in terms of four submatrices of the Zoeppritz coefficient matrix, two submatrices associated with each of the two media.

4.2.4) and the seismic signature is more complicated. A fracture (which is generally defined as a low-velocity layer) can excite significant reflected and transmitted waves. Apart from making the seismic response frequency-dependent (as indicated by the Eq. 1.1.1 and Eq. 1.1.2, Coates and Schoenberg, 1995), fractures introduce significant amplitude and velocity changes in the seismic waves, but also the phase varies.

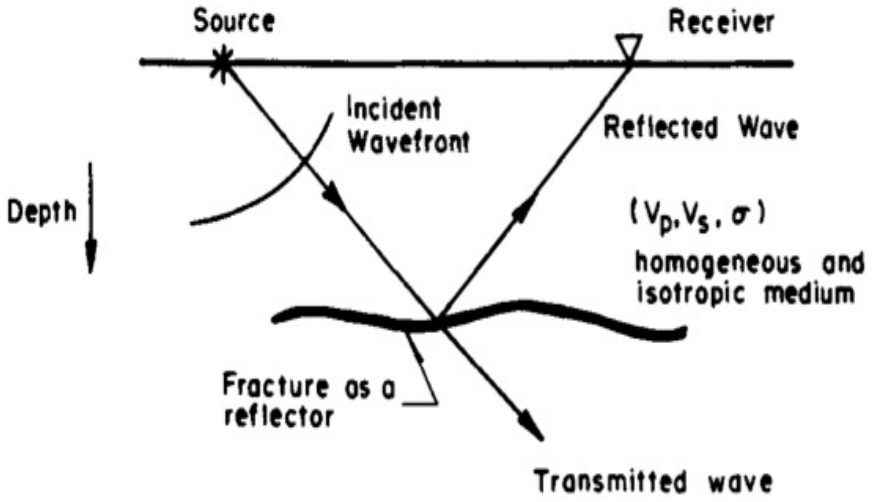

FIGURE 4.2.4. Wave propagation across a fracture resulting in reflected and transmitted waves (only P-waves are shown) (Boadu and Long, 1996).

The effects of a single fractures have been studied in detail by Boadu and Long (1996): the reflected P-waves undergo considerable change in pulse shape and have much smaller amplitudes compared with the incident wave (for the transmitted waves this effect is much less significant), see Fig. 4.2.5. In the frequency domain, the effect of the fracture is again much more significant for the reflected than for the transmitted P-wave. The amplitude in the spectrum of the reflected P-wave is much lower than the incident wave; moreover, its peak frequency is higher. In the spectrum of the transmitted P-P wave it is possible to notice that the higher frequencies undergo the strongest attenuation (Fig. 3.6): indeed the relative amplitude of the lowest frequencies (from 0 to about 300 Hz) is not affected by the presence of fractures; on the contrary, a difference in the amplitude between the fractured and unfractured media is visible for the higher frequencies; in addition, the presence of fractures yields a decrease of the peak frequency.

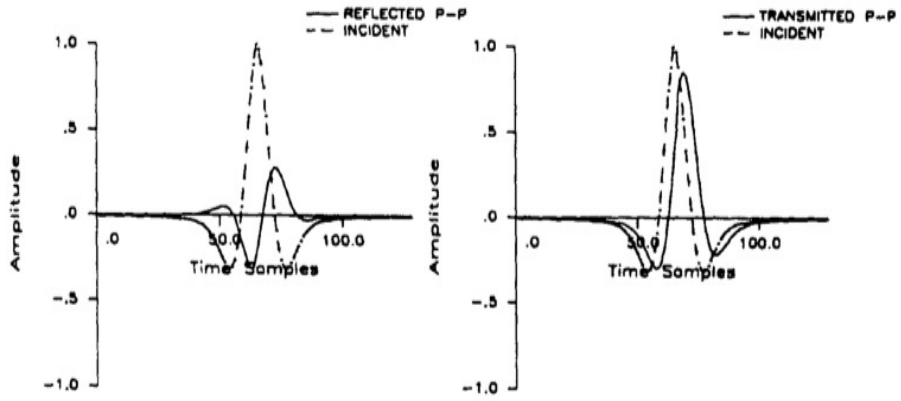

FIGURE 4.2.5. Reflected and transmitted waves at a single fracture: the reflected P-wave undergoes significant change in shape and has a much smaller amplitude compared with the incident wave; for the transmitted P-wave the effect is less evident (Boadu and Long, 1996).

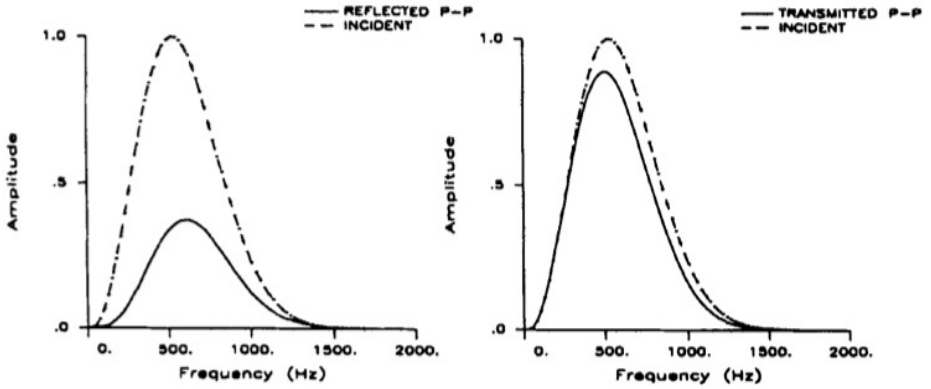

FIGURE 4.2.6. Spectra of waveforms for reflected and transmitted waves at a single fracture: the effect of the fracture is again much more significant for the reflected than for the transmitted P-wave:the amplitude in the spectrum of the reflected P-wave is strongly decreased by the presence of the fracture (Boadu and Long, 1996).

4.2.2. Diffractions from the fracture tips. Diffraction is the phenomenon of transmission of energy by non-geometric ray paths. When a wave impinges upon a fracture, which can be considered as a truncated reflector, then the wavefront bends around the tip of the fracture giving rise to a diffracted wave. The tip acts as a secondary source of wavefronts (according to the Huygens' Principle of secondary wavefronts) that are spread out in all directions, included the so called "shadow zone", where, according to ray theory, no waves could propagate (Reynolds, 1997), as shown in Fig. 4.2.7:

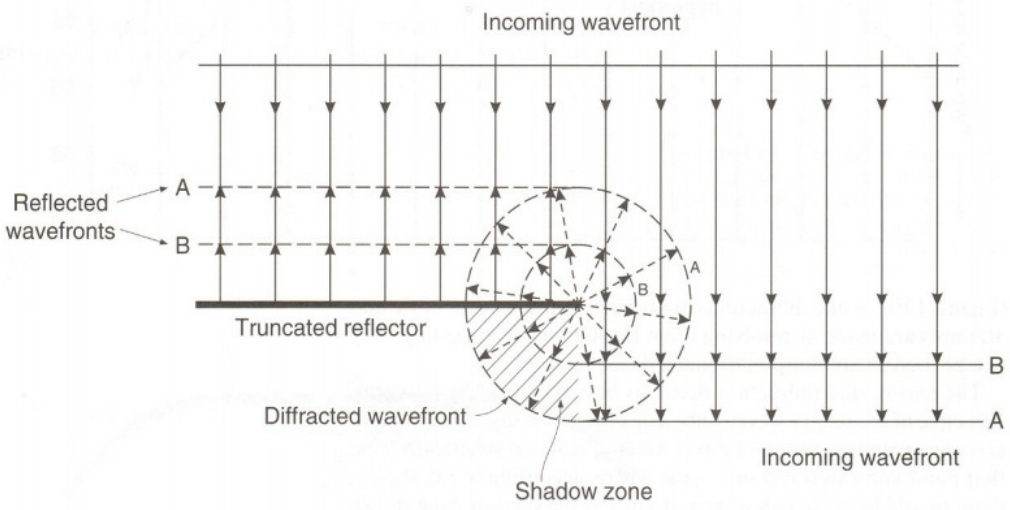

FIGURE 4.2.7. Diffracted wavefronts arising from a truncated reflector (Reynolds, 1997). The tip of the fracture acts a secondary source of waves that are spread out in all directions (in the shadow zone as well).

Diffraction and scattering are two different phenomena, but the use of these terms in the literature is often confusing. In order to better distinguish these two phenomena, consider the plot in Fig. 4.2.8, which gives an overview of approaches to wave propagation in random media. The classification of approaches is shown in terms of the scale length of heterogeneity (a), the seismic wavelength (λ) and distance travelled (L): scattering theory of waves is relevant for the description of wave propagation when the seismic wavelength becomes significant in comparison to the scale length of the underlying seismic heterogeneity of the medium; in this case, ray theory is inadequate in explaining seismic wave propagation in such complex media. Diffraction can be viewed as an intermediate effect between scattering and multipathing (which consists in the reflections of the waves along different paths due to the presence of strong lateral variations in velocity and which is described by the ray theory).

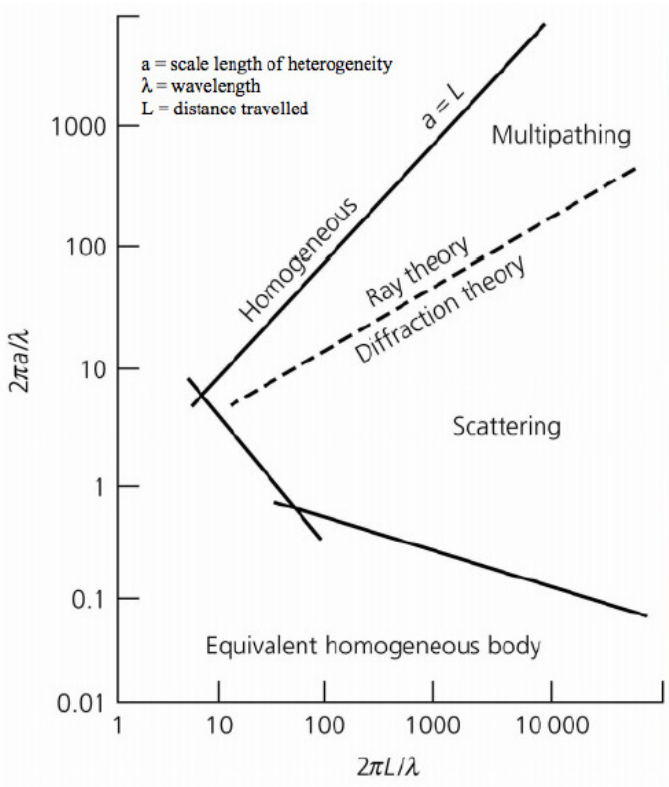

FIGURE 4.2.8. An overview of approaches to wave propagation in random media. The classification of approaches is shown in terms of the scale length of heterogeneity (a), the seismic wavelength (λ) and distance travelled (L). Picture from a lecture by Prof. Rawlison.

4.2.3. Influence of the fracture features. The influence of several fracture features (fracture length, orientation, density, distribution) has been tested in several works. For the purpose of this thesis, it is important to mention the results by Vlastos et al. (2003) and Hall and Wang (2012).

Vlastos et al. (2003) have demonstrated by numerical simulations the importance of the spatial distribution of fractures, which affects the multiple scattering. They have also demonstrated the effect of the fracture length relatively to the wavelength, but this has been already largely discussed.

Hall and Wang (2012) have demonstrated that longer fractures attenuate more than the smaller ones (Fig. 4.2.9): varying the fracture length from 0.1λ to 4λ, where λ is the wavelength, fractures which are long compared to the wavelength attenuate more than those which are short (Hall and Wang, 2012); moreover, as the fractures length increases, reflection becomes more and more predominant over scattering (as already demonstrated by Vlastos et al. (2003)). They have also shown that the fractures orientation has a significant influence on the seismic signal, especially when the

fracture length is less than or comparable to the wavelength: the fracture oriented in the direction of propagation affect the wavefield more than those perpendicular (Fig. 4.2.10), which means that the diffractions from the fractures are more disruptive than the reflections: the reason is that in the case of vertical fractures the incident wave front reaches the fracture at an angle greater than the critical angle which causes a higher loss of energy (and therefore of coherence).

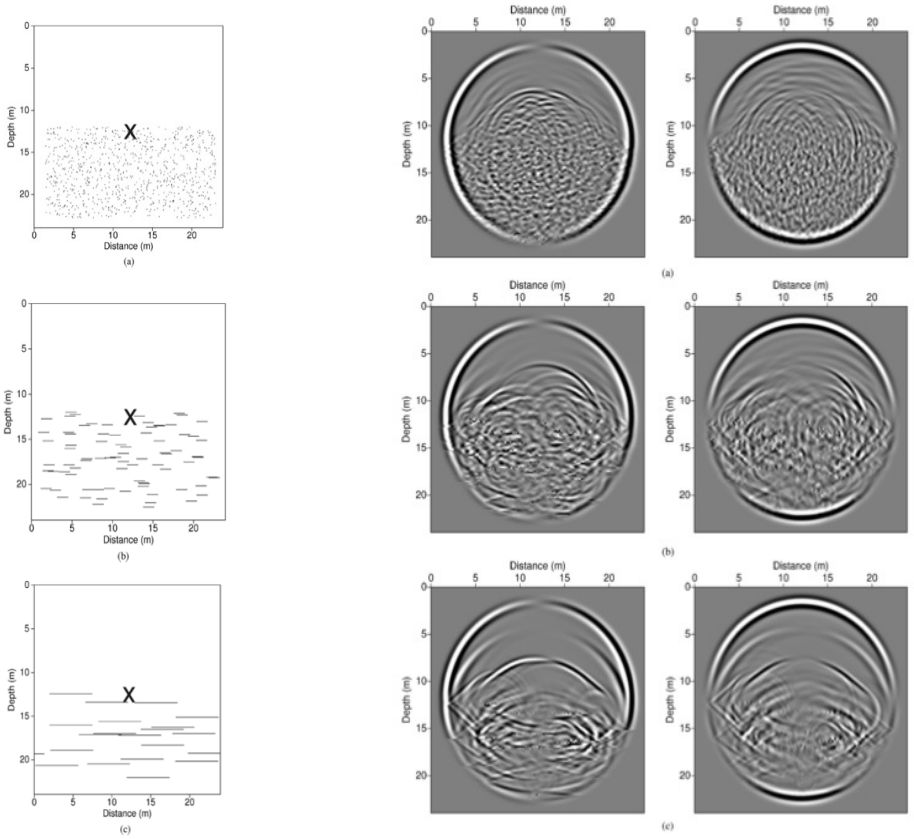

FIGURE 4.2.9. Models with different fracture lengths and relative snapshots of the horizontal (left) and vertical (right) components of velocity: Varying the fracture length from 0.1λ to 4λ, where λ is the wavelength, shows that fractures which are long compared to the wavelength attenuate more than those which are short (Hall and Wang, 2012). Moreover it is possible to notice that, as the fractures length increases, reflection becomes more and more predominant over scattering.

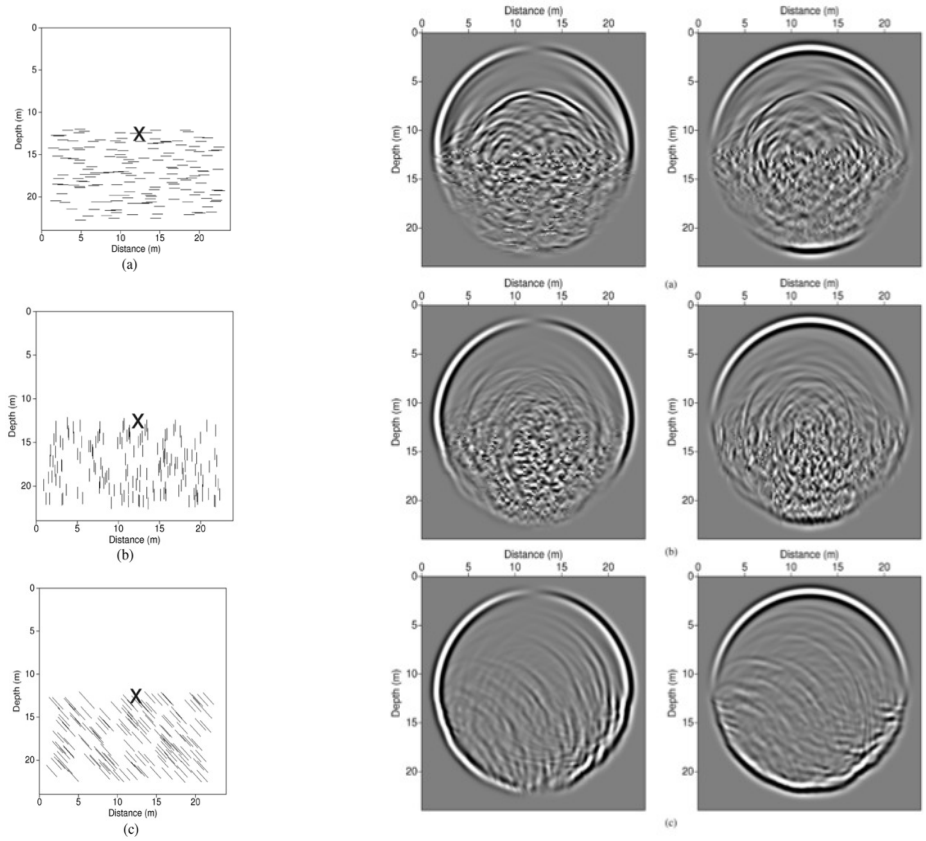

FIGURE 4.2.10. Models with different fractures orientation and relative snapshots of the horizontal (left) and vertical (right) components of velocity: the horizontal fractures seem to affect the wave front less than vertical ones (Hall and Wang, 2012).

CHAPTER 5

2D Synthetic seismic modeling

In this chapter it is described the modeling procedure, starting from the the density and velocity modes created in Matlab and going on with the simulation of the seismic wave propagation in FDELMODC. Some typical outputs have been included as a useful preview of the further results.

5.1. Density and velocity models in MATLAB

In order to test the seismic signature of fractures several synthetic seismic modelings have been performed. As a first step, a 2D density model and a 2D velocity model[1] have been produced by means of the program MATLAB. An example of the graphic outputs is shown in Fig. 5.1.1

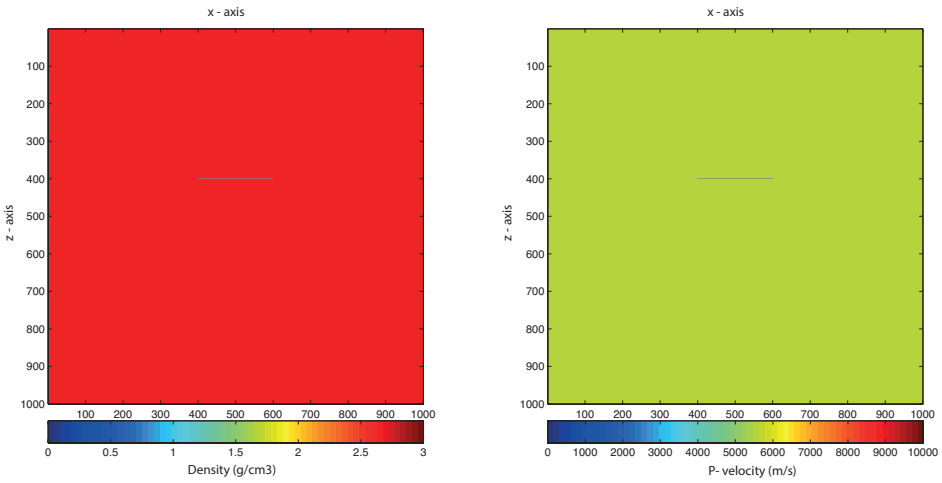

FIGURE 5.1.1. Example of the MATLAB output: on the left-hand side the Density model is shown, on the right-hand side the Velocity model.

It has been assigned a density of 2.65 g/cm^3 and a velocity of 5490 m/s to the background model, which has been assumed to be homogeneous. For what concerns the fractures, they have been assigned a density of 1 g/cm^3 [2]and a velocity of 1690

[1]Only compressional P-waves have been considered in this work, hence the velocity here is the P-velocity

[2]The fractures have been modeled as water-filled fractures

m/s. In the case of a layered model, it has been assigned a density of 2.65 g/cm^3 and a velocity of 5490 m/s to the medium which contains the fractures and a density of 2.00 g/cm^3 and a velocity of 2700 m/s to the layers surrounding the fractured medium. Fractures are randomly positioned in the center of the model, between 1250m and 3750m. In the case of a layered medium, only the middle layer, 1500m thick, contains random fractures.

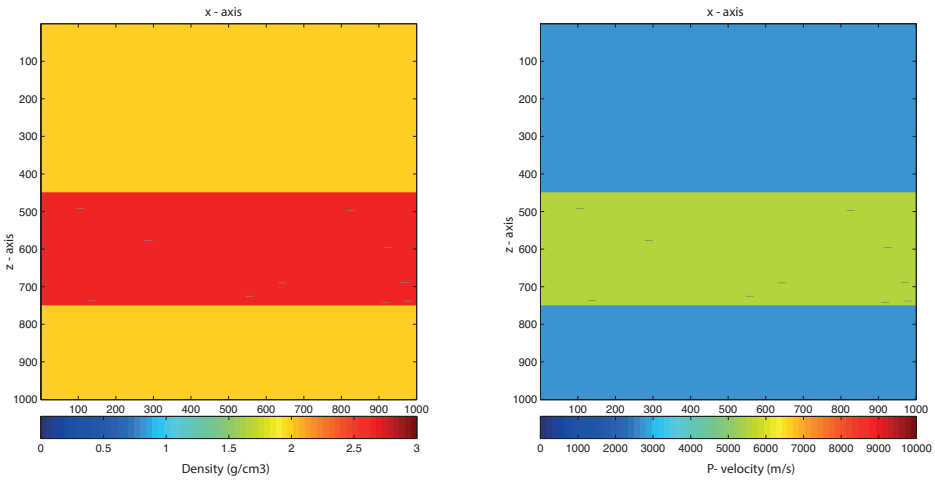

FIGURE 5.1.2. Density model (on the left-hand side) and Velocity model (on the right-hand side) for the layered model.

5.2. Finite-Difference Method (FDELMODC)

Seismic wave propagation in media with discrete fracture distributions has been modeled with the numerical approach by using the 2D finite-difference method. Fractures are treated as highly compliant interfaces with a vanishing width in the 2D finite-difference grid (the scale on which they can occur is often smaller than the grid size in numerical modeling).

The density and velocity models created in Matlab have been used as an input for the program FDELMODC, which models seismic wave propagation by approximating the derivatives in the 2D wave equation by finite-differences (the only difference with the wave equation described in Chapter 1 is that in this case the x- and z-components of the velocity must be considered).

Several input parameters have been defined, as shown in Tab. 1:

Parameters	**Value**
Time step in the model[3]	0.0004 [s]
Discrete grid distance (dx = dz)	5.0
Tapering window length (grid points)[4]	800
Time shift of the peak in time domain[5]	0.05 [s]
Number of sampling points in time domain	1024
Peak frequency [6]	22 [Hz]
Model dimensions (grid points)[7]	1000
x-coordinate of the first and the last receiver	(0,0) , (5000,5000) [m]
z-coordinate of the first and last receiver	(0,4000) , (0,4000) [m]
x-distance between receivers	5 [m]
Desired sampling in the receiver data	0.0012 [s]
x-coordinate of the source position	2500 [m]
z-coordinate of the source position	0 [m]
Number of shots	1
Time window	2.5 [s]

Tab. 1: Table of the modeling parameters chosen in FDELMODC

For what concerns the survey setting, the source is positioned at the surface in a split-spread array of 1000 receivers. A second array of 1000 receivers is positioned at a depth of 4000m. The receivers at the surface record the reflected wavefield, whereas those at a depth of 4000m record the transmitted wavefield. A schematic representation of the model dimensions, source and receivers positions is given in Fig. 5.2.1. The shown receiver positions are related to the six synthetic seismic traces that have been selected further in this work to compare the wiggle traces of the different models. The selected offsets are: 0, -1275m, -2500m (corresponding to the traces number 500, 250 and 1 for the receivers at the surface, 1501, 1251 and 1002 for the receivers at 4000m).

[3]The time step has been chosen according to the Stability condition which relates to the discrete grid distance: $\sqrt{\frac{\lambda+2\mu}{\rho}}\frac{\triangle t}{h} \leq 0.606$

[4]Absorbing tapered boundaries have been chosen in order to suppress (or mostly attenuate) reflections from the sides of the model

[5]This time shift has been introduced in order to avoid a peak in the wavelet at t=0

[6]Considering a Vp of 5490 m/s, this results in a **wavelength** of **249.5 m**

[7]Considering that dx=5, this means that the effective dimensions of the model is 5000x5000 m

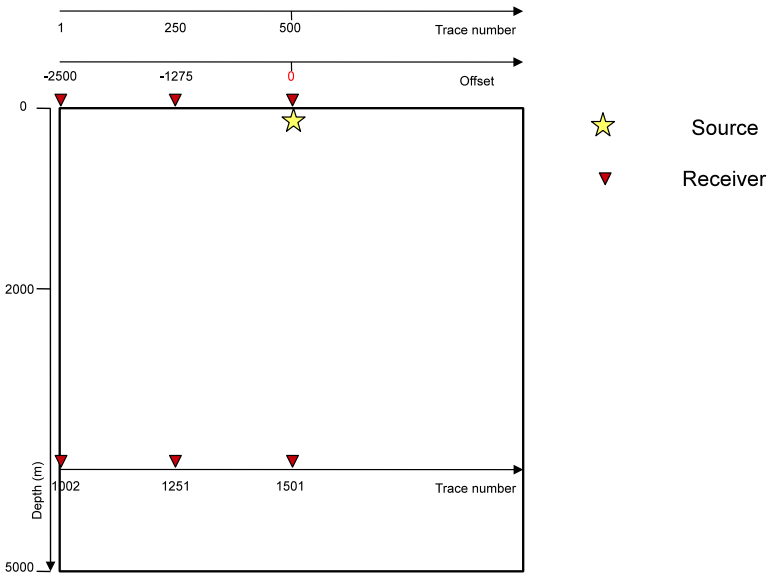

FIGURE 5.2.1. Schematic representation of model dimensions (5000x5000 m), source and receivers positions

Once the modeling has been performed, there are several available outputs. In Fig. 5.2.2, Fig. 4.5 and Fig. 5.2.4 some typical FDELMODC graphic outputs are shown:

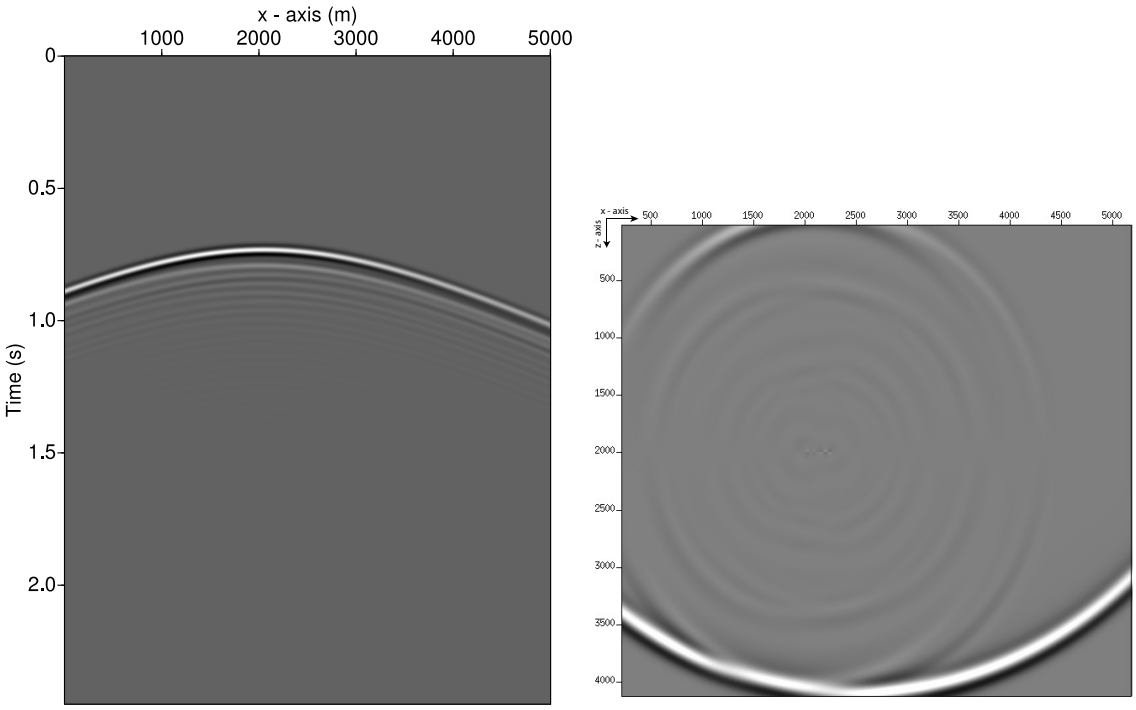

(A) (B)

FIGURE 5.2.2. Examples of a modeled receivers measurements (Fig. 5.2.2a) and of a snapshot (Fig. 5.2.2b).

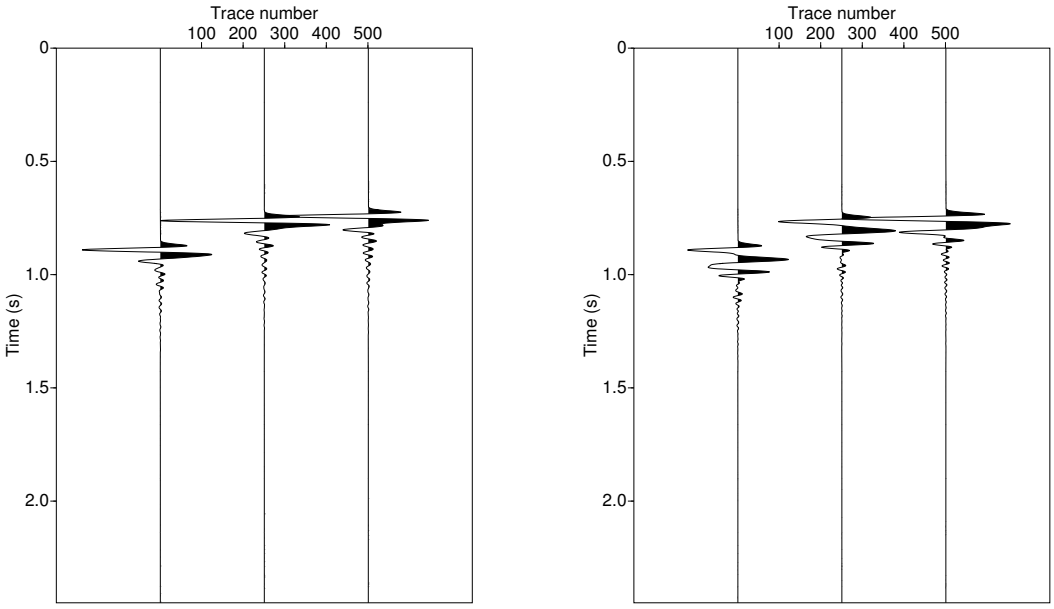

(A) (B)

FIGURE 5.2.3. Example of wiggle traces relative to two different models

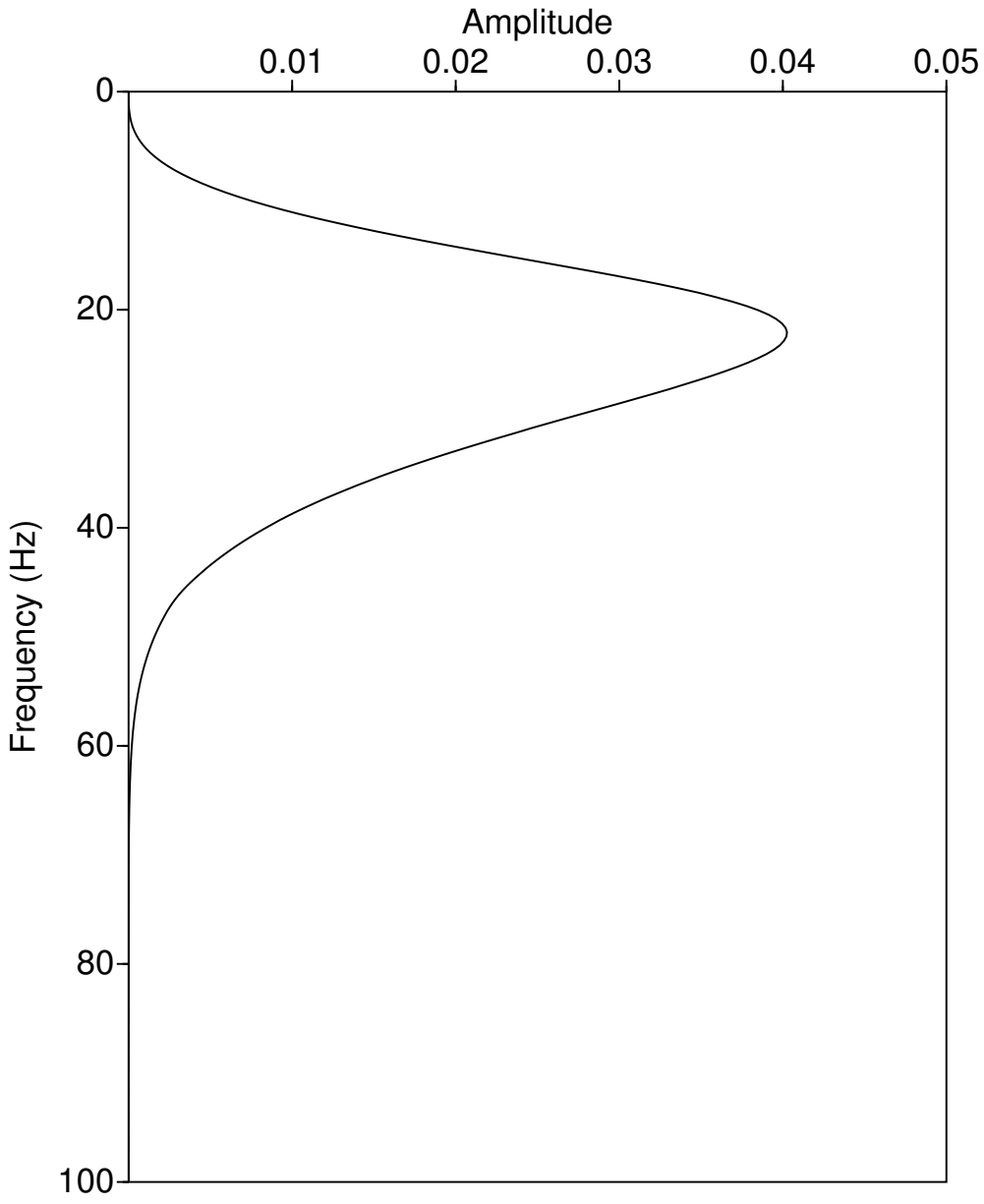

FIGURE 5.2.4. Example of the amplitude spectra which results from the superposition of all the different amplitude spectra relative to a specific receivers array. By doing the superposition over all the traces, the resulting spectrum represents an "averaged" output, which is not subjected to the specific conditions (like the relative source-receiver distance).

CHAPTER 6

Results from the one-fracture model

6.1. Introduction

2D synthetic seismic models have been created to analyze the fracture signatures. In order to test the influence of each fracture feature (orientation, fracture length, fractures density), it has been chosen to vary only one parameter at a time, keeping the other two fixed. In this chapter, the effect of the fracture orientation and length will be described. In the next chapter, the influence of all the three parameters will be analyzed; in addition, the seismic signature of fractures in a layered homogeneous medium will be investigated. The model with no fractures represents the reference for all the other models: each variation from the unperturbed condition that it represents will be attributed to the presence of the fractures. Obviously this statement implies a series of assumptions that represent the limitations of this approach, but this will be discussed later in the Discussion.

Fig. 5.1 and Fig. 5.2 respectively show the wiggle traces and the amplitude spectra referred to the model without any fractures. They will be used for any further comparisons as reference outputs.

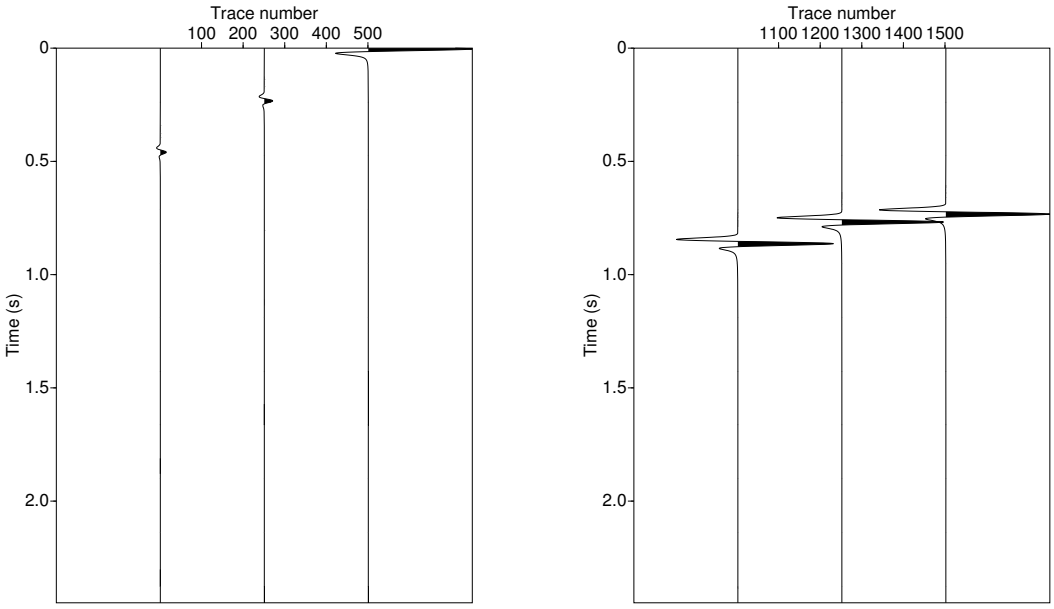

(A) (B)

FIGURE 6.1.1. Wiggle traces recorded from the receivers at the surface (Fig. 5.1a) and at a depth of 4000m (Fig.5.1b) for the model without fractures.

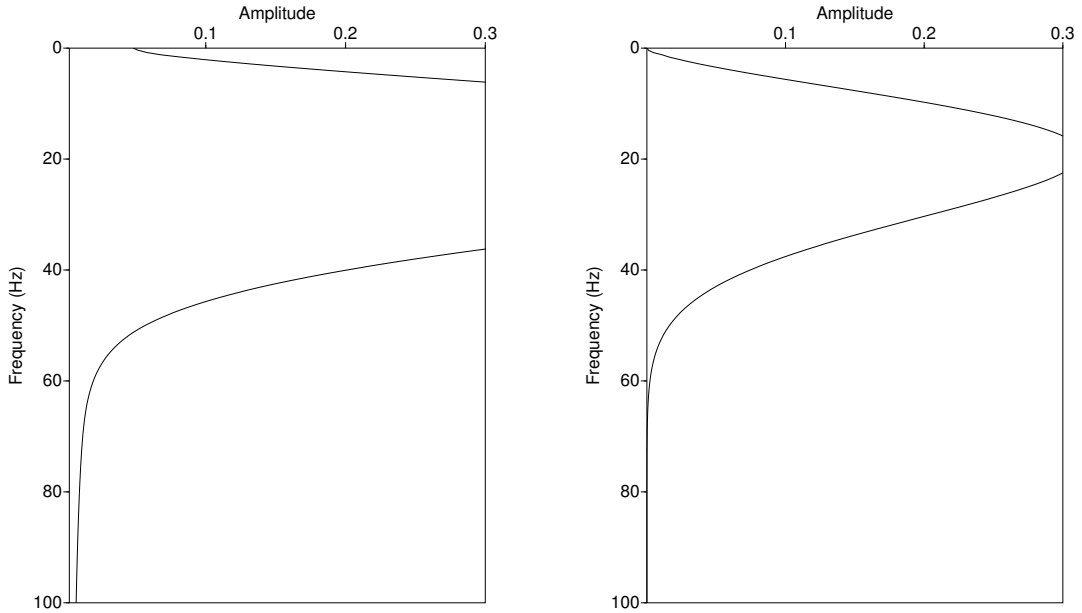

(A) (B)

FIGURE 6.1.2. Amplitude spectra for the traces recorded by the receivers at the surface (Fig. 5.2a) and at the depth of 4000m (Fig. 5.2b) for the model without fractures.

6.2. Orientation effect

The first experiment has been performed on a very simple model characterized by a homogeneous half space ($\rho = 2.65\text{g/cm}^3$, $v_p = 5490m/s$) which contains a single fracture; its length has been fixed to 100 m (almost half wavelength). In order to test the effect of the fracture orientation, three different models have been considered in which the fracture is horizontal, vertical and at 45°[1]. In Fig. 6.2.1 there is a schematic representation of the three models (note that the length of the fractures has been exaggerated for visualization purpose):

[1]For what concerns the angle convention in this work, it must be pointed out that the angles are defined according to an anti-clockwise rotation.

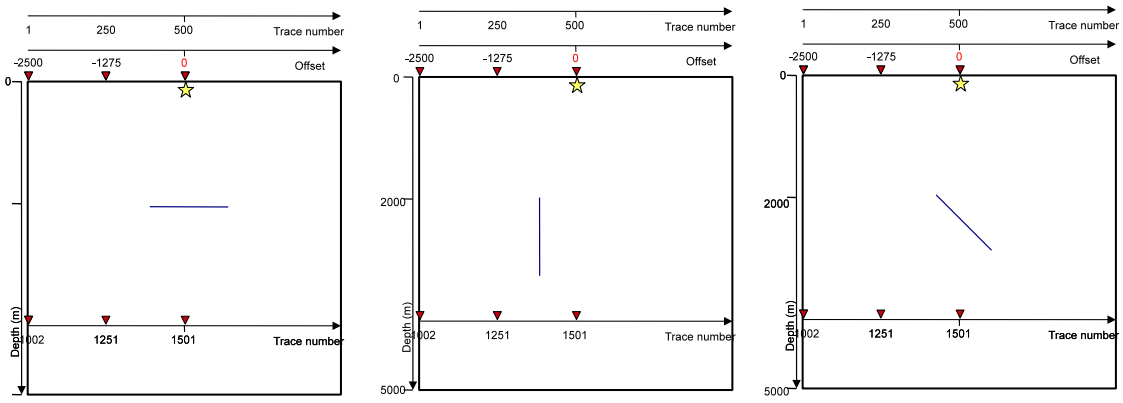

FIGURE 6.2.1. From left to right: model with one horizontal fracture, with one vertical fracture and with a fracture at 45°. The star represents the source position, the triangles the receiver positions.

A first comparison among the different models is done by analyzing the wiggle traces. It is important to point out the difference between the outputs referred to the receivers at the surface and those referred to the receivers at 4000m: in the first case the direct field has been removed from the total wavefield (since the direct waves traveling along the surface are not influenced by the presence of fractures), on the contrary in the second case the total wavefield has been considered (because the transmitted waves are affected by the fractures). This distinction is valid for all the further cases.

The wiggle traces referred to the offsets 0, -1275m and -2500m are shown in Fig. 6.2.2(for the receivers at the surface) and in Fig. 6.2.3(for the receivers at a depth of 4000m):

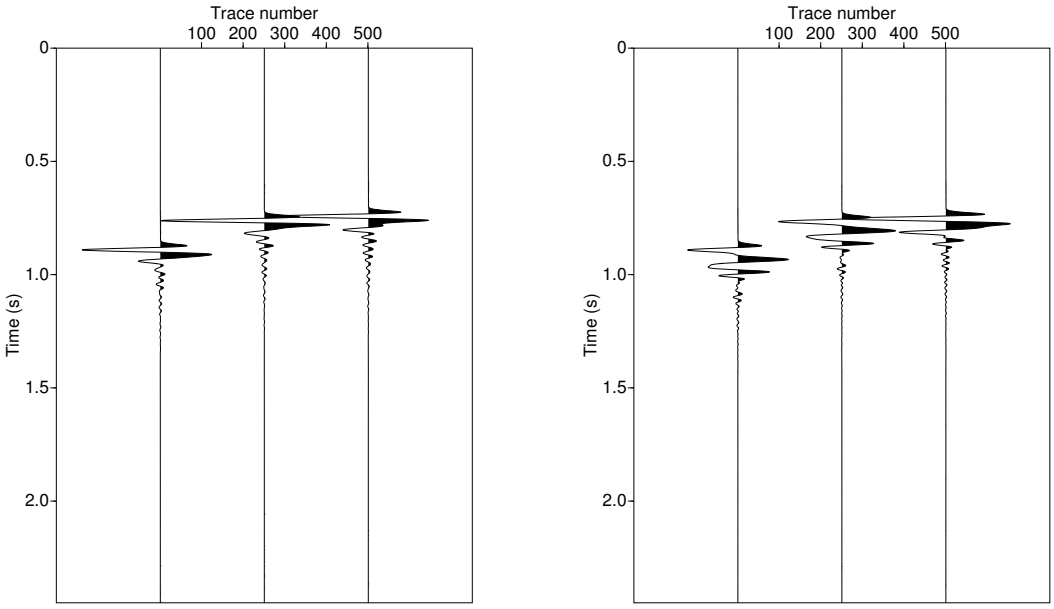

(A)

(B)

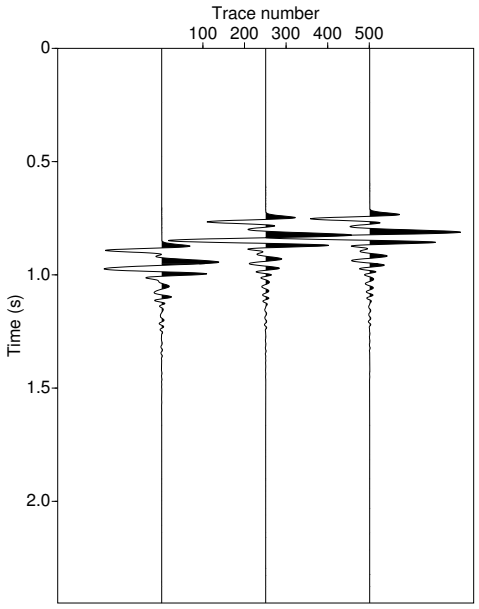

(C)

FIGURE 6.2.2. Wiggle traces recorded from the receivers at the surface. Fig.6.2.2a Wiggle traces for the model with one horizontal fracture; Fig.6.2.2b Wiggle traces for the model with one fracture at 45°; Fig.6.2.2c Wiggle traces for the model with one vertical fracture.

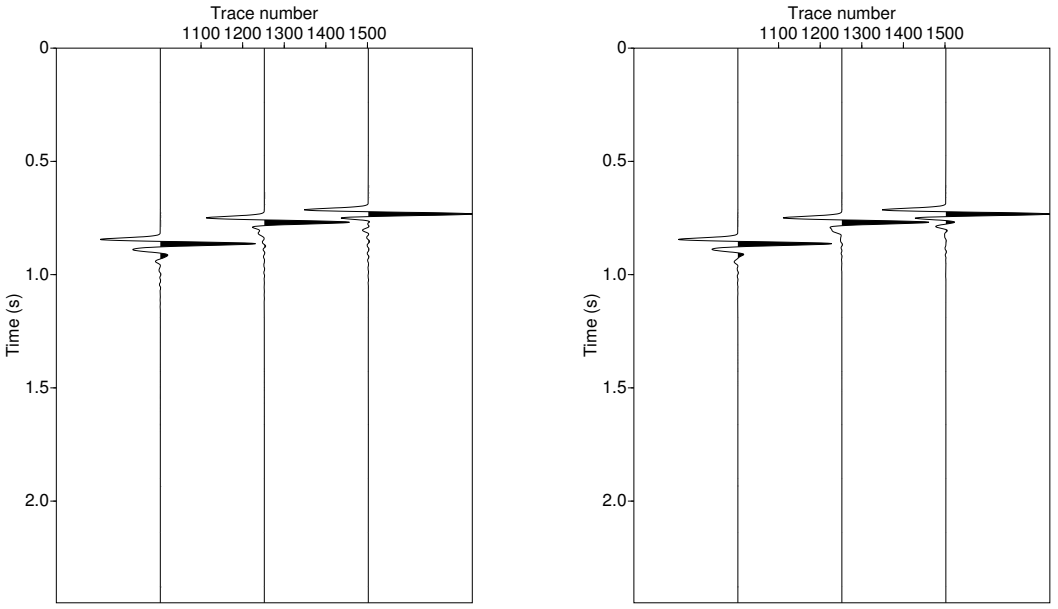

(A)

(B)

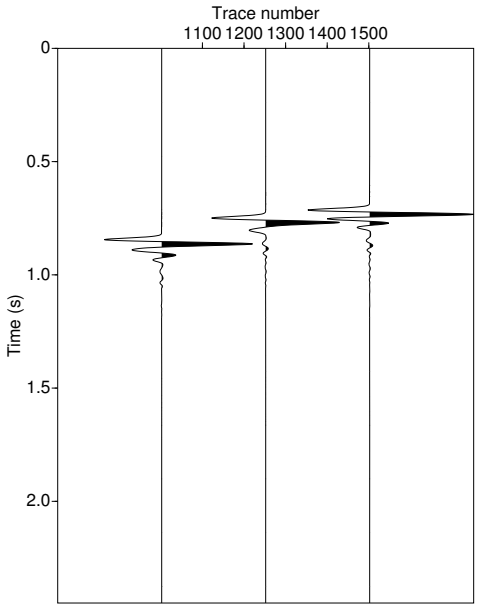

(C)

FIGURE 6.2.3. Wiggle traces recorded from the receivers at the depth of 4000m. Fig. 5.5a Wiggle traces for the model with one horizontal fracture; Fig. 5.5b Wiggle traces for the model with one fracture at 45°; Fig. 5.5c Wiggle traces for the model with one vertical fracture.

The presence of the fracture is clearly revealed by the diffraction events (Fig. 6.2.2 and Fig. 6.2.3) and by the "ringing" waves recorded at later times with respect to the first arrivals (Fig. 6.2.2 and Fig. 6.2.3). These "tails" are particularly evident when the reflected wavefield is considered; in particular, they have a higher amplitude in the case of a horizontal and a vertical fracture compared to the one inclined at 45°.

In Fig.6.2.4 and Fig. 6.2.5 it is shown the total recorded pressure wavefield for the three different models respectively for the receivers at the surface and the receivers at 4000m:

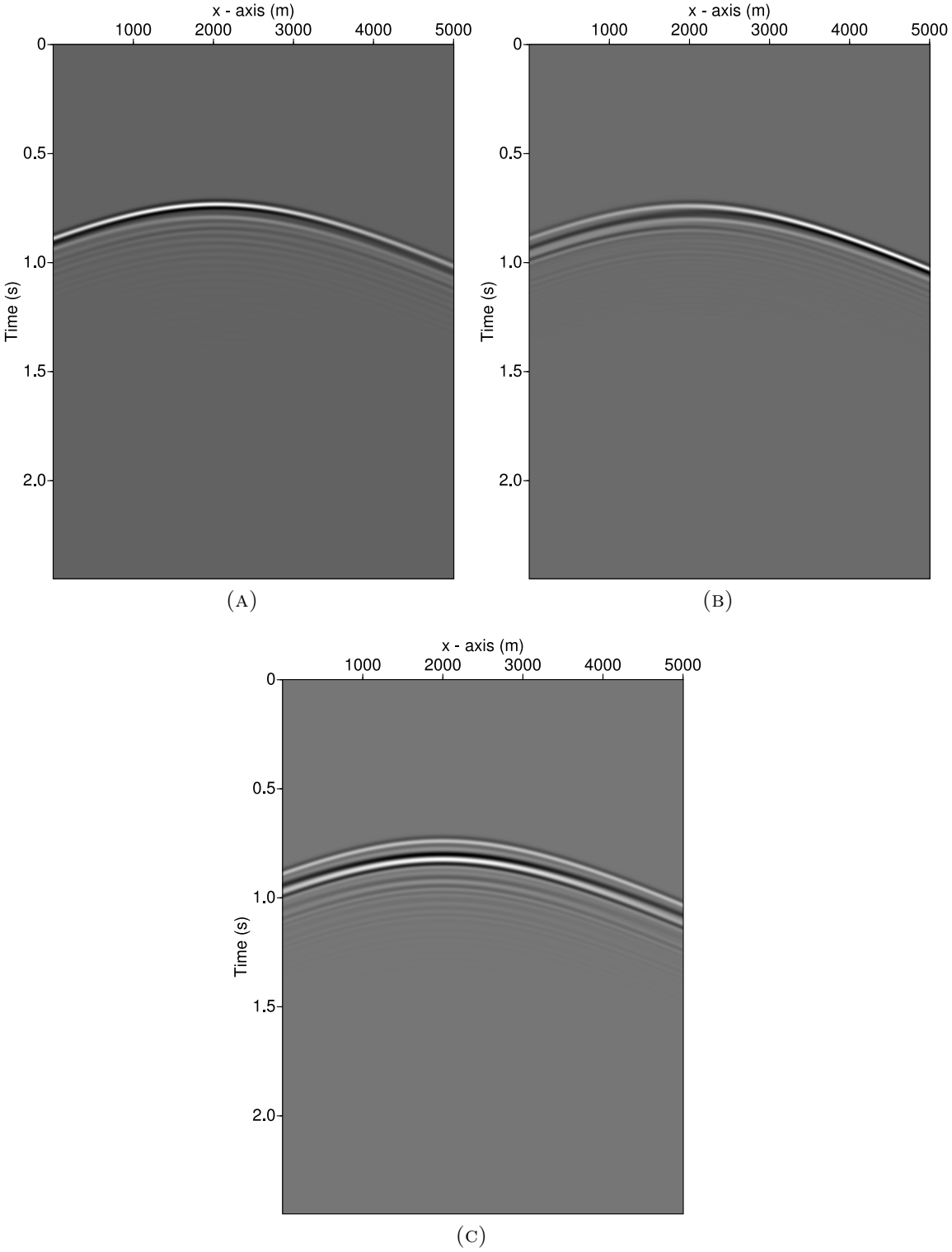

FIGURE 6.2.4. Pressure wavefield recorded at the receivers on the surface; from the left to the right: model with one horizontal fracture (Fig. 6.2.4a), with a 45° inclined fracture (Fig. 6.2.4b) and with a vertical fracture (Fig. 6.2.4c). It is possible to notice the diffracted hyperbolae and the late arrivals.

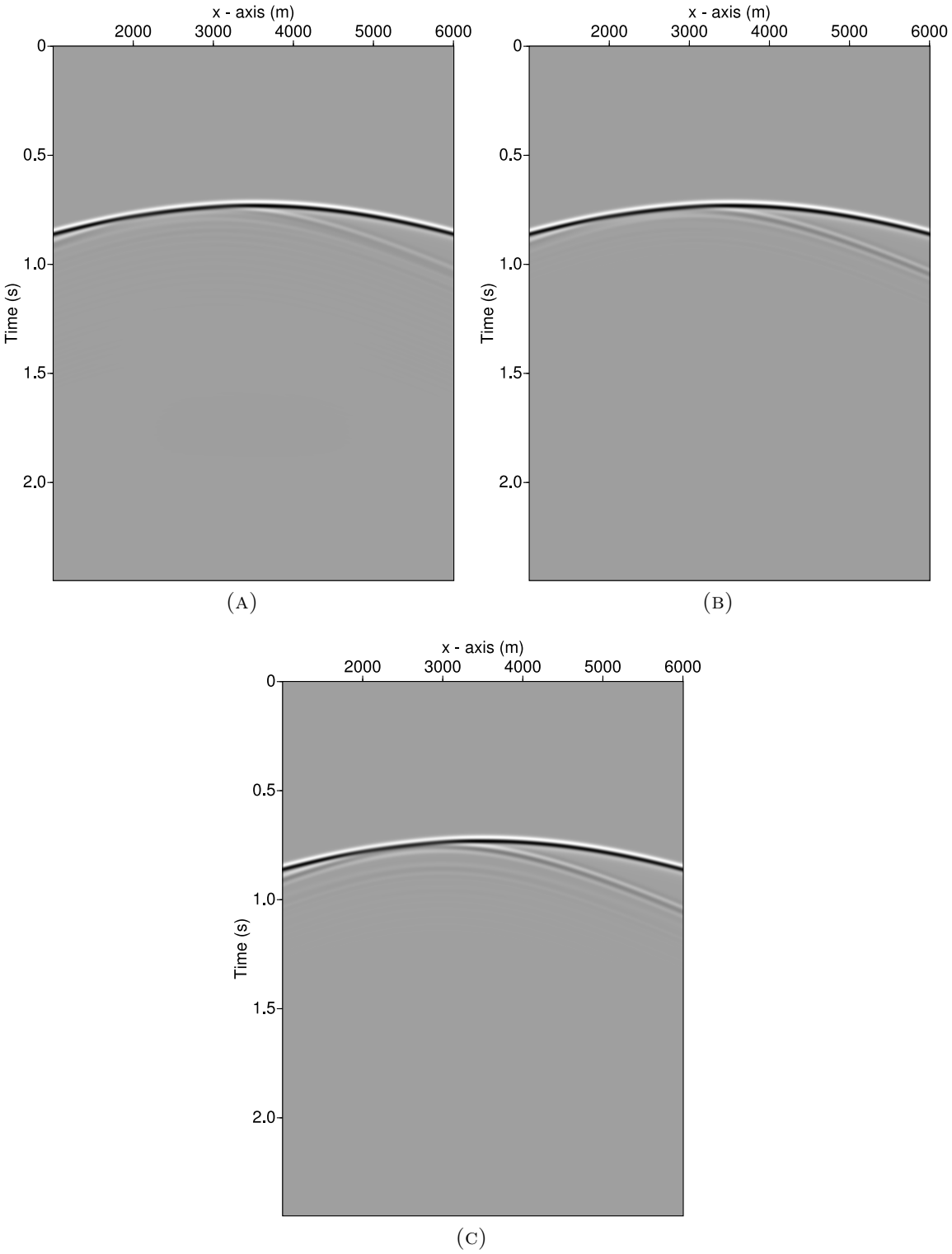

FIGURE 6.2.5. Pressure wavefield recorded at the receivers at 4000m; from the left to the right: model with one horizontal fracture (Fig. 6.2.5a), with a 45° inclined fracture (Fig. 6.2.5b) and with a vertical fracture (Fig. 6.2.5c). The diffracted and transmitted wavefield are visible; the late arrivals are present in this case as well, but less than in the previous case.

The recognizable events in Fig. 6.2.4 are mainly diffracted hyperbolae followed by late arrivals whose amplitude decreases with time. In Fig. 6.2.5, both transmitted and diffracted events are visible. Looking at the snapshot in Fig. 6.2.6 (referred to the model with one horizontal fracture), the fracture seems to act as a point scatterer[2]: the incident wavefield is spherically spread out as it interacts with the fracture ("scattered wavefront" in Fig. 6.2.6). Moreover, the fracture represents the center for several concentric wavefronts; the amplitude of the wavefronts decreases going from the most external circle towards the fracture. The late arrivals (after the first scattered wave) cannot be identified as a *coda wave*, since it is generally associated to the multiple scattering (which occurs when a wave is repeatedly scattered by several scatterers, that is by several fractures). The "tail" after the first arrivals could be caused by scattering within the fracture (maybe due to the grid spacing chosen for the modeling).

[2]In the literature, a "point scatterer" is described as a "point diffractor", as it generates a diffraction hyperbola as seismic response. For this reason, referring to Fig. 5.6 and Fig. 6.2.5, the visible events are described as "diffracted events". This is valid for all the similar cases.

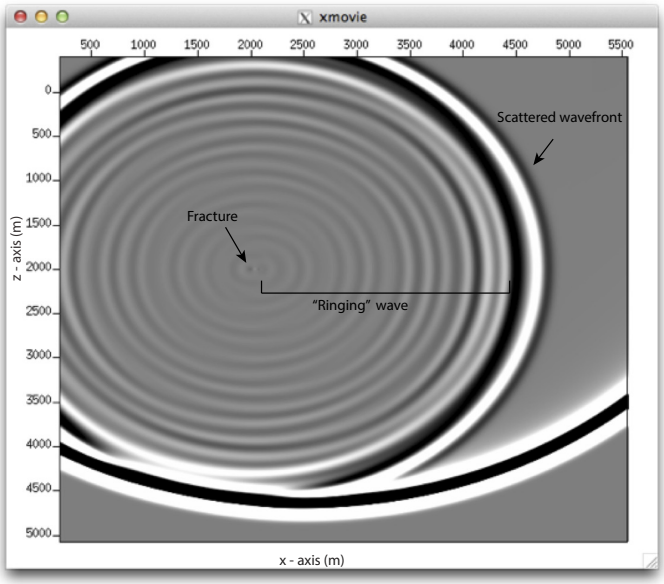

FIGURE 6.2.6. Snapshot of the vertical component of the velocity. Model with a 100m long horizontal fracture. The fracture seems to act as a point scatterer: the incident wavefield is spherically spread out as it interacts with the fracture. The fracture represents the center for several concentric wavefronts; the amplitude of the wavefronts decreases going from the most external circle towards the fracture.

The effect of the orientation has been tested in the frequency domain as well by comparing the amplitude spectra for the three models. In Fig. 6.2.7 the results relative to the receivers at the surface are shown, in Fig. 6.2.8 the ones relative to the receivers at 4000m:

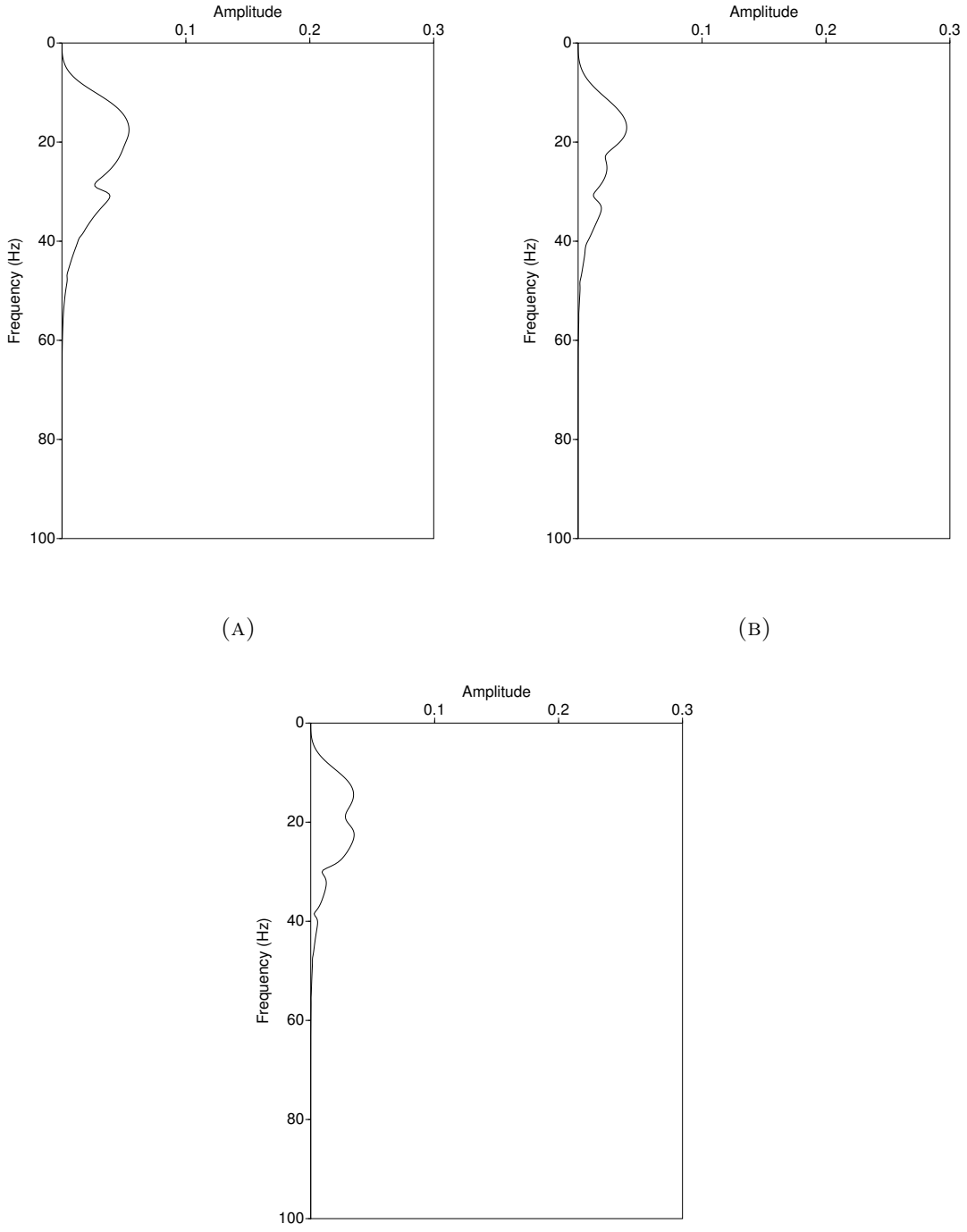

(A)

(B)

(C)

FIGURE 6.2.7. From the left to the right: amplitude spectra for the model with one horizontal fracture (Fig. 6.2.7a), a 45° inclined fracture (Fig.6.2.7b) and a vertical fracture (Fig. 6.2.7c). Results related to the receivers at the surface. The spectrum relative to the model with one horizontal fracture has the highest amplitude, but the most prominent effect of the orientation change is the variation of the shape of the spectra.

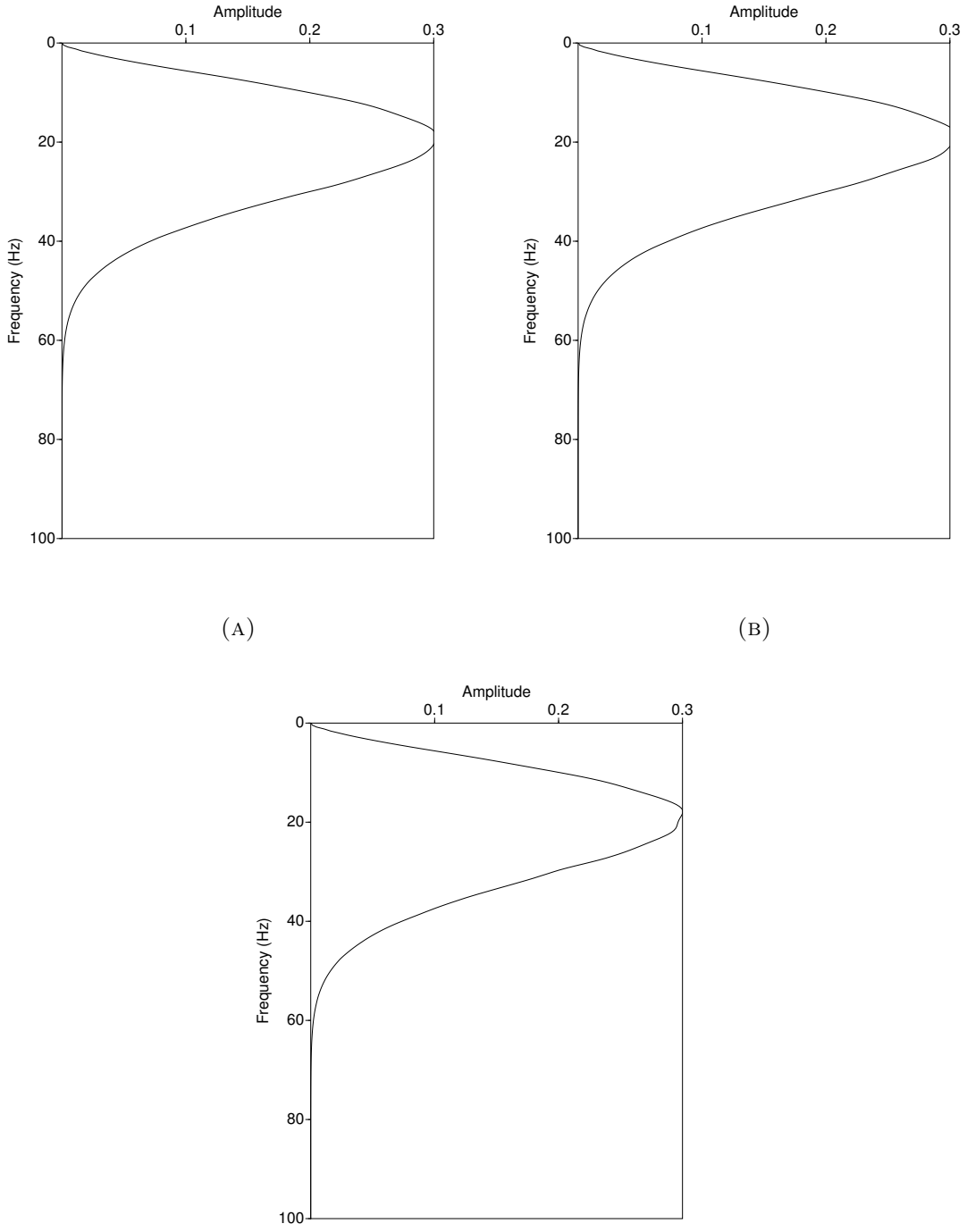

(A)

(B)

(C)

FIGURE 6.2.8. From the left to the right: amplitude spectra for the model with one horizontal fracture (Fig. 6.2.8a), a 45° inclined fracture (Fig.6.2.8b) and a vertical fracture (Fig. 6.2.8c). Results related to the receivers at the depth of 4000m. These spectra are less affected by the presence of the fracture and by the different orientation compared to the previous figure.

The amplitude spectra in Fig. 6.2.7 show relatively low amplitudes, but it should kept in mind that the direct field has been removed. Having said that, their difference can be attributable to the different orientation of the fracture in the three models; in particular, the spectrum relative to the model with one horizontal fracture has the highest amplitude, due to the highest energy density that is back-scattered from a discontinuity which is parallel to the receivers array. On the other hand, the spectra in Fig. 6.2.8 are less affected by the presence of the fracture and by the different orientation; it can be said that the strongest decrease in the peak amplitude occurs for the vertical fracture (Fig. 6.2.8c).

6.3. Fracture length effect

The second experiment differs from the first one only for the choice of the variable parameter. This time, the orientation of the fracture has been fixed, meaning that the fracture length represents the only varying parameter. Several tests have been made for each of the previous three models:

- fracture length $\sim$ wavelength (= 250 m)
- fracture length $\sim$ 1/2 wavelength (= 100 m)
- fracture length $\sim$ 1/5 wavelength (= 50 m)
- fracture length $\sim$ 1/10 wavelength (= 25 m)

For practical reasons it is not possible to show all the results. In the following, only the results for the model with one horizontal fracture will be shown.

The first comparison is made among the wiggle traces referred to the offsets 0, -1275m and -2500m. Fig. 6.3.1 is related to the receivers at the surface, Fig. 6.3.2 to the receivers at the depth of 4000m:

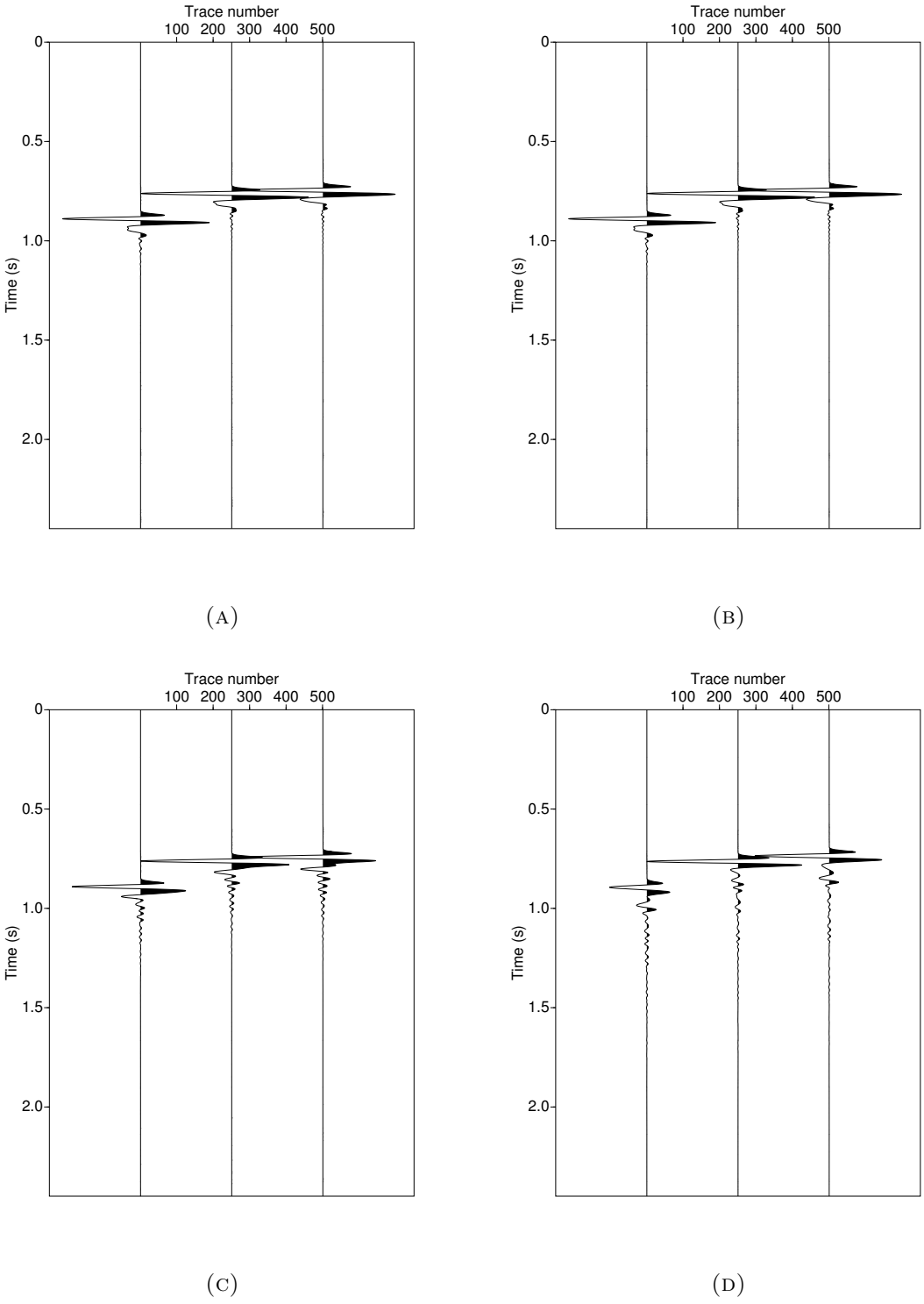

(A) (B)

(C) (D)

FIGURE 6.3.1. Wiggle traces for the receivers at the surface for different fracture length (horizontal fracture): f.l. = 25m (Fig. 6.3.1a); f.l.=50m (Fig. 6.3.1b); f.l.=100m (Fig. 6.3.1c); f.l.=250m (Fig. 6.3.1d). The amplitude of the diffracted events decreases as the fracture length increases.

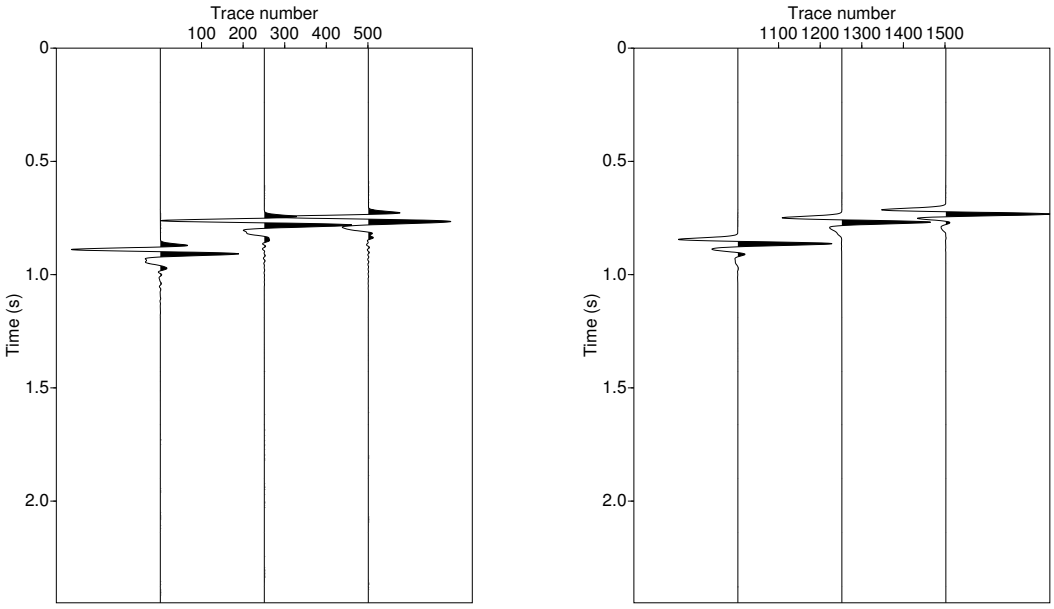

(A)

(B)

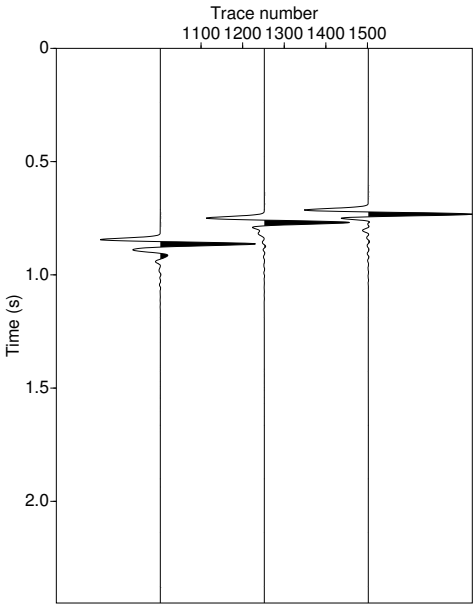

(C)

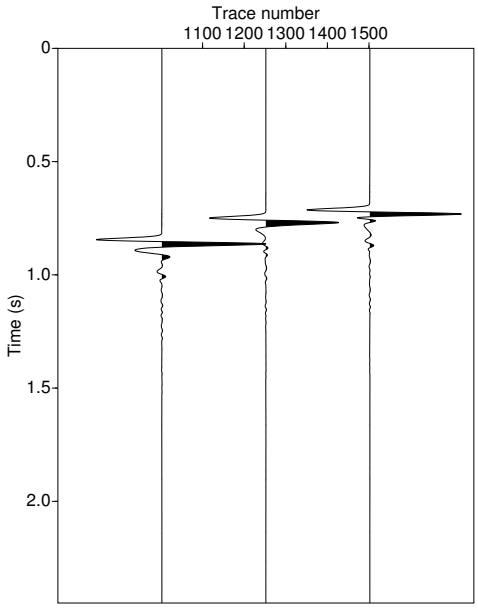

(D)

FIGURE 6.3.2. Wiggle traces for the receivers at the depth of 4000m for different fracture lengths (horizontal fracture): f.l. = 25m (Fig. 6.3.2a); f.l.=50m (Fig. 6.3.2b); f.l.=100m (Fig. 6.3.2c); f.l.=250m (Fig. 6.3.2d). Note the wavefield attenuation when the fracture length approaches the wavelength

Fig. 6.3.1 shows that the amplitude of the diffracted events decreases as the fracture length increases; moreover, when the fracture length approaches the wavelength, the seismic signal starts to become more complex (Fig. 6.3.1d). In addition, if the fractures are too small compared to the wavelength (Fig. 6.3.1a), they do not produce any "ringing" waves, which appears when the fractures approach a length that is about one fifth of the wavelength (Fig. 6.3.1b); increasing the fracture length, the "ringing" wave length (therefore its time duration) increases (Fig. 6.3.1c and Fig. 6.3.1d). For the transmitted wavefield it appears only starting from fractures lengths of about half-wavelength (Fig. 6.3.2c). Moreover, it is possible to notice the wavefield attenuation when the fracture length approaches the wavelength (Fig. 6.3.2d); as for the reflected wavefield, the seismic signal starts to become more complex.

In Fig. 6.3.3 and Fig. 6.3.4 it is shown the total recorded pressure wavefield for the four different fracture lengths respectively for the receivers at the surface and the receivers at 4000m:

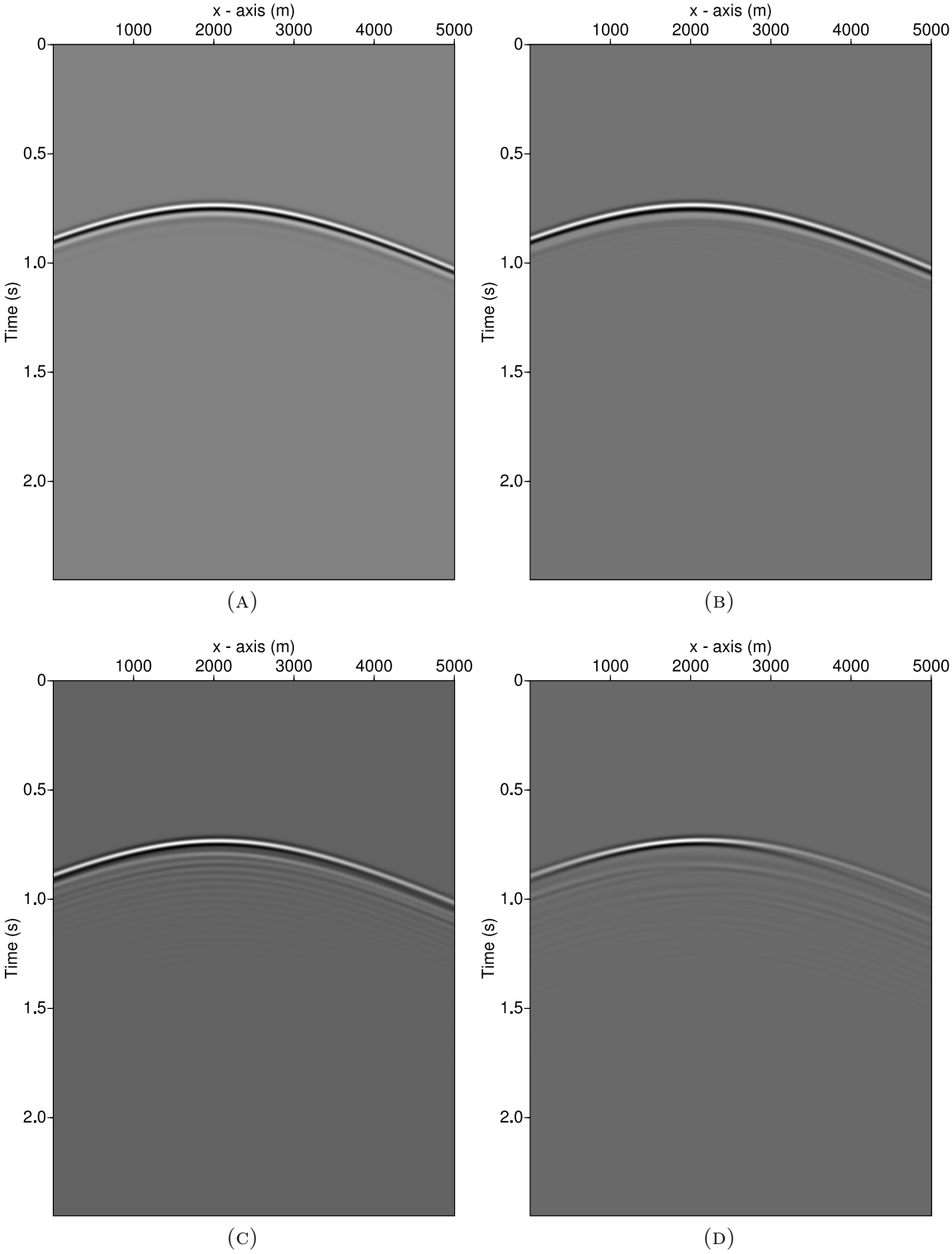

FIGURE 6.3.3. Pressure wavefield recorded at the receivers on the surface for different fracture lengths (horizontal fracture): f.l. = 25m (Fig. 6.3.3a); f.l.=50m (Fig. 6.3.3b); f.l.=100m (Fig. 6.3.3c); f.l.=250m (Fig. 6.3.3d).

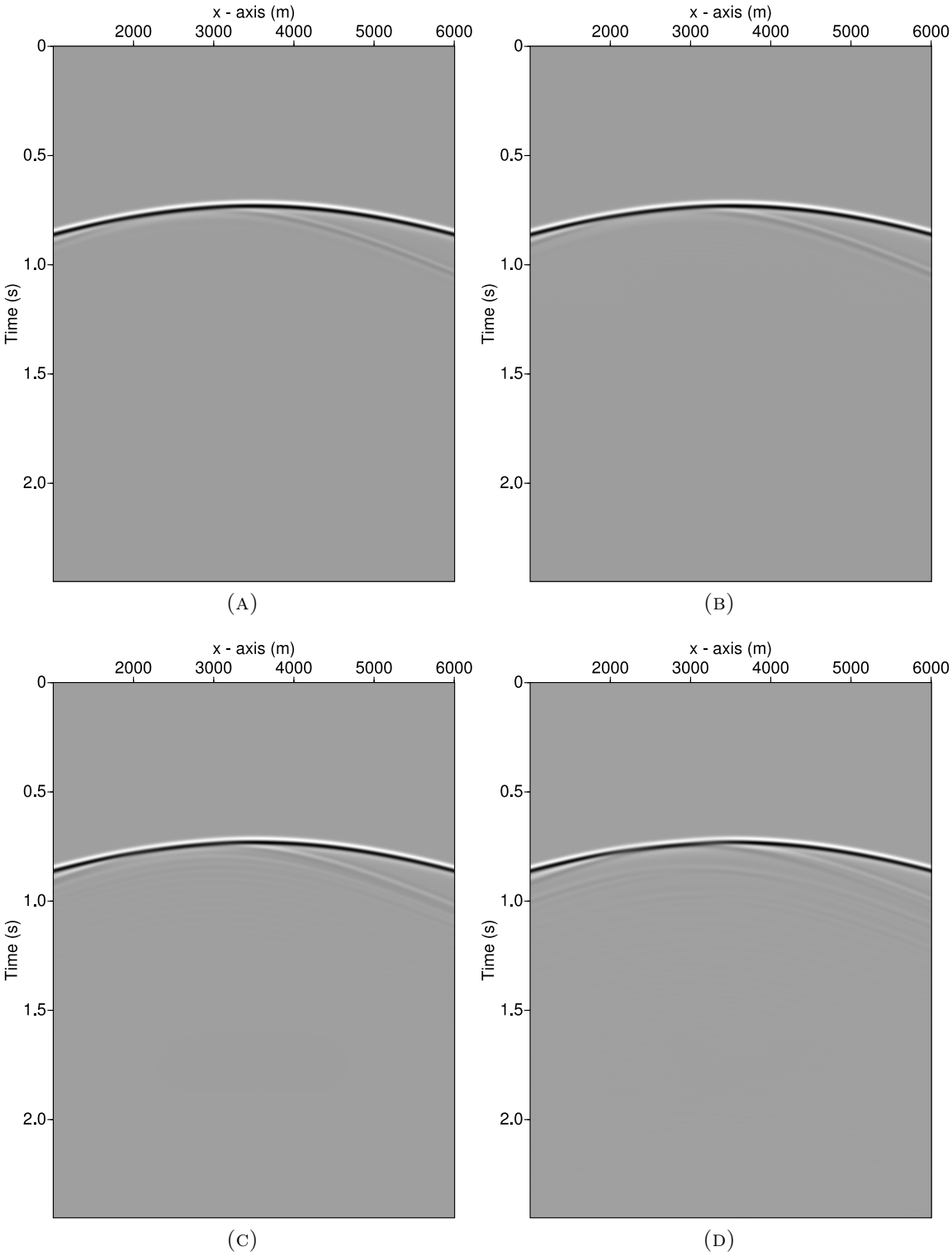

FIGURE 6.3.4. Pressure wavefield recorded at the receivers on the surface for different fracture lengths (horizontal fracture): f.l. = 25m (Fig. 6.3.4a); f.l.=50m (Fig. 6.3.4b); f.l.=100m (Fig. 6.3.4c); f.l.=250m (Fig. 6.3.4d).

Fig. 6.3.3 and Fig. 6.3.4 basically confirm what has been said about the wiggle traces. In particular, it is possible to notice that the diffraction hyperbola in Fig.6.3.3d shows a decreased amplitude along the two sides and that a second diffraction hyperbola at later times start to be visible. This can be due to the onset of the separation of the diffracted wavefields from the fracture tips, which could not occur for lower fracture lengths.

The effect of the fracture length has been tested in the frequency domain as well by comparing the amplitude spectra for the four different fracture lengths. The results are shown in Fig. 6.3.5 and Fig. 6.3.6 for the receivers at the surface and the receivers at 4000m respectively:

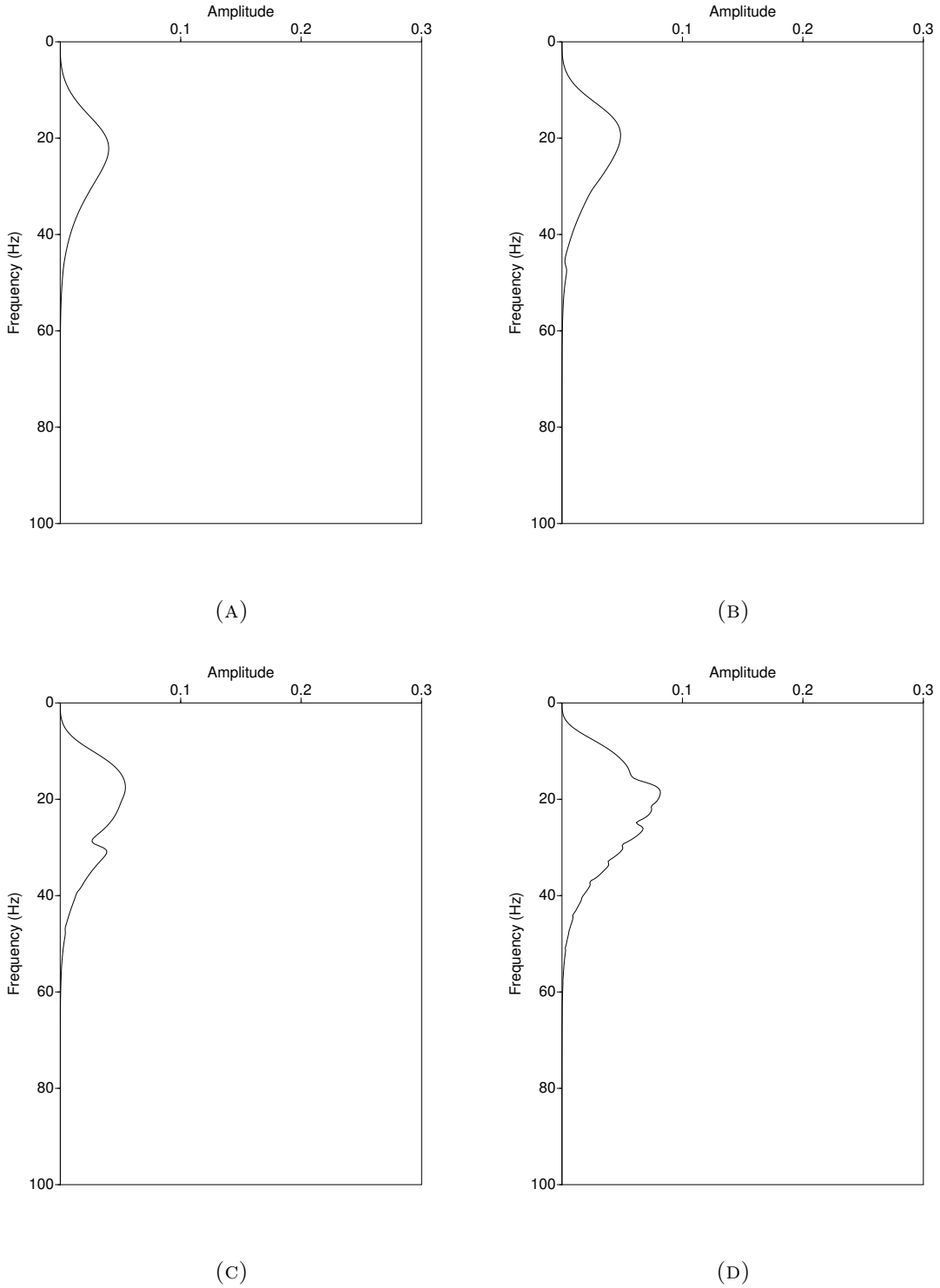

FIGURE 6.3.5. Amplitude spectra for the model with one horizontal fracture for different fracture lengths. From the left to the right: f.l. = 25m (Fig. 6.3.5a); f.l.=50m (Fig. 6.3.5b); f.l.=100m (Fig. 6.3.5c); f.l.=250m (Fig. 6.3.5d). Results related to the receivers at the surface. As the fracture length increases, the amplitude of the spectra increases; moreover, the spectrum in Fig. 6.3.5d is much less smooth if compared to the other ones.

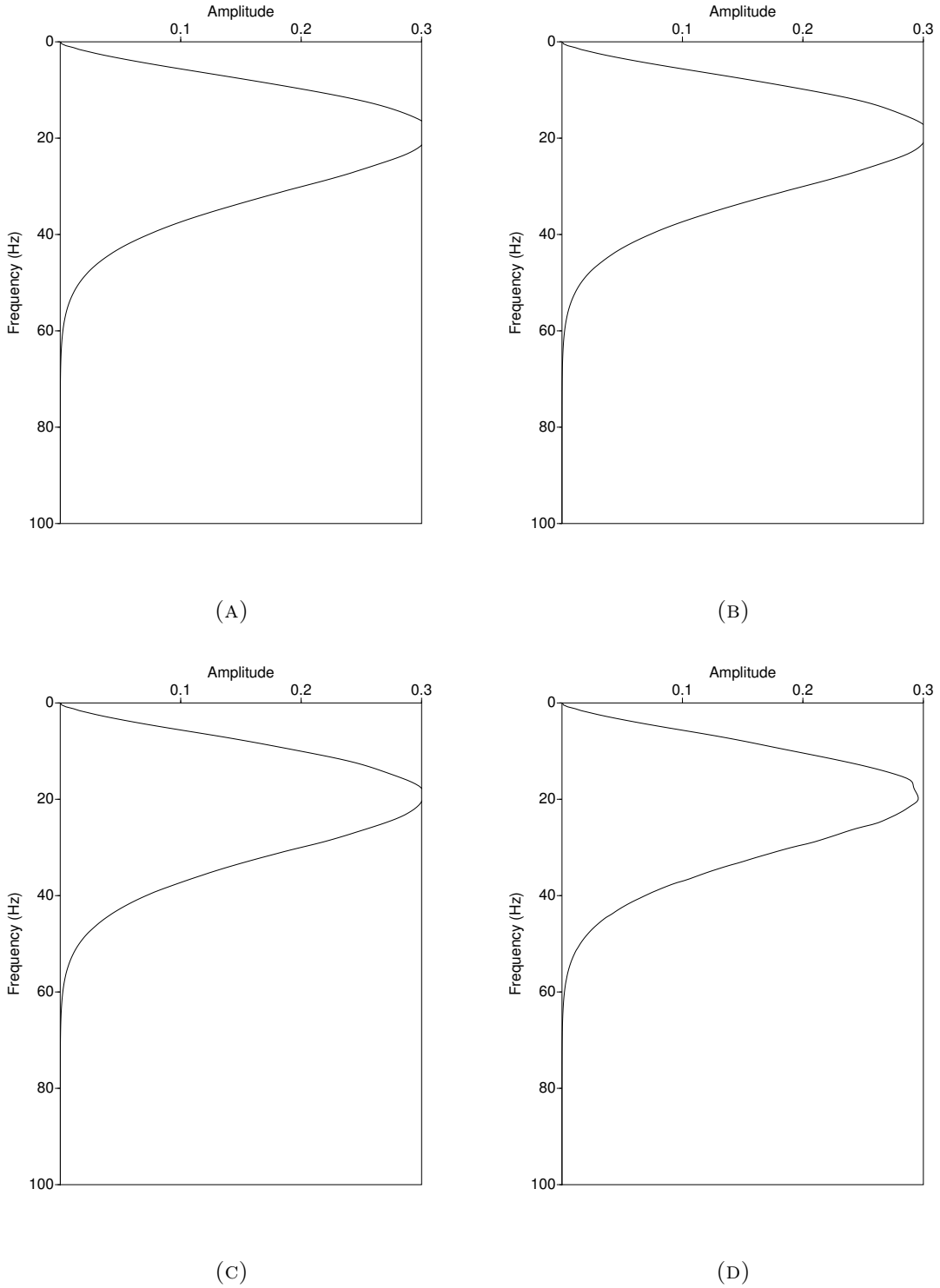

(A) (B)

(C) (D)

FIGURE 6.3.6. Amplitude spectra for the model with one horizontal fracture for different fracture lengths. From the left to the right: f.l. = 25m (Fig. 6.3.6a); f.l.=50m (Fig. 6.3.6b); f.l.=100m (Fig. 6.3.6c); f.l.=250m (Fig. 6.3.6d). Results related to the receivers at the depth of 4000m.

In Fig. 6.3.5, as the fracture length increases, the amplitude of the spectra increases; this could be explained considering that when the fracture length increases, a higher seismic energy is back-scattered towards the surface. As the fracture length increases, there is a decrease in the peak frequency, but as the fractures approach the wavelength, a shift of the peak frequency towards higher values occurs. Moreover, the spectrum in Fig. 6.3.5d is much less smooth if compared to the other ones, maybe due to diffractions from the tips that start to get separated: in fact, it is similar to the spectrum of the vertical fracture in Fig. 1.2.7c, for which the wavefields diffracted by the two tips were already separated for a fracture length of 100m. Much less effects are visible in Fig. 5.9c; it can only be said that the strongest decrease in the peak amplitude occurs for the longest fracture (Fig. 5.16d).

CHAPTER 7

Results from the multiple-fractures models

7.1. Introduction

In this chapter, which includes the results from all the multiple fractures models, the influence of all the three parameters (fracture orientation, fracture length and fractures density) will be described. For practical reasons, the outputs related to the reference model (without fractures) are shown again in Fig. 7.1.1 and Fig. 7.1.2 :

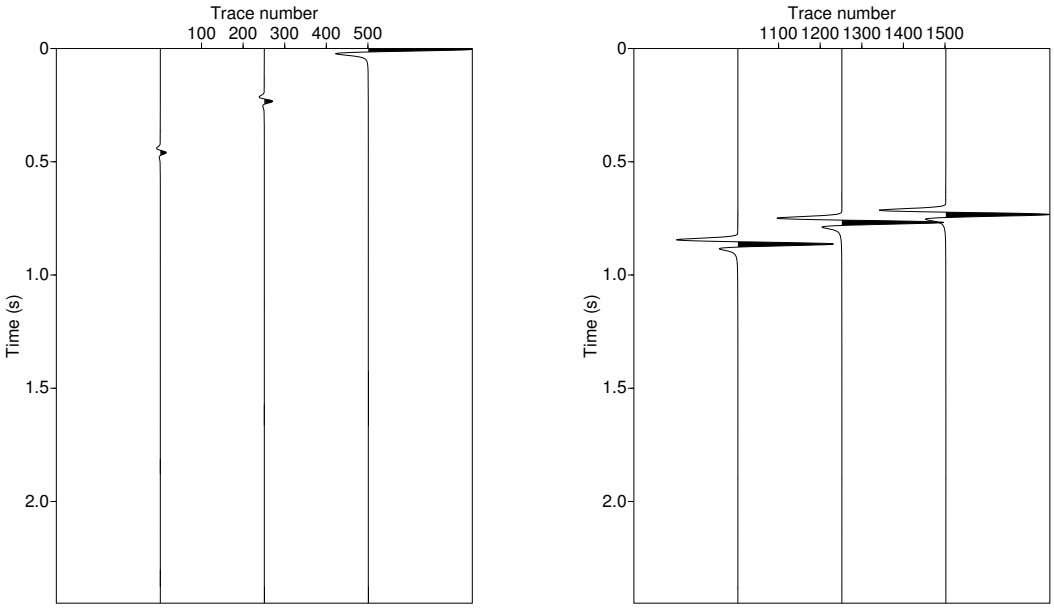

(A) (B)

FIGURE 7.1.1. Wiggle traces recorded from the receivers at the surface and at a depth of 4000m for the model without fractures.

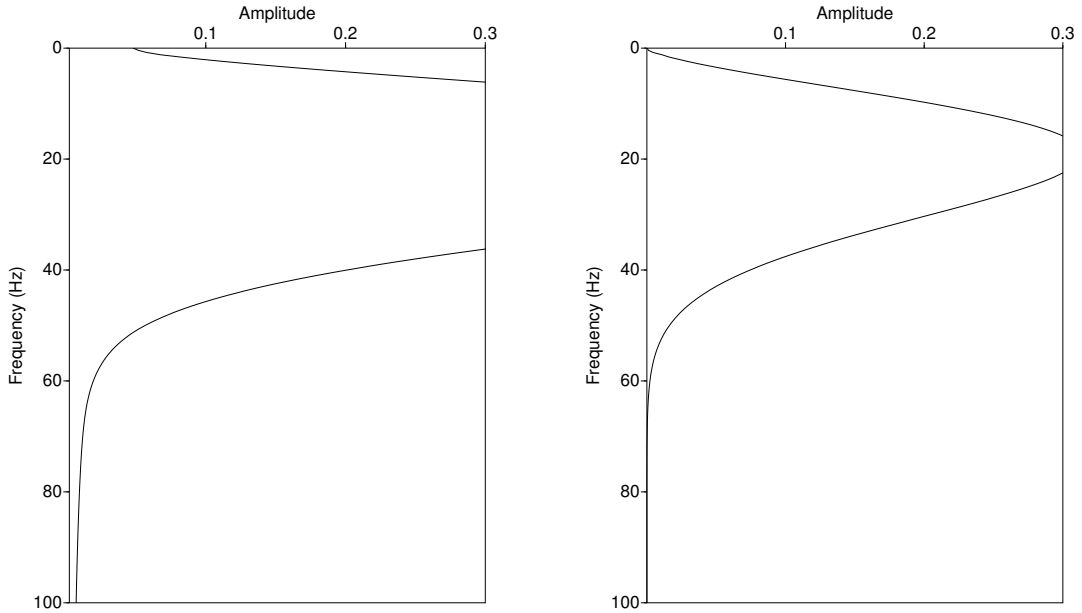

(A) (B)

FIGURE 7.1.2. Amplitude spectra for the traces recorded by the receivers at the surface (Fig. 7.1.2a) and at the depth of 4000m (Fig. 7.1.2b) for the model without fractures.

7.2. Orientation effect

In order to test the influence of the fracture orientations, frequency-wavenumber (f-k) plots can be implemented as an useful to tool, since they are used to examine the direction and apparent velocity of seismic waves. Five f-k plots have been produced for the models with one-hundred 100m long fractures and with the following different fracture orientations: horizontal, at 20°, at 45°, at 70°, vertical (Fig. 7.2.1 for the receivers at the surface, Fig. 7.2.2 for those at the depth of 4000m):

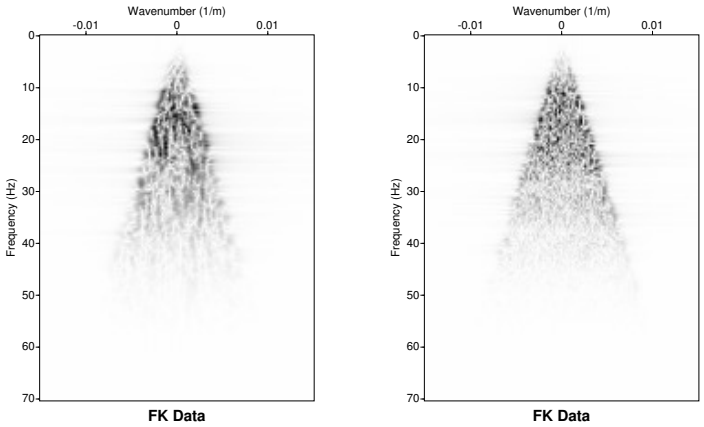

(A)

(B)

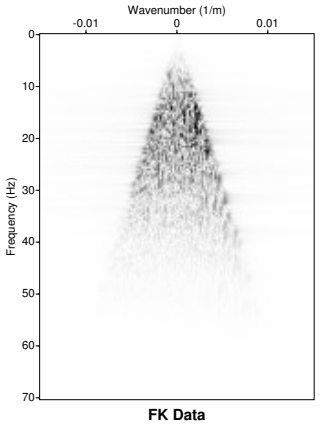

(C)

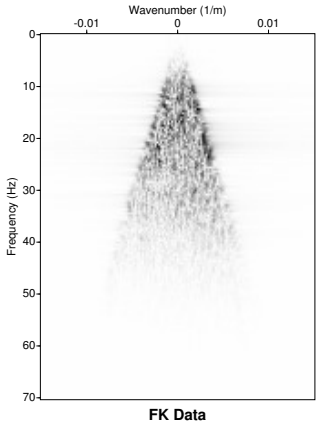

(D)

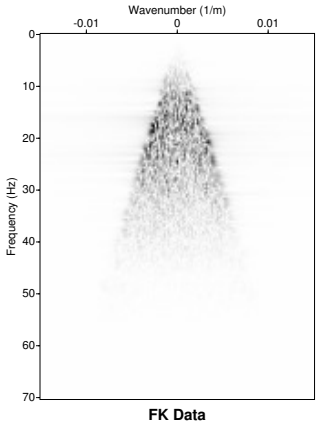

(E)

FIGURE 7.2.1. F-k plots for the models with a hundred 100m long fractures. Each plot corresponds to a different fractures orientation. From left to right: horizontal fractures (Fig. 7.2.1a); 20° inclined fractures (Fig. 7.2.1b); 45° inclined fractures (Fig. 7.2.1c); 70° inclined fractures (Fig. 7.2.1d); vertical fractures (Fig. 7.2.1e). Results related to the receivers at the surface.

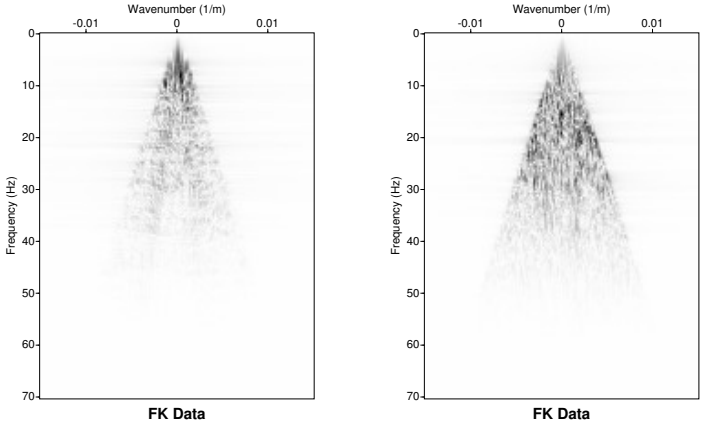

(A)

(B)

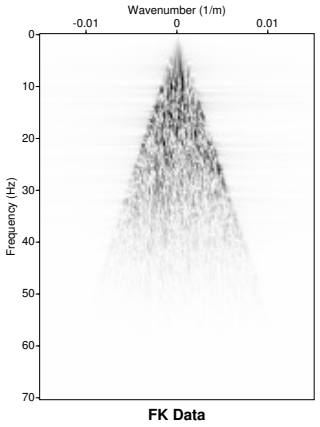

(C)

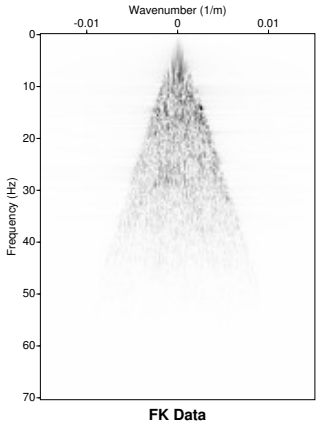

(D)

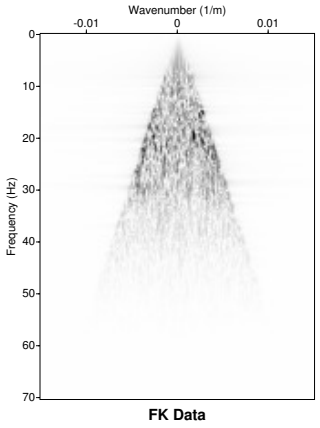

(E)

FIGURE 7.2.2. F-k plots for the models with a hundred 100m long fractures. Each plot corresponds to a different fractures orientation. From left to right: horizontal fractures (Fig. 7.2.2a); 20° inclined fractures (Fig. 7.2.2b); 45° inclined fractures (Fig. 7.2.2c); 70° inclined fractures (Fig. 7.2.2d); vertical fractures (Fig. 7.2.2e). Results related to the receivers at the depth of 4000m.

In Fig. 7.2.1 the imprint of the fractures orientation is represented by the different energy density distribution: in the case of horizontal fractures (Fig. 7.2.1a) the reflected energy density has the highest amplitude and it is evenly distributed in the f-k region; when inclined fractures are present (Fig. 6.3b, Fig. 6.3c and Fig. 6.3d), the overall energy density diminishes but local peaks are present that indicate a preferential direction of approach of the reflected waves crossing the array at the surface (due to the fracture orientation). Less information is contained in the results of the f-k analysis applied to the transmitted wavefield in Fig. 7.2.2 .

7.3. Fracture length and orientation effect

Models with one hundred horizontal and vertical fractures have been created for different fracture lengths:

- fracture length $\sim$ wavelength (= 250 m)
- fracture length $\sim 1/2$ wavelength (= 100 m)
- fracture length $\sim 1/5$ wavelength (= 50 m)
- fracture length $\sim 1/10$ wavelength (= 25 m)

First the results relative to horizontal fractures models are presented. The wiggle traces referred to the offsets 0, -1275m and -2500m are shown in Fig. 7.3.1 (for the receivers at the surface) and in Fig. 7.3.2 (for the receivers at a depth of 4000m):

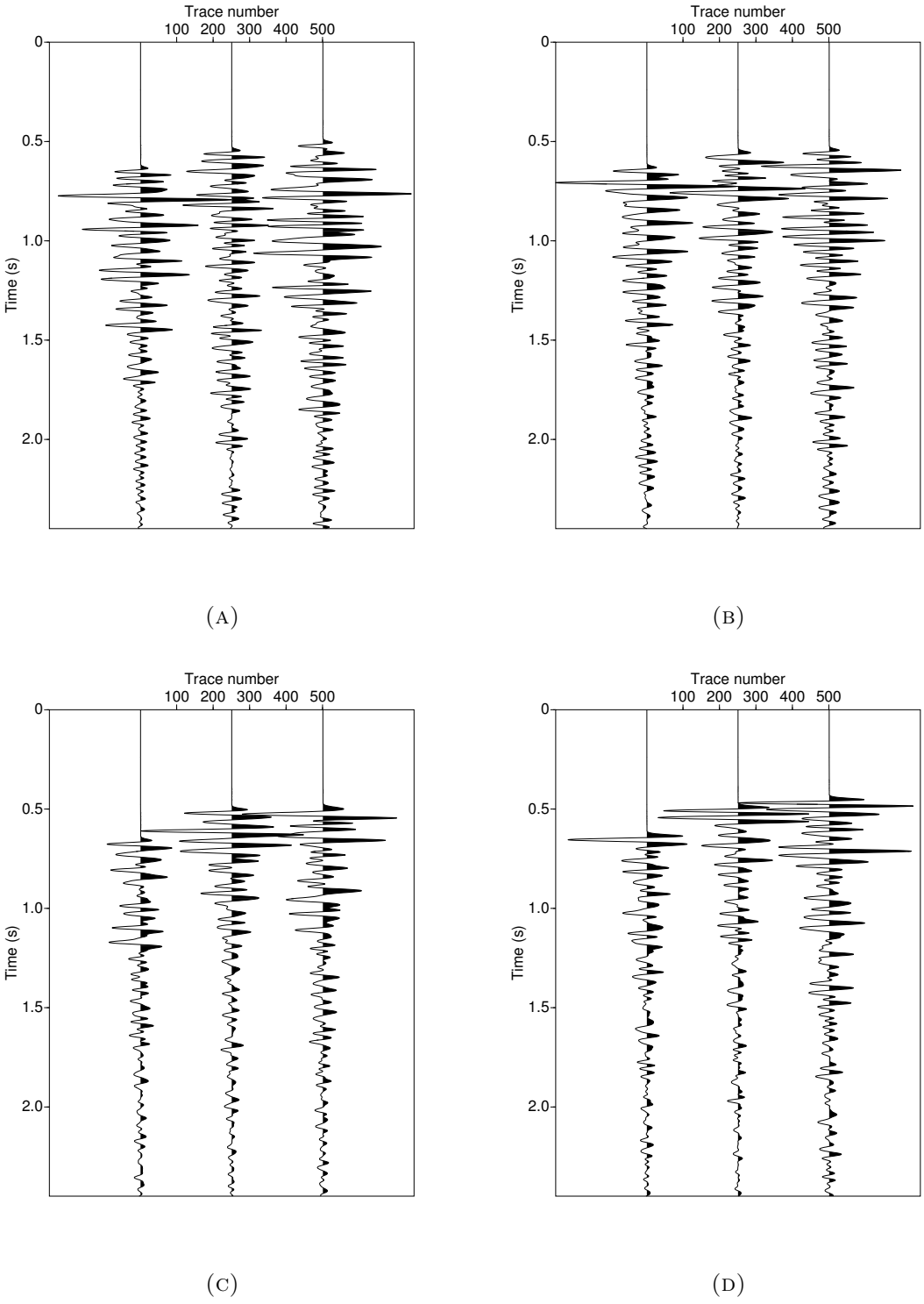

(A) (B)

(C) (D)

FIGURE 7.3.1. Wiggle traces for the receivers at the surface for different fracture lengths (one hundred horizontal fractures): f.l. = 25m (Fig. 7.3.1a); f.l.=50m (Fig. 7.3.1b); f.l.=100m (Fig. 7.3.1c); f.l.=250m (Fig. 7.3.1d). As the fracture length increases, longer coda waves are produced (scattering is more and more significant).

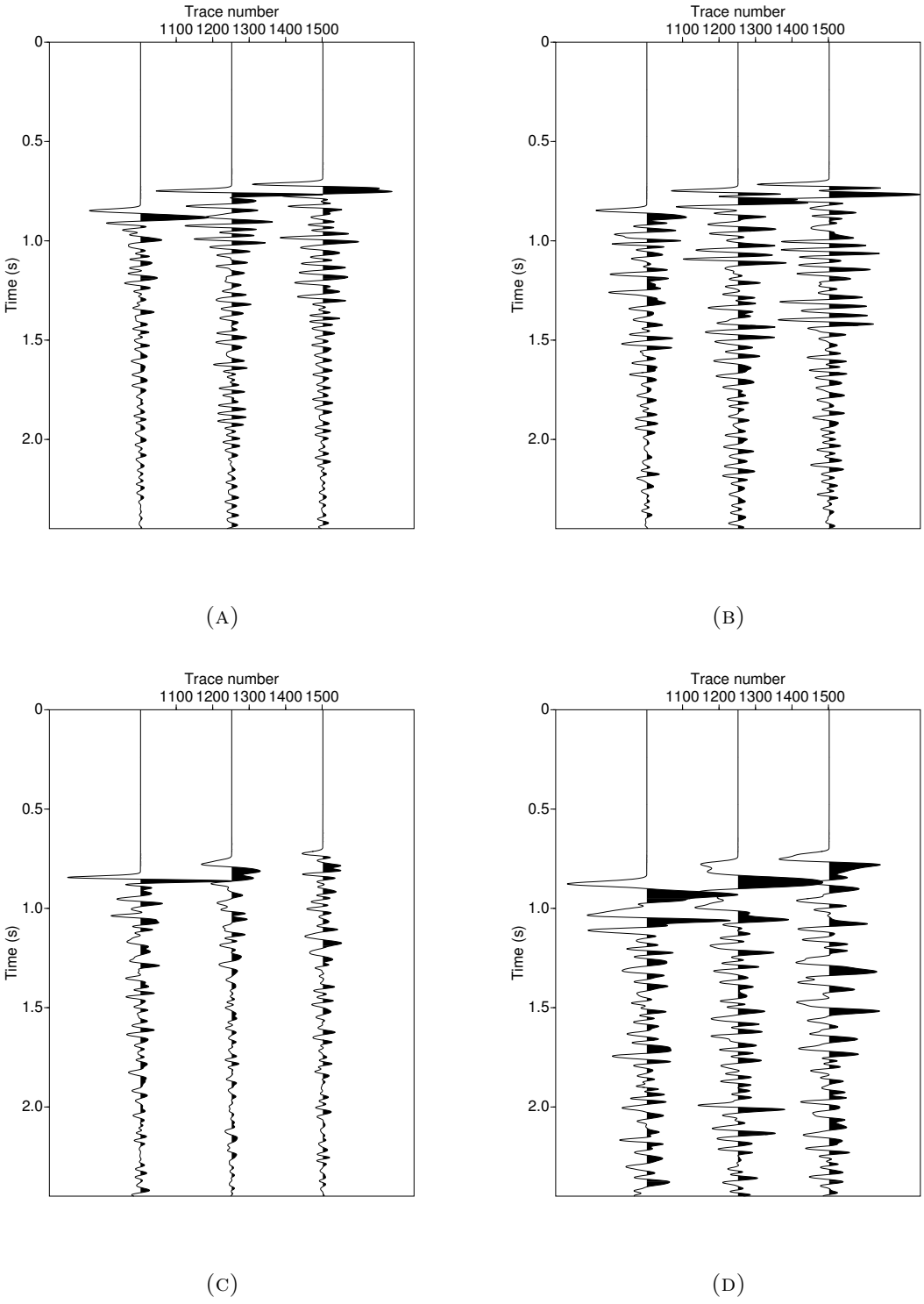

(A) (B)

(C) (D)

FIGURE 7.3.2. Wiggle traces for the receivers at the depth of 4000m for different fracture lengths (one hundred horizontal fractures): f.l. = 25m (Fig. 7.3.2a); f.l.=50m (Fig. 7.3.2b); f.l.=100m (Fig. 7.3.2c); f.l.=250m (Fig. 7.3.2d). It seems there is a strong attenuation for 100m long fractures; moreover, when the fractures length approaches the wavelength, the amplitude of the signal is very high even at late times.

The effect of the fractures is basically revealed by the complex traces, that now include all the waves diffracted and/or scattered from the fractures and the coda waves. This time, the use of the term "*coda waves*", defined as ringing-type and non-coherent signals recorded after the direct arrival resulting from multiple scattering, is justified. Fig. 7.3.1 shows that for fractures 25m long (Fig. 7.3.1a) the coda waves are shorter; as the fracture length increases, longer coda waves are produced. Fig. 7.3.2 shows less clear results: it seems there is a strong attenuation for 100m long fractures (Fig. 7.3.2c); moreover, when the fractures length approaches the wavelength (Fig. 7.3.2d), the amplitude of the signal is very high even at late times and the frequency seems to be lower if compared to the other three models.

The results in the frequency domain are shown in Fig. 7.3.3 and Fig. 7.3.4 for the receivers at the surface and the receivers at 4000m respectively:

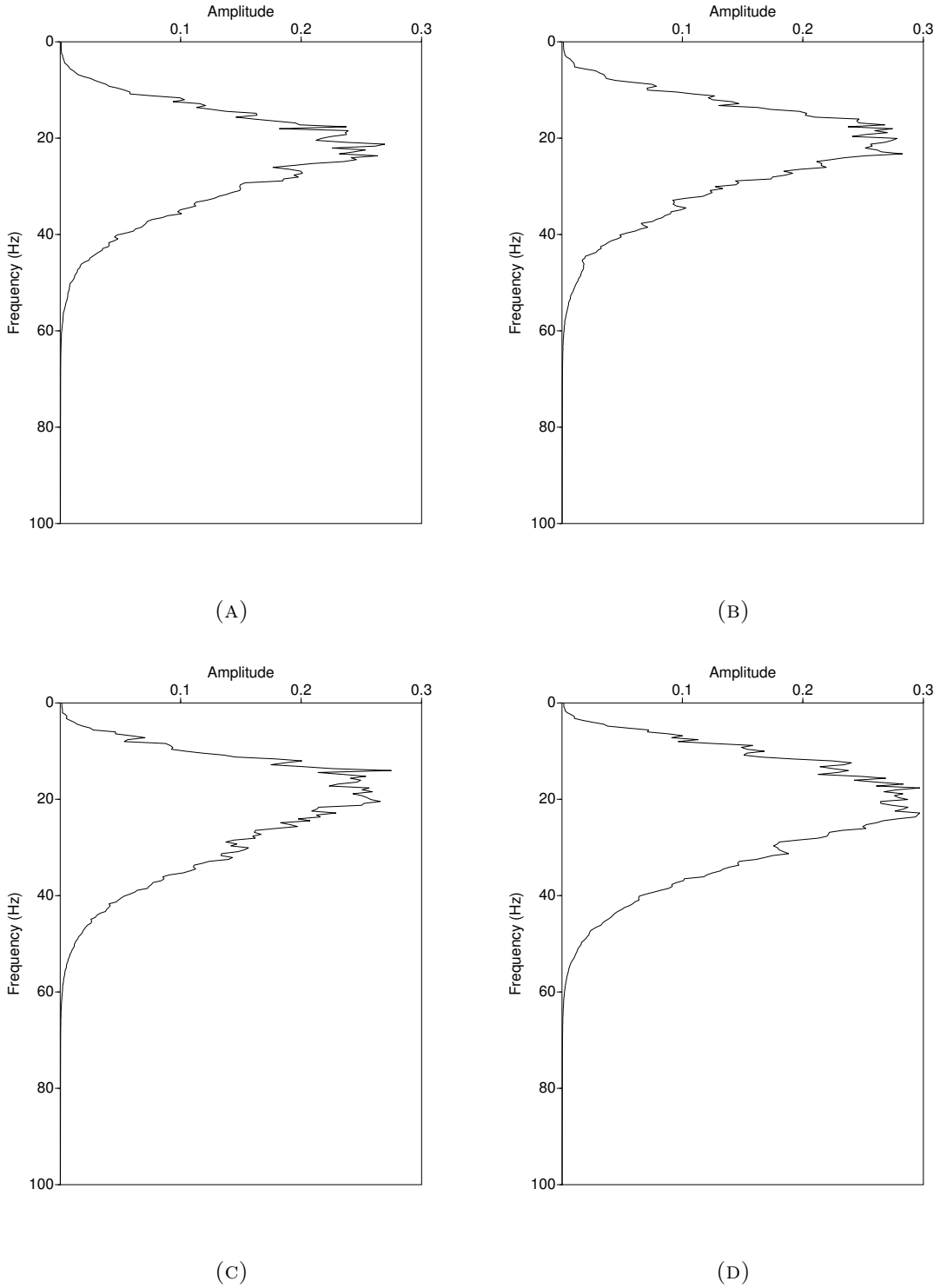

FIGURE 7.3.3. Amplitude spectra for the models with one hundred horizontal fractures but with different fracture lengths. From the left to the right: f.l. = 25m (Fig. 7.3.3a); f.l.=50m (Fig. 7.3.3b); f.l.=100m (Fig. 7.3.3c); f.l.=250m (Fig. 7.3.3d). Results related to the receivers at the surface. It is visible a clear increase in the peak amplitude when the fractures length approaches the wavelength. Moreover, as the fractures length increases, a shift of the peak frequency towards higher frequencies can be noticed.

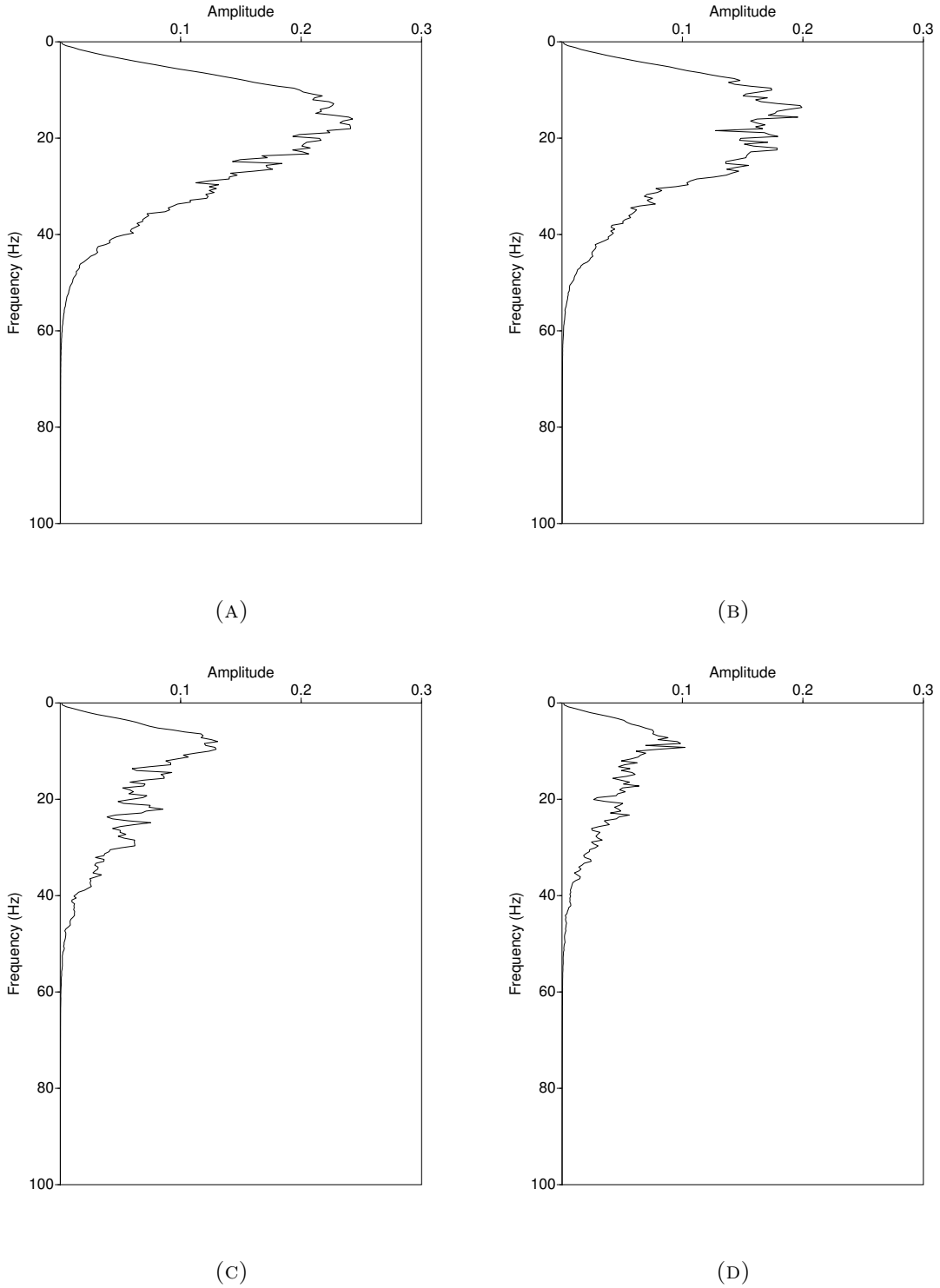

FIGURE 7.3.4. Amplitude spectra for the models with one hundred horizontal fractures but with different fracture lengths. From the left to the right: f.l. = 25m (Fig. 7.3.4a); f.l.=50m (Fig. 7.3.4b); f.l.=100m (Fig. 7.3.4c); f.l.=250m (Fig. 7.3.4d). Results related to the receivers at the depth of 4000m. Net decrease in the peak amplitude as the fractures length increases and shift of the peak amplitude towards lower frequencies this time.

Fig. 7.3.3 shows an increase in the peak amplitude when the fractures length approaches the wavelength (Fig. 7.3.3d), which could be explained considering that a higher seismic energy is back-scattered towards the surface (maybe the contribution of the reflected wave to the overall spectrum starts to increase). Moreover, as the fractures length increases, a shift of the peak frequency towards higher frequencies can be noticed. On the other hand, Fig. 7.3.4 shows a net decrease in the peak amplitude as the fractures length increases, which can be explained with a higher attenuation of the transmitted waves crossing longer fractures; in addition, it can be noticed a shift of the peak amplitude towards lower frequencies this time. Moreover, the higher frequencies seem to be much more affected by the presence of longer fractures, as their amplitude in the spectrum is strongly reduced. Eventually, it is possible to notice that in Fig. 7.3.4c and Fig. 7.3.4d there is also a decrease in the maximum frequency (from 60 Hz to 57Hz and 55Hz respectively).

The same results are now presented for the vertical fractures models. The wiggle traces referred to the offsets 0, -1275m and -2500m are shown in Fig. 7.3.5 (for the receivers at the surface) and in Fig. 7.3.6 (for the receivers at a depth of 4000m):

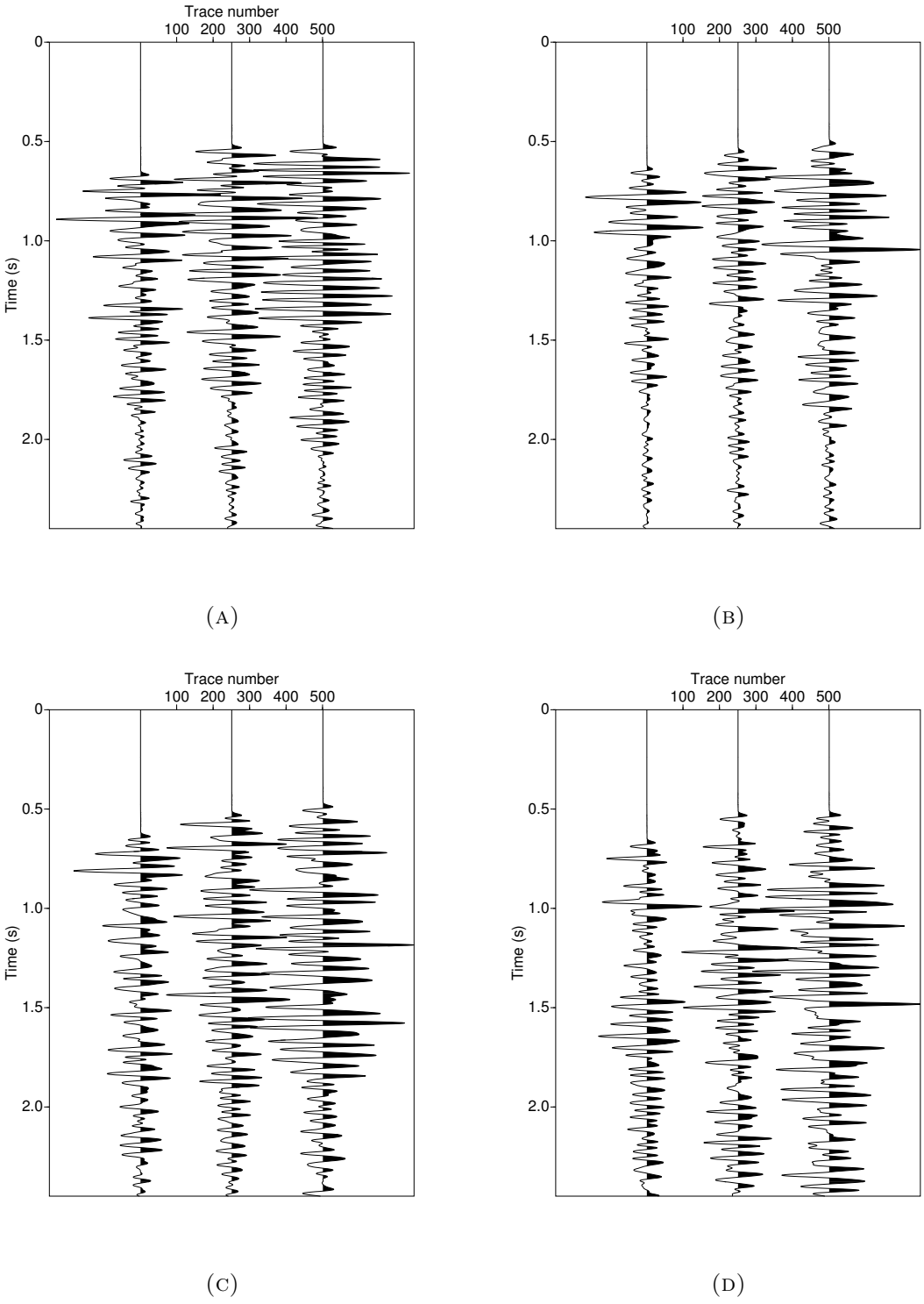

(A) (B)

(C) (D)

FIGURE 7.3.5. Wiggle traces for the receivers at the surface for different fracture lengths (one hundred vertical fractures): f.l. = 25m (Fig. 7.3.5a); f.l.=50m (Fig. 7.3.5b); f.l.=100m (Fig. 7.3.5c); f.l.=250m (Fig. 7.3.5d).

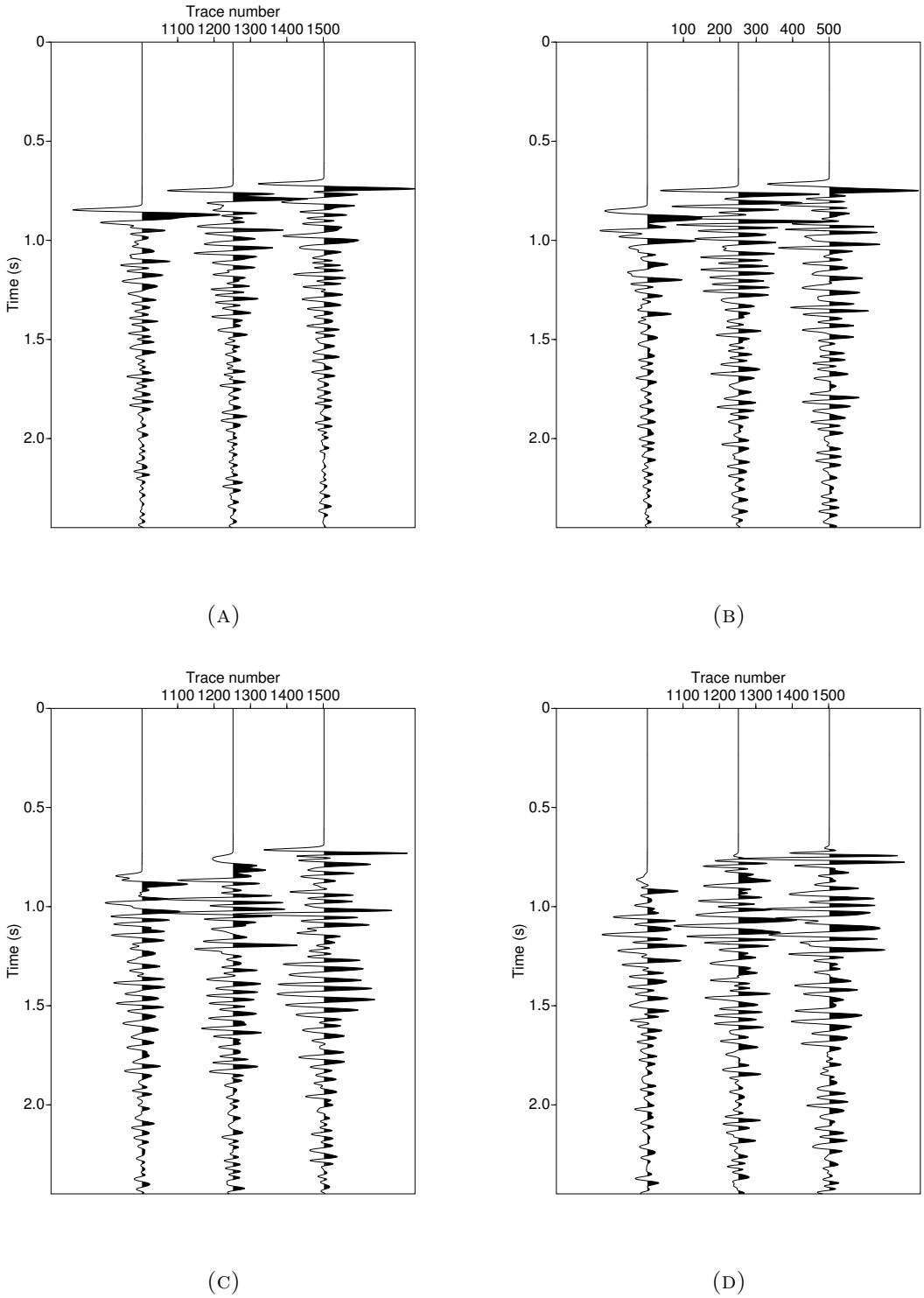

(A) (B)

(C) (D)

FIGURE 7.3.6. Wiggle traces for the receivers at the depth of 4000m for different fracture lengths (one hundred vertical fractures): f.l. = 25m (Fig. 7.3.6a); f.l.=50m (Fig. 7.3.6b); f.l.=100m (Fig. 7.3.6c); f.l.=250m (Fig. 7.3.7d).

If compared to Fig. 7.3.1 , Fig. 7.3.5 shows different outputs: coda waves appear at very late times or they do not appear at all as the fracture length increases (Fig.7.3.5c and Fig. 7.3.5d); this could be simply related to the selected time window (which ends at 2.5s). On the other hand, for the transmitted wavefield, coda waves are visible already for a fracture length of 1/10 of the wavelength (Fig. 7.3.6a) and their amplitude increases as the fracture length increases (Fig.7.3.6). Note the strong attenuation of the transmitted wavefield in Fig. 7.3.6c and Fig. 7.3.6d.

The comparison has been made in the frequency domain as well. The results are shown in Fig. 7.3.7 and Fig. 7.3.8 for the receivers at the surface and the receivers at 4000m respectively:

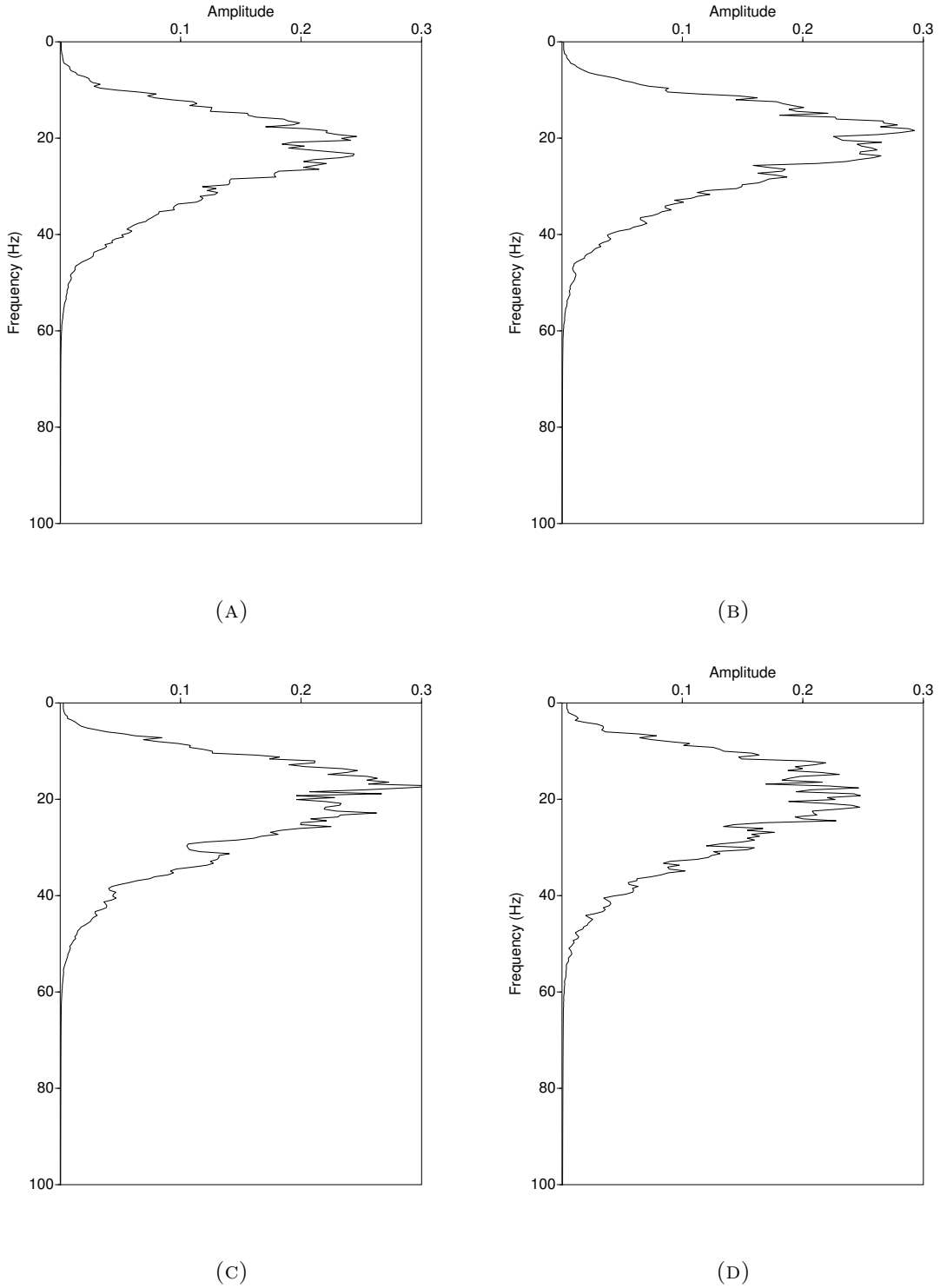

(A) (B)

(C) (D)

FIGURE 7.3.7. Amplitude spectra for the models with one hundred vertical fractures but with different fracture lengths. From the left to the right: f.l. = 25m (Fig. 7.3.7a); f.l.=50m (Fig. 7.3.7b); f.l.=100m (Fig. 7.3.7c); f.l.=250m (Fig. 7.3.7d). Results related to the receivers at the surface. It can be seen a shift of the peak frequency towards lower frequencies as fractures length increases.

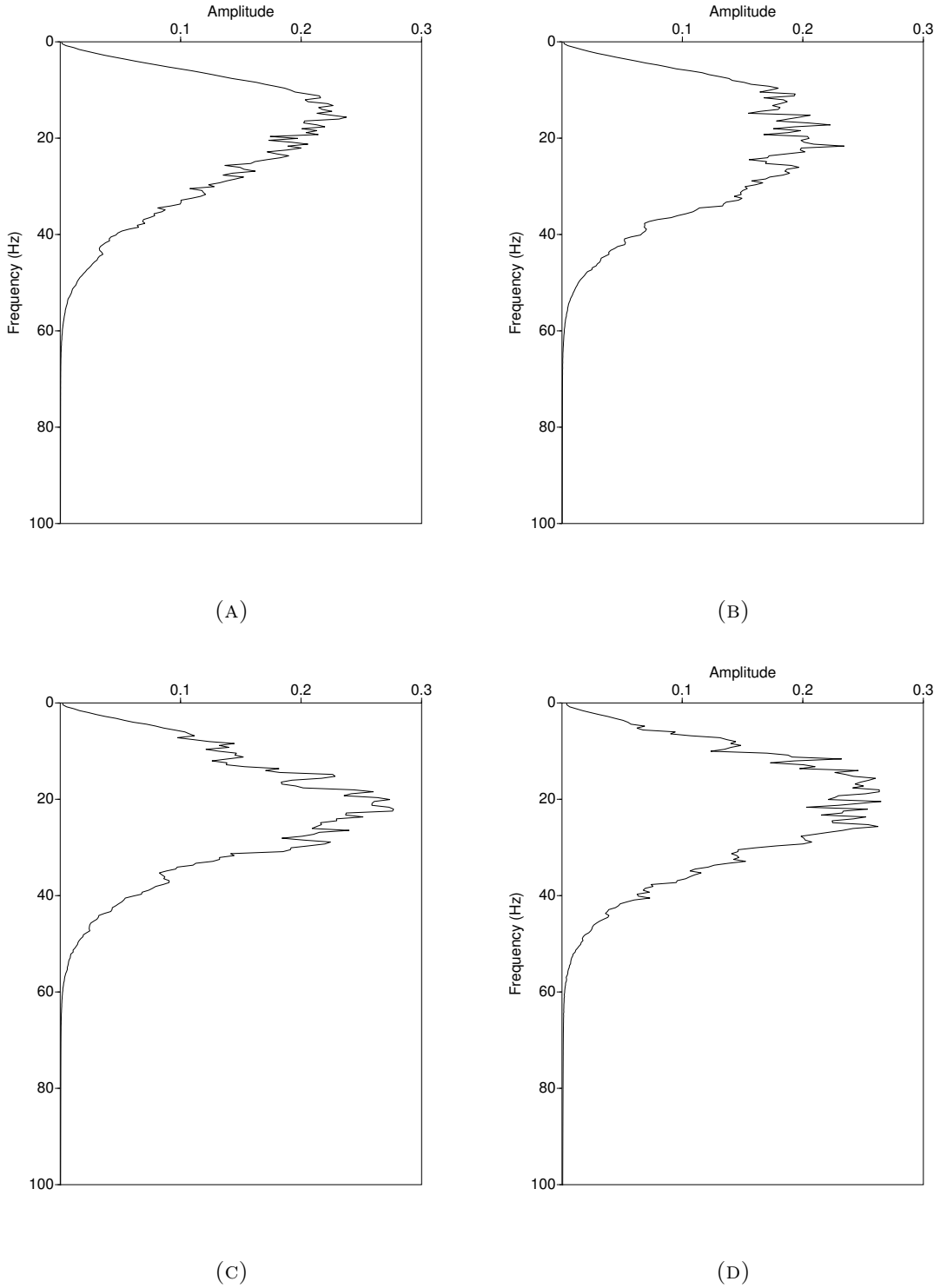

(A) (B)

(C) (D)

FIGURE 7.3.8. Amplitude spectra for the models with one hundred vertical fractures but with different fracture lengths. From the left to the right: f.l. = 25m (Fig. 7.3.8a); f.l.=50m (Fig. 7.3.8b); f.l.=100m (Fig. 7.3.8c); f.l.=250m (Fig. 7.3.8d). Results related to the receivers at the depth of 4000m. It can be seen a shift of the peak frequency towards higher frequencies.

If compared to the model with one hundred horizontal case, the opposite trend occurs: for the reflected wavefield there is a shift of the peak frequency towards lower frequencies as fractures length increase (Fig. 7.3.7), while for the transmitted wavefield there is a shift towards higher frequencies (7.3.8).

7.4. Fractures density effect

The effect of the fracture density on the seismic signature has been tested for horizontal fractures that have a length of about half wavelength (100m). The seismic response of two, three, five, ten, twenty, fifty, seventy and one hundred fractures has been simulated. Here only the results for the models with two, ten, fifty and one hundred fractures will be presented.

The wiggle traces referred to the offsets 0, -1275m and -2500m are shown in Fig. 7.4.1(for the receivers at the surface) and in Fig. 7.4.2(for the receivers at a depth of 4000m):

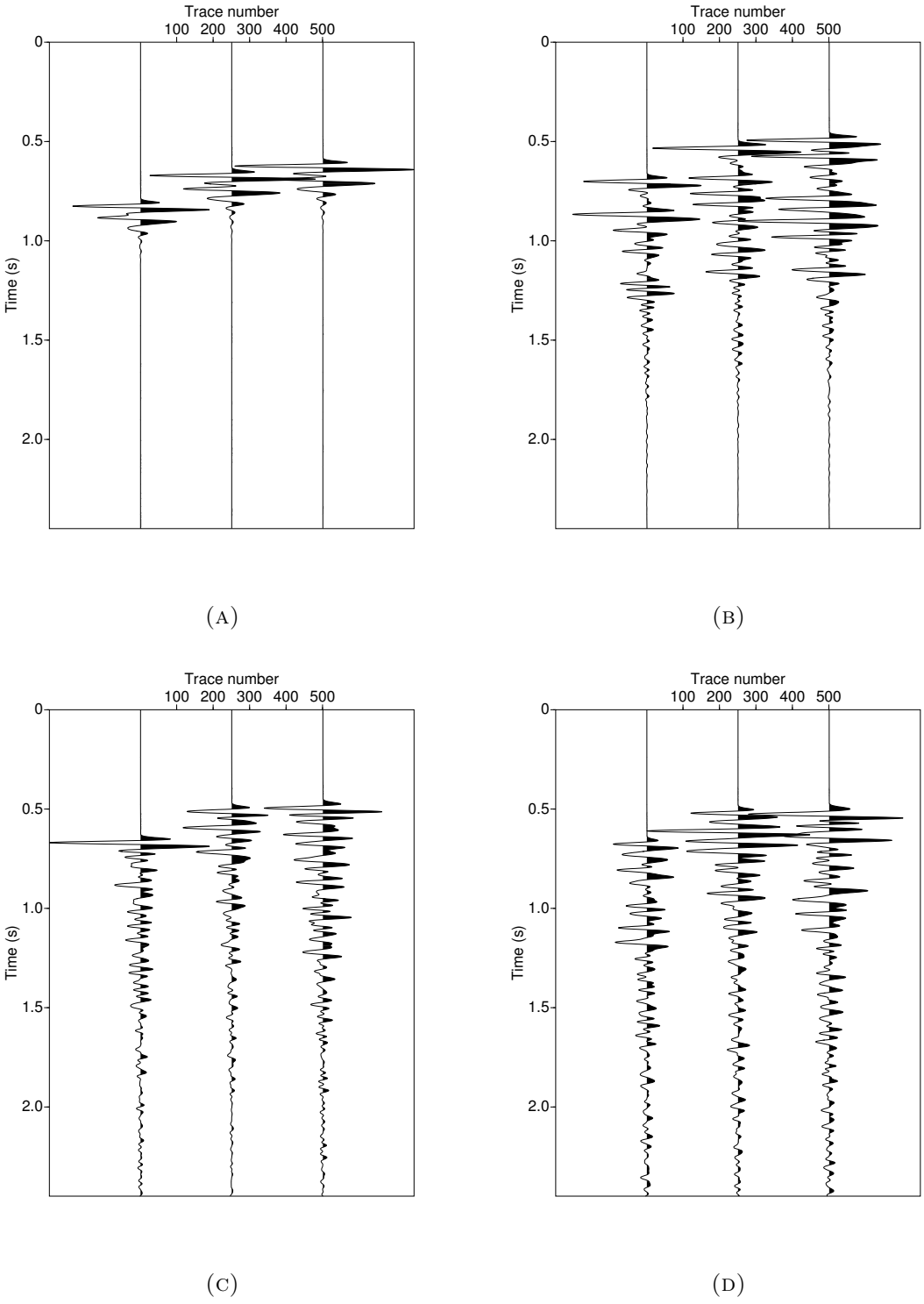

(A) (B)

(C) (D)

FIGURE 7.4.1. Wiggle traces for the receivers at the surface for different fracture densities (100m long horizontal fractures): two fractures (Fig. 7.4.1a); ten fractures (Fig. 7.4.1b); fifty fractures (Fig. 7.4.1c); one hundred fractures (Fig. 7.4.1d). The seismic signal is more and more complicated as the fractures number increases, which results in longer coda waves as well.

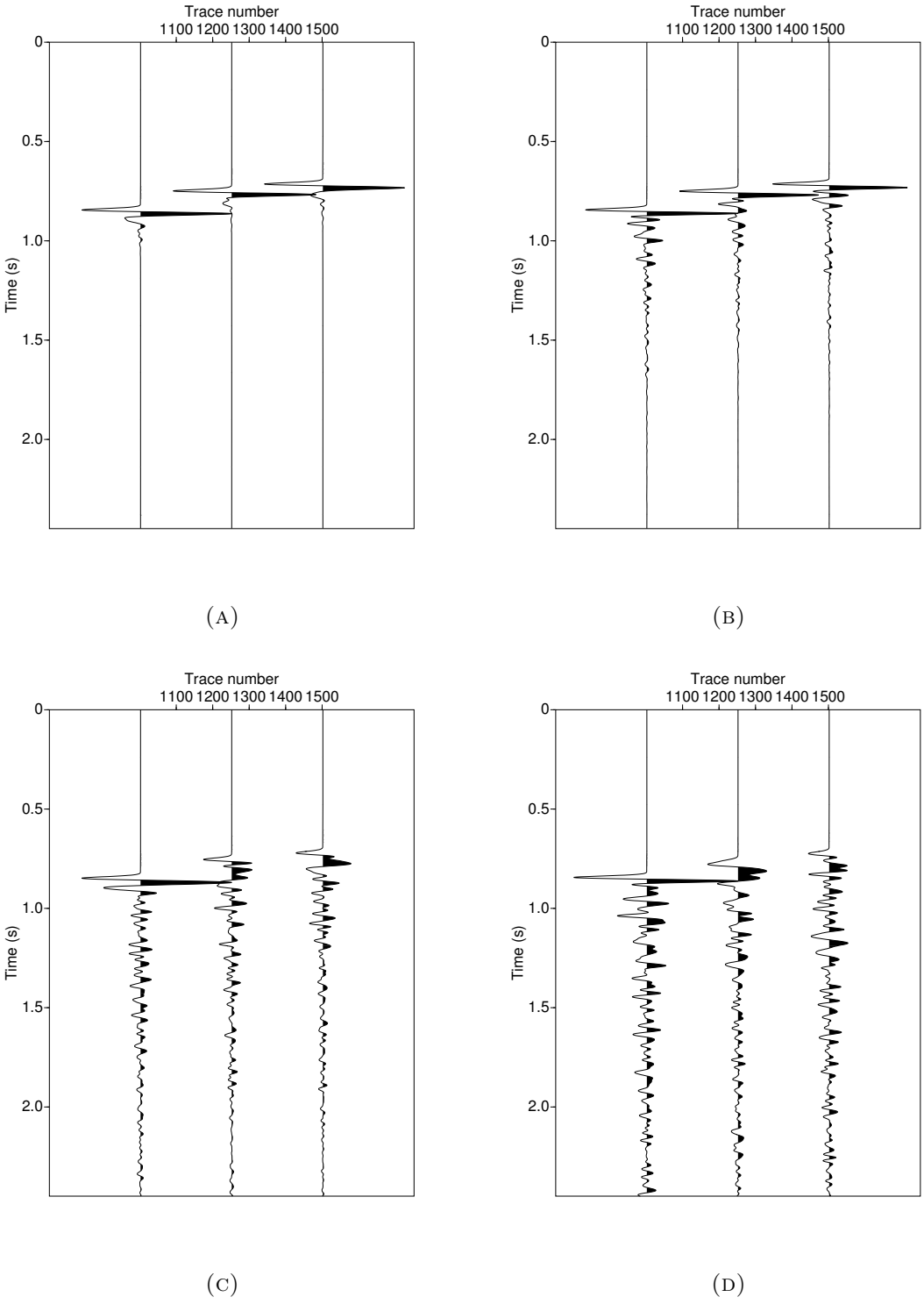

(A) (B)

(C) (D)

FIGURE 7.4.2. Wiggle traces for the receivers at the depth of 4000m for different fracture densities (100m long horizontal fractures): two fractures (Fig. 7.4.2a); ten fractures (Fig. 7.4.2b); fifty fractures (Fig. 7.4.2c); one hundred fractures (Fig. 7.4.2d). It is clearly visible the attenuation of the incident field due to the high fractures number and the longer coda waves as in the previous case.

Fig. 7.4.1 shows that the seismic signal is more and more complicated as the fractures number increases, which results in longer coda waves as well. In Fig. 7.4.2 it is clearly visible the attenuation of the incident field due to the high fractures number (Fig. 7.4.2c and Fig. 7.4.2d) and the longer coda waves as in the previous case.

In Fig. 7.4.3 and Fig. 7.4.4 it is shown the total recorded pressure wavefield for the three different models respectively for the receivers at the surface and the receivers at 4000m:

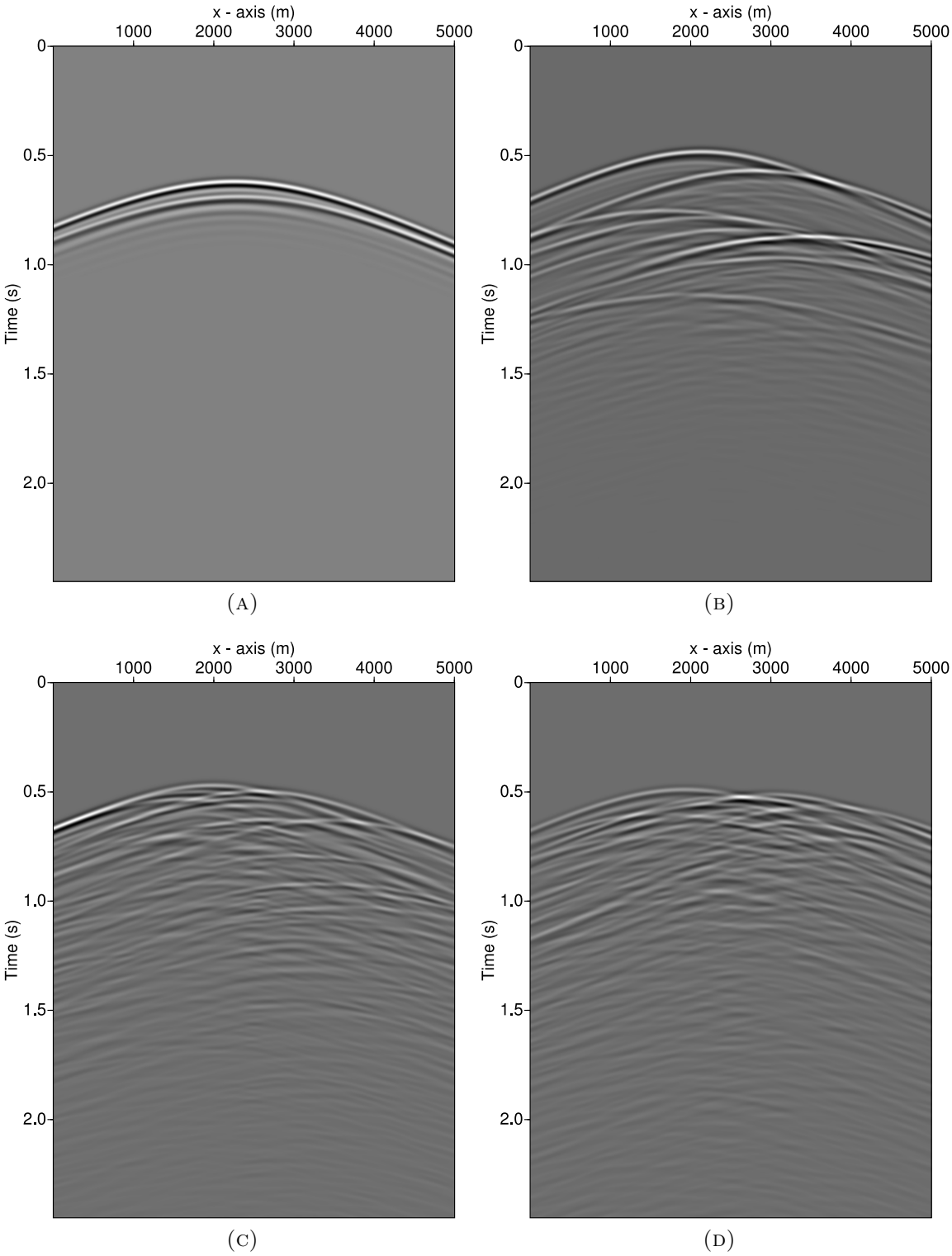

FIGURE 7.4.3. Pressure wavefield recorded at the receivers on the surface for different fractures densities (100m long horizontal fractures): two fractures (Fig. 7.4.3a); ten fractures (Fig. 7.4.3b); fifty fractures (Fig. 7.4.3c); one hundred fractures (Fig. 7.4.3d). The pressure wavefield becomes more and more complicate as the fractures number increases.

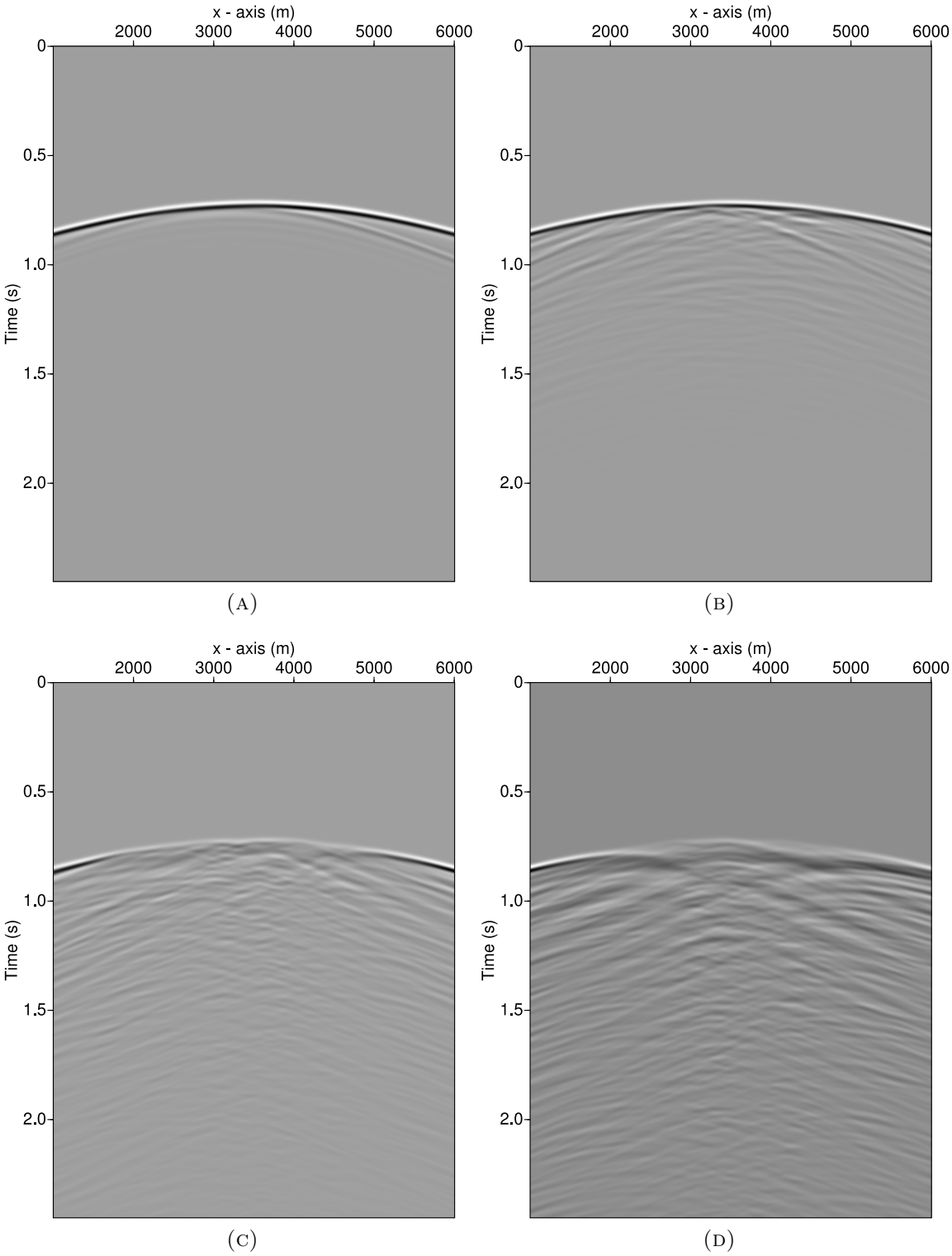

FIGURE 7.4.4. Pressure wavefield recorded at the receivers at the depth of 4000m for different fractures densities (100m long horizontal fractures): two fractures (Fig. 7.4.4a); ten fractures (Fig. 7.4.4b); fifty fractures (Fig. 7.4.4c); one hundred fractures (Fig. 7.4.4d). The attenuation of the transmitted wavefield clearly increases as the fractures number overcomes the number of ten.

Fig. 7.4.3 clearly shows the influence of the fractures on the seismic signature, which becomes more and more complicated as the fractures number increases (note the high number of diffraction hyperbolae that interfere with each other). The same occurs in Fig. 7.4.4, where the attenuation of the transmitted wavefield clearly increases as the fractures number overcomes the number of ten.

The effect of the fractures number variation has been tested in the frequency domain as well by comparing the amplitude spectra for the four different models. The results are shown in Fig. 7.4.5 and Fig. 7.4.6 for the receivers at the surface and the receivers at 4000m respectively:

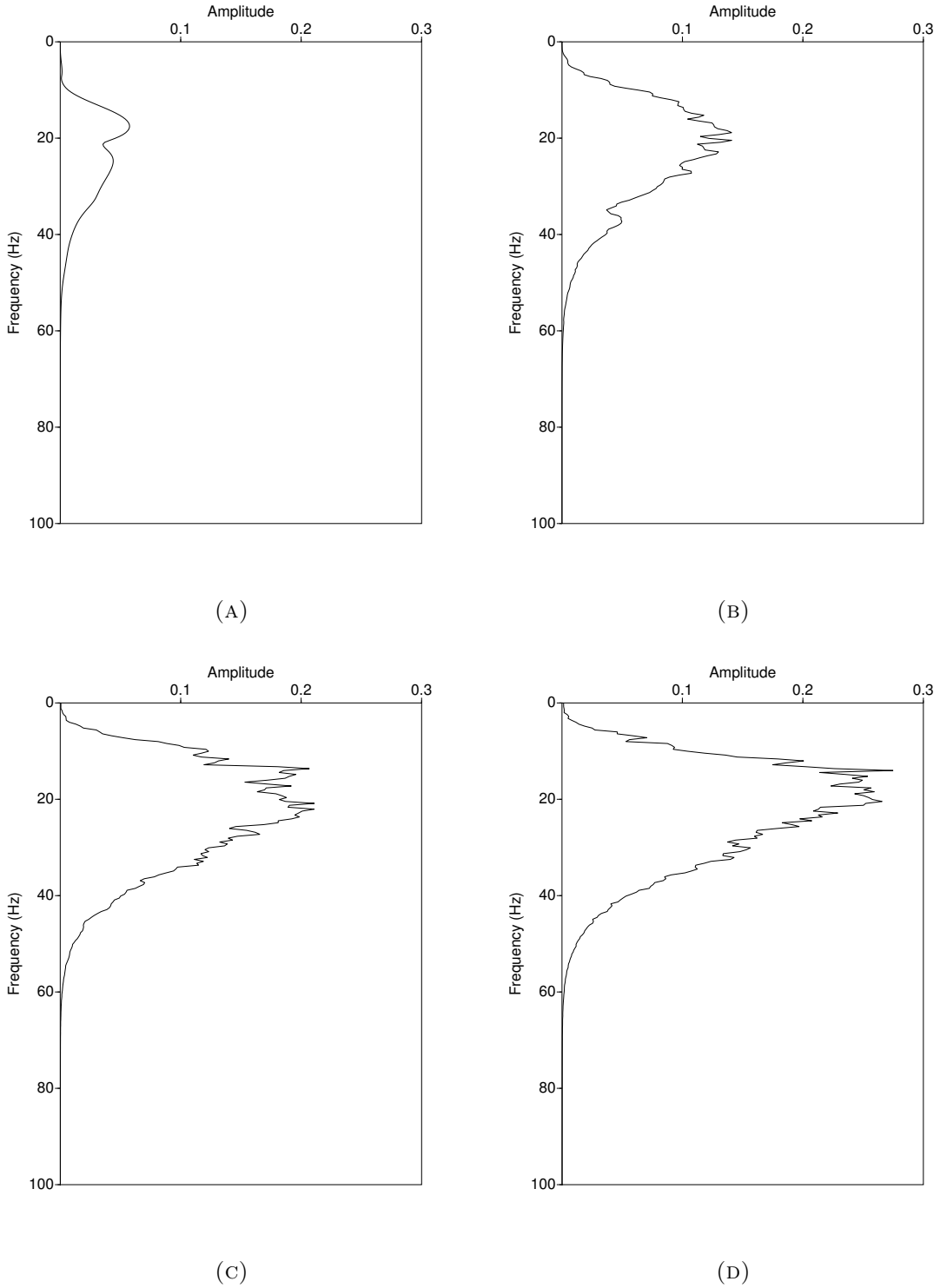

FIGURE 7.4.5. Amplitude spectra for the models with 100m long horizontal fractures but with different fracture densities. From the left to the right: two fractures (Fig. 7.4.5a); ten fractures (Fig. 7.4.5b); fifty fractures (Fig. 7.4.5c); one hundred fractures (Fig. 7.4.5d). Results related to the receivers at the surface. The amplitude of the spectra increases as the fractures number increases.

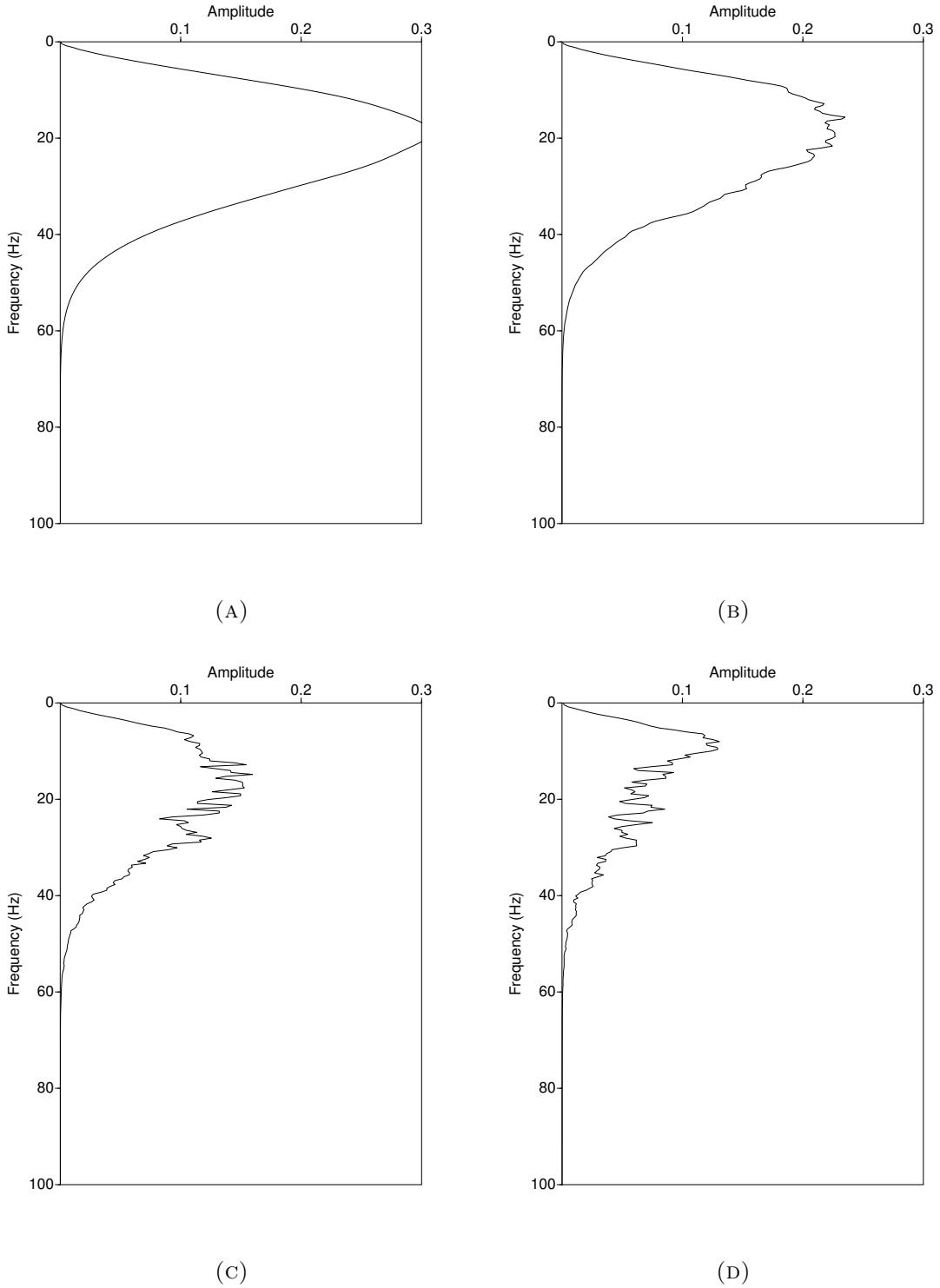

FIGURE 7.4.6. Amplitude spectra for the models with 100m long horizontal fractures but with different fracture densities. From the left to the right: two fractures (Fig. 7.4.6a); ten fractures (Fig. 7.4.6b); fifty fractures (Fig. 7.4.6c); one hundred fractures (Fig. 7.4.6d). Results related to the receivers at the depth of 4000m. As the fractures become more numerous, the amplitude of the spectrum clearly decreases.

In Fig. 7.4.5 the amplitude of the spectra increases as the fractures number increases (due to the contributions from more fractures). On the contrary, for the transmitted field (Fig. 7.4.6) the trend is opposite: as the fractures become more numerous, the amplitude of the spectrum clearly decreases, due to the stronger attenuation imposed by a higher number of fractures. Moreover, it seems that the higher frequencies are more attenuated than the lower ones (Fig. 7.4.6c and Fig. 7.4.6d). Eventually, in Fig. 7.4.6d it is possible to notice a decrease in the maximum frequency as well (from 60 Hz to about 55 Hz).

7.5. Layering effect

In this section it will be described the effect of a fractured layer in a otherwise homogeneous medium. The three-layers model that has been created is described in Chapter 2 (see Fig. 4.2). Only the middle layer contains one hundred horizontal fractures and it is characterized by a density and a velocity that differ from the surrounding medium. The outputs referred to the layered model with the fractured layer have been compared to those referred to the layered model which does not contain any fractures. Fig. 7.5.1a-b shows the results related to the receivers at the surface: it can be noticed that the reflection from the top of the layer is completely disrupted by the presence of the diffraction hyperbolae generated by the fractures inside the layer (Fig. 7.5.1b). On the other hand, the reflection from the bottom of the layer is still visible and it seems not to be affected by the presence of fractures. Fig. 7.5.1c-d shows the results for the receivers at 4000m: the direct field which reaches the top of the fractured layer is severely disrupted by the presence of the fractures (Fig. 7.5.1d) but it is somehow "reconstructed" by the several diffraction hyperbolae produced by the fractures. On the contrary, the wavefield transmitted across the bottom of the layer is not visible at all.

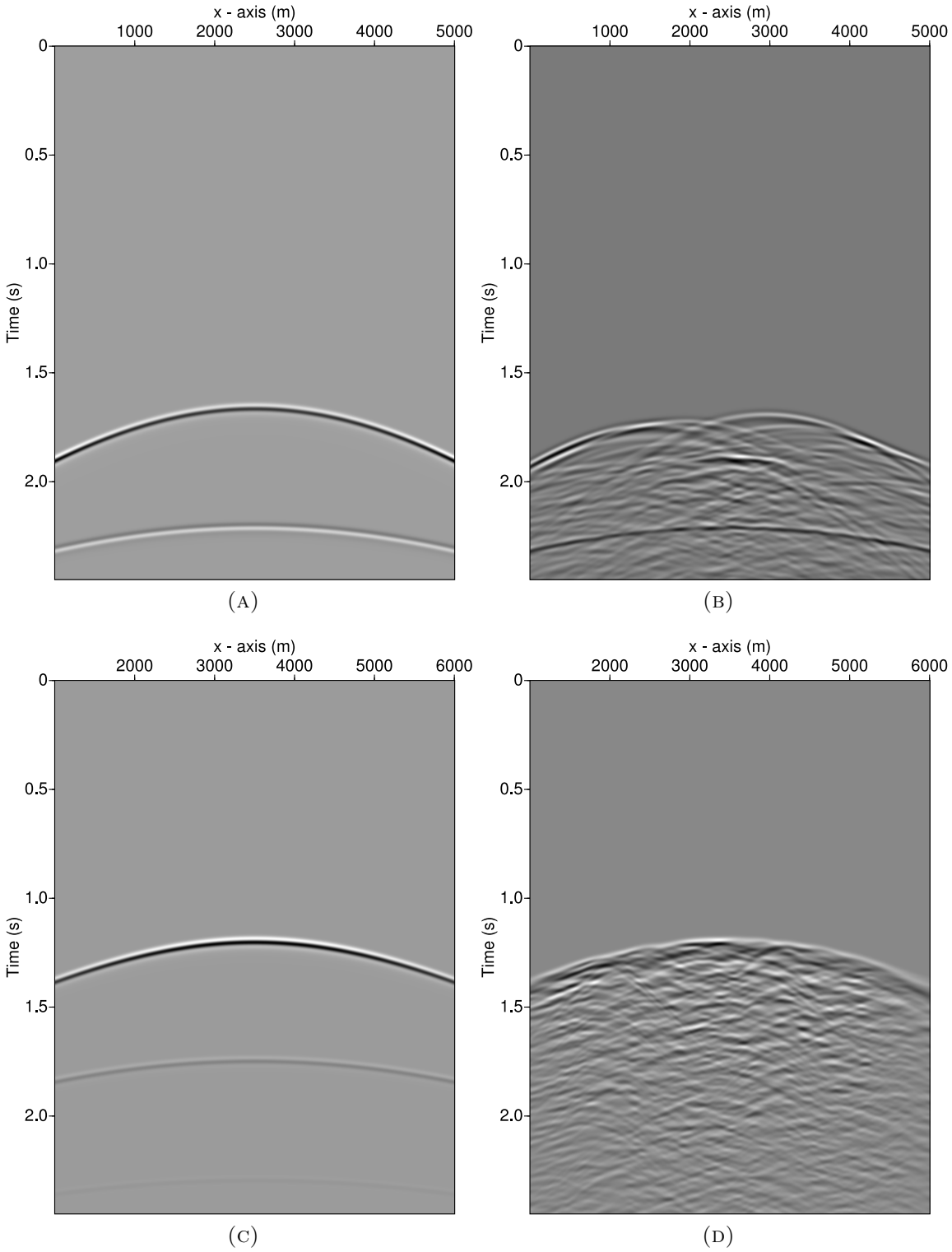

FIGURE 7.5.1. Comparison between the pressure wavefield recorded in the layered medium without fractures (Fig. 7.5.1a-c) and the layered medium with the one hundred fractures in the middle layer (Fig. 7.5.1b-d). The reflection from the top of the layer is completely disrupted by the presence of the fractures inside the layer. On the other hand, the reflection from the bottom of the layer is still visible. The direct field reaching the top of the fractured layer is severely disrupted but it is somehow "reconstructed" by the diffraction hyperbolae. On the contrary, the wavefield transmitted across the bottom of the layer is not visible at all.

The comparison has been made in the frequency domain as well: for what concerns the wavefield recorded at the surface, the amplitude spectrum does not show a significant decrease in the peak amplitude (Fig.7.5.2a) if compared to the spectrum of the incident wavefield (7.5.2b). More significant is the difference in the peak amplitude between the spectrum of the wavefield transmitted across the fractured layer (Fig. 7.5.2d) and across the unfractured layer (Fig. 7.5.2c).

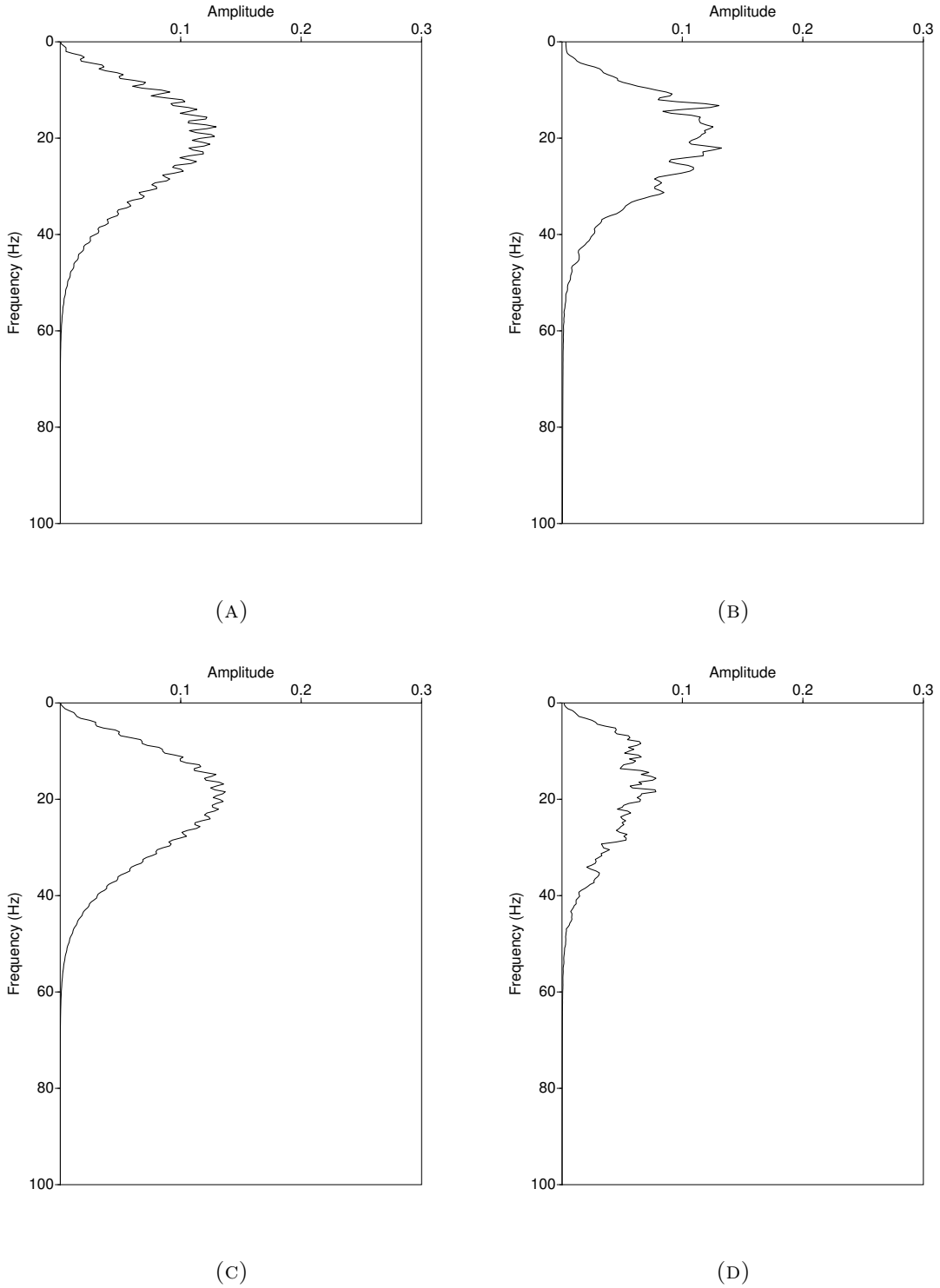

FIGURE 7.5.2. Comparison between the amplitude spectra referred to the layered medium without fractures (Fig. 7.5.2a-c) and the layered medium with the one hundred fractures in the middle layer (Fig. 7.5.2b-d). For what concerns the wavefield recorded at the surface, the amplitude spectrum does not show a significant decrease in the peak amplitude when compared to the spectrum of the incident wavefield. More relevant is the difference in the peak amplitude between the spectrum of the wavefield transmitted across the fractured layer and across the unfractured layer.

The layered model with the fractured layer has been also compared to the model which contains one hundred horizontal fractures as well, but these are randomly distributed in a otherwise homogeneous model. In Fig. 7.5.3 and Fig. 7.5.4 it is shown the total recorded pressure wavefield for the two models respectively for the receivers at the surface and the receivers at 4000m:

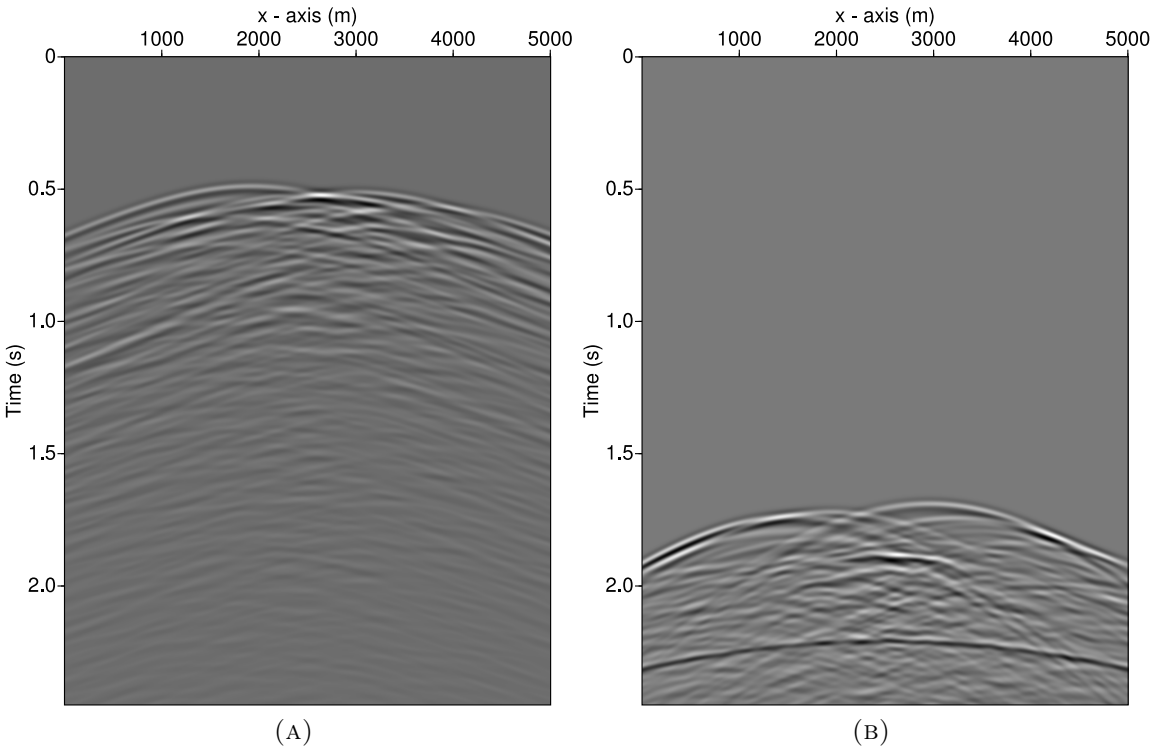

(A) (B)

FIGURE 7.5.3. Pressure wavefield recorded at the receivers at the surface for the no layered medium (Fig. 7.5.3a) and the layered medium (Fig. 7.5.3).

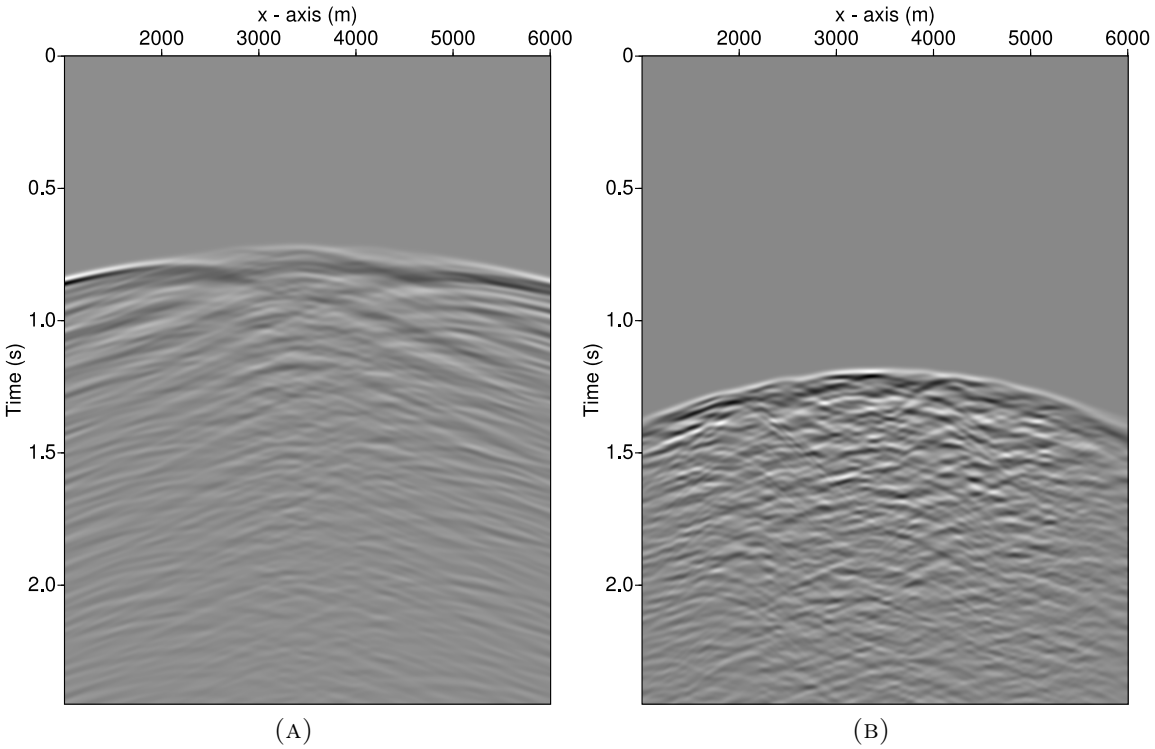

(A) (B)

FIGURE 7.5.4. Pressure wavefield recorded at the receivers at the depth of 4000m for the no layered medium (Fig. 7.5.4a) and the layered medium (Fig. 7.5.4b).

In Fig. 7.5.3 and Fig. 7.5.4b it can be noticed that the fractured layer determines a higher superposition of diffraction events due to the higher fractures density[1], which obviously yield a much more complex wavefield. Considering the frequency domain, Fig. 6.23 and Fig. 6.24 show the amplitude spectra for the two models respectively for the receivers at the surface and those at a depth of 4000m:

[1]Here meant not as the fractures number, since it is still one hundred, but as the ratio of the number of fractures to the area

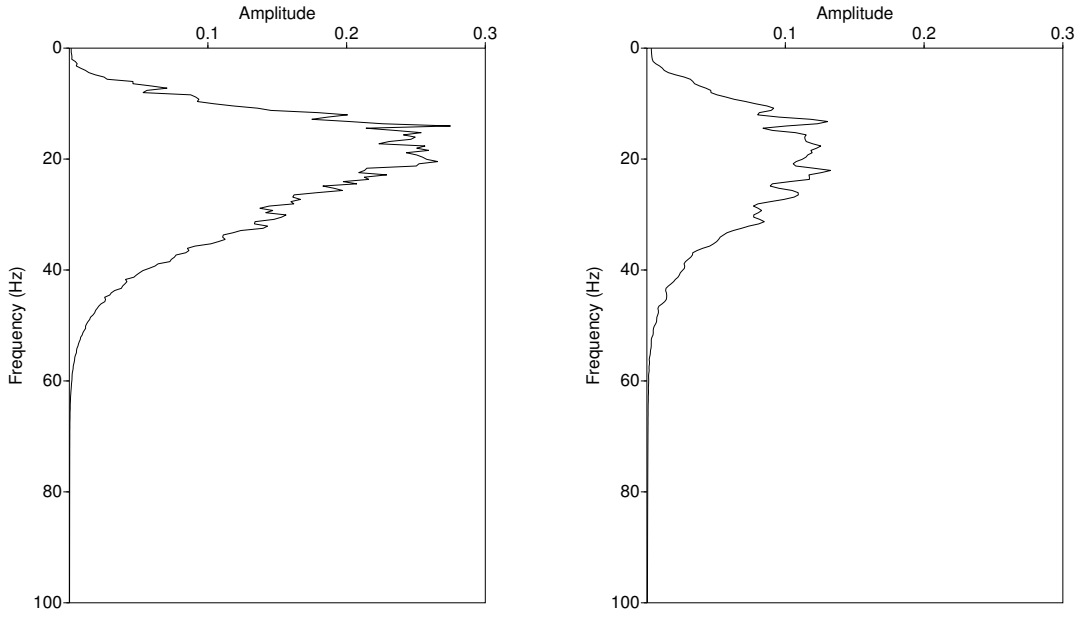

(A) (B)

FIGURE 7.5.5. Amplitude spectra for the no layered medium (Fig. 7.5.5a) and the layered medium (Fig. 7.5.5b). Results related to the receivers at the surface. The peak amplitude for the layered model is much lower than the unlayered model.

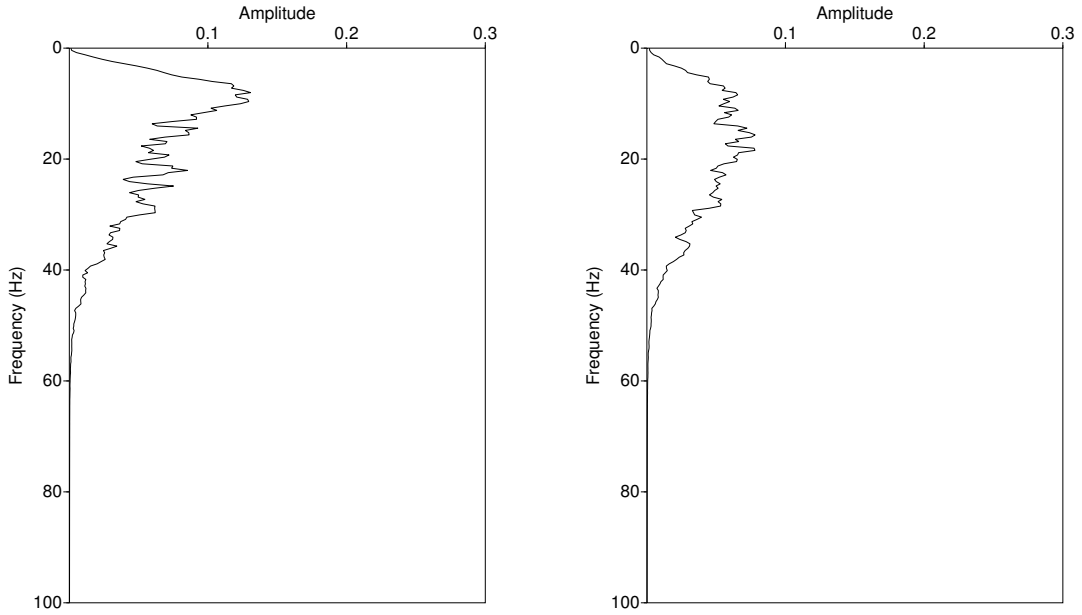

(A) (B)

FIGURE 7.5.6. Amplitude spectra for the no layered medium (Fig. 7.5.6a) and the layered medium (Fig. 7.5.6b). Results related to the receivers at the depth of 4000m. The spectrum for the case of the layered medium is more homogeneous and shows a higher peak frequency if compared to the no layered medium.

Fig. 6.23 shows that the introduction of the fractured layer yields a strong decrease of the peak amplitude, maybe due to the higher distance of the fractures from the array and to the destructive interference of the diffractions in the layer which has a high fracture density[2]. In Fig. 6.24 it is possible to notice a more homogeneous spectrum for the case of the layered medium and a higher peak frequency if compared to the no layered medium.

[2]Here meant not as the fractures number, since it is still one hundred, but as the ratio of the number of fractures to the volume

CHAPTER 8

Discussion

The seismic signatures of a 2D discrete network of fractures have been investigated by performing several numerical modeling tests by means of the program FDELMODC. Different modeling outputs (wiggle traces, pressure wavefield, spectrum in the frequency domain, f-k plots etc.) have been analyzed in order to test the individual effects of the fractures features as the orientation, the length and the density; the layering effect has been tested as well. As a starting point, models with a single fracture were produced in order to investigate the influence of a single fracture on the seismic record and in particular the influence of its orientation and its length. Then the modeling test was made more complicated by introducing discrete fractures distributions and by testing the effect of the change of their length, orientation and density. Eventually, a three-layer model with fractures contained only in the middle layer was modeled as representative of the most realistic case.

The effect of fractures on velocities and attenuation of the seismic waves has been largely discussed in the literature (Boadu and Long, 1996; Pyrak—Nolte et al., 1987). The results discussed in this work have clearly shown the attenuation effect (in the time and frequency domain) which interests a wavefield propagating in a fractured medium; however, they have not revealed any significant velocity changes in the wavefield propagating in a fractured medium compared to that propagating in a medium without fractures, proving that P-waves are not good in revealing possible time delays due to the presence of fractures. The analysis in the time domain has prevented any quantitative determinations of a possible time delay which can be attributed to the presence of fractures: indeed the wavelet referred to the medium with fractures and that without fractures do not show any significant time difference in the onset arrivals; in cases like this, which differ from the earthquakes applications, identifying a possible time delay in the time domain becomes a subjective issue, which also depends on the chosen sampling interval. In future, analysis of the phase difference may give more quantitative results[1] (personal communication, Prof. Ghose 2012). Anyhow, these results are not surprising, since it was already demonstrated (Xu and King, 1989; Hardage, June 2011) that P-velocities decrease by a often negligible amount when the medium changes from non-fractured to a medium with aligned fractures, whereas S-waves show significant time delays.

[1] $\triangle t = \frac{\varphi}{2\pi f}$, where φ is the phase difference and f is the frequency

The imprint of the presence of a fracture on a seismic signal is basically revealed by the creation of reflected, diffracted, refracted and scattered waves. In order to test the effect of the orientation, single-fracture models were produced that include a 100m-long fracture (almost half wavelength): for this 'fracture length to wavelength ratio', diffracted and scattered waves are expected to be predominant over the reflected waves.

The orientation effect has shown significant effects already in the models with a single fracture, especially for what concerns the reflected wavefield: in particular, the vertical fracture seems to produce the strongest effect, as it generates two diffraction hyperbolae corresponding to the waves diffracted by the two fracture tips (unexpectedly, the diffraction from the bottom tip seems to have the strongest amplitude, maybe due to interference phenomena). For the specific position of the vertical fracture relatively to the receivers array at the surface, it produces only strong diffracted waves (from the two tips) that have the most significant influence on the incident wavefield. In both the models with the horizontal and vertical fracture it is particularly evident a "ringing" wave following the first scattered wave whose amplitude decreases with time (Fig. 8.0.1a): this "tail" cannot be identified as a *coda wave*, since this is usually referred to waves that undergo multiple scattering in a fracture network (causing energy dispersion and an amplitude decrease with time); for this reason, this term will be used only to define the late arrivals for the models with multiple fractures. A possible interpretation of the "ringing" waves could be that they are caused by scattering within the fracture (related to the grid spacing chosen for the modeling): the increasing fracture length could increase the path along which the wave get trapped, yielding longer "ringing" waves. For this specific 'fracture length to wavelength ratio', the fracture acts as a point scatterer (see Fig. 8.0.2): the incident wavefield is spherically spread out as it interacts with the fracture ("scattered wavefront" in the figure), which give rise to a diffraction hyperbola in the time section (visible in Fig. 8.0.1b). This is in agreement with the results by Vlastos et al. (2003) and Hall and Wang (2012).

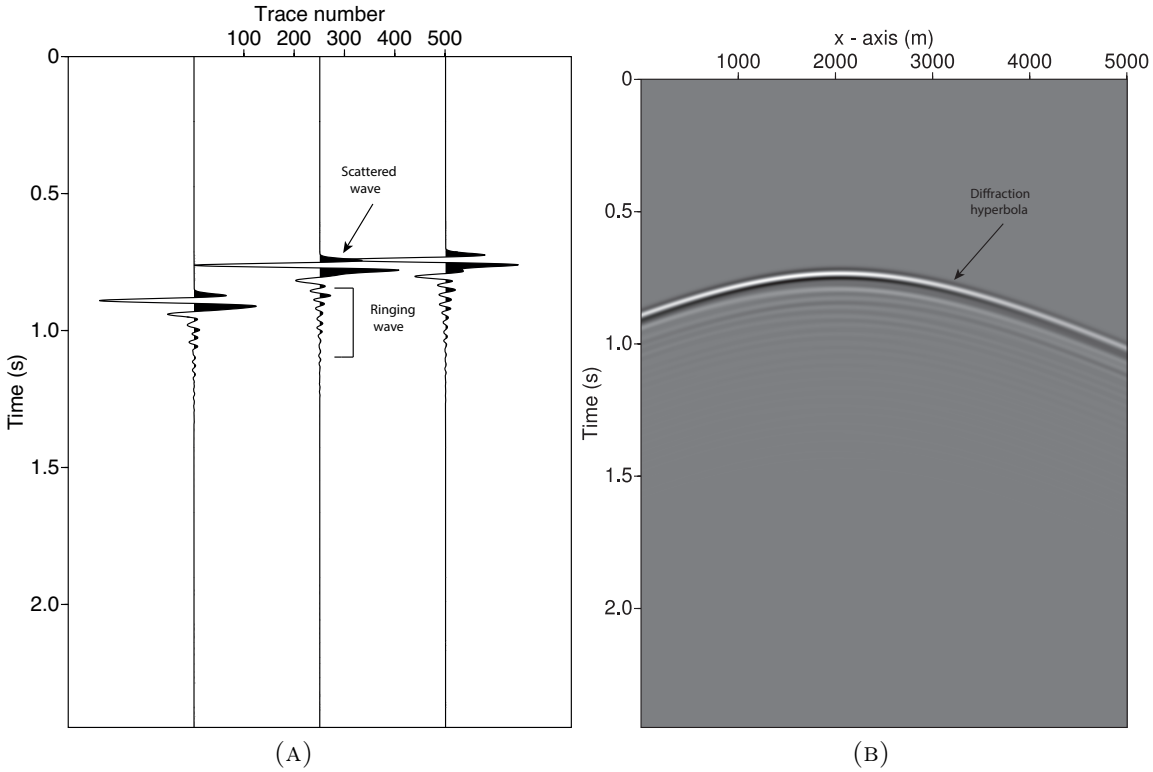

FIGURE 8.0.1. Fig. 8.0.1a shows the wiggle traces referred to the model with one horizontal fracture for the receivers at the surface. It is possible to recognize the scattered wave and the late arrivals ("ringing" wave). Fig. 8.0.1b shows the pressure wavefield recorded at the receivers at the surface. The diffraction hyperbola is generated by the fracture acting as a point scatterer. The late arrivals are visible as well.

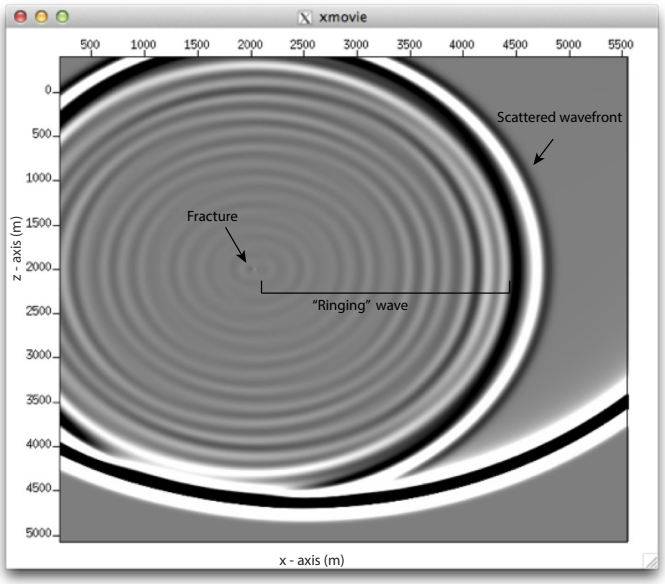

FIGURE 8.0.2. Snapshot of the vertical component of the velocity. Model with a 100m long horizontal fracture. The fracture seems to act as a point scatterer: the incident wavefield is spherically spread out as it interacts with the fracture. The fracture represents the center for several concentric wavefronts; the amplitude of the wavefronts decreases going from the most external circle towards the fracture.

The effect of the orientation has been tested in the frequency domain as well by comparing the amplitude spectra relative to the different models: the reflected wavefield seems to be the more affected by the change in the fracture orientation (Fig.8.0.3) than the transmitted one, as already pointed out for the wiggle traces. The spectrum related to the model with one horizontal fracture (Fig. 8.0.3a) is characterized by the highest amplitude, due to the strongest back-scattered wavefield contribution. On the other hand, the spectra relative to the models with one fracture at 45° and one vertical fracture (Fig. 8.0.3b-c) show a similar peak amplitude (which occurs at about 18 Hz for the 45°-fracture model and at about 22 Hz for the vertical-fracture model); moreover, they are characterized by a much stronger attenuation of the high-frequencies components if compared to the model with one horizontal fracture, which is maybe an effect of the disruptive action of the diffractions that

are more effective in these two models. In particular, when the fracture is vertical, the higher frequencies undergo the strongest attenuation (see the abrupt decrease of the amplitude starting from 30Hz, Fig. 8.0.3c):

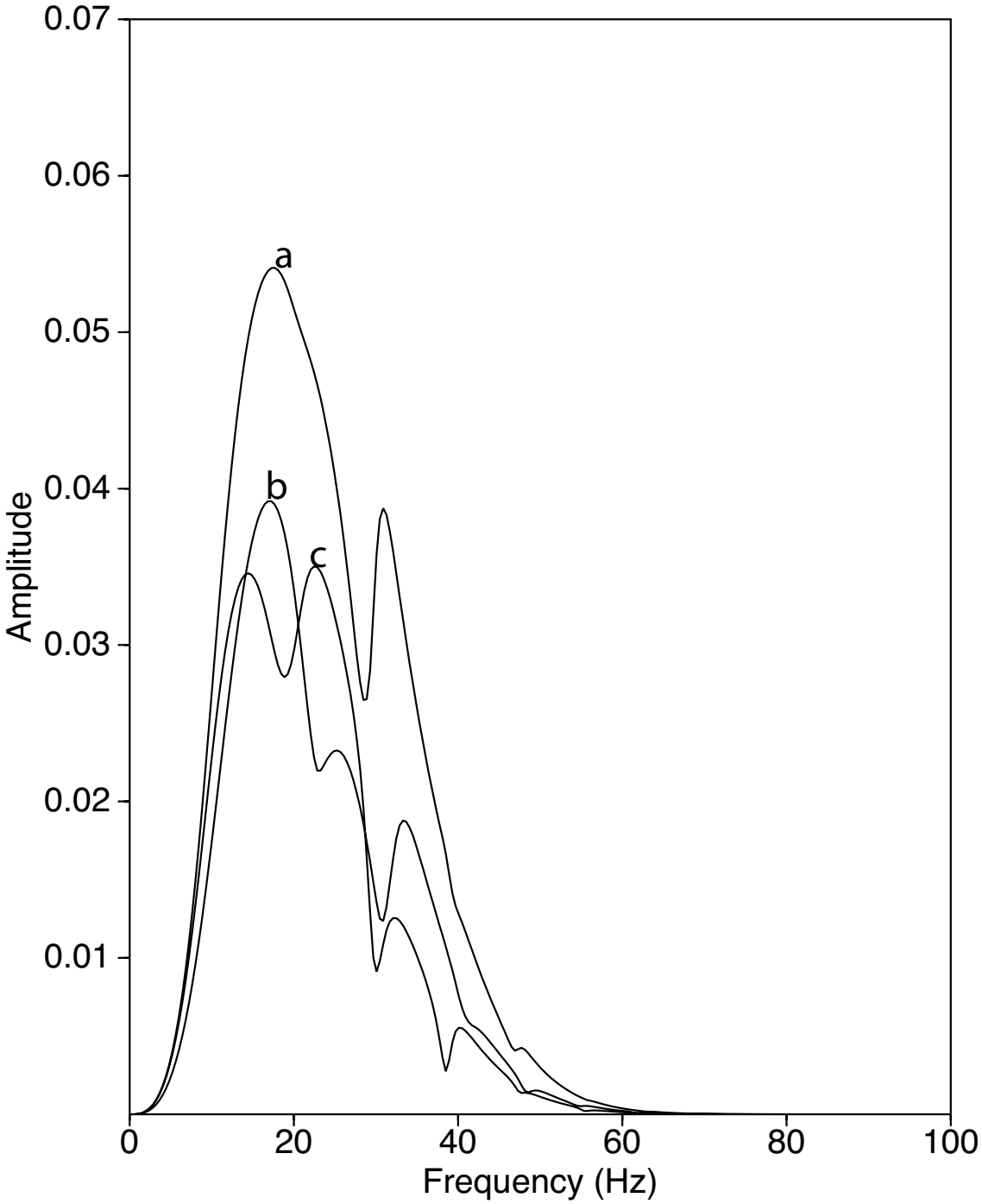

FIGURE 8.0.3. Amplitude spectra for the model with one 100m-long horizontal fracture (a), a 45° inclined fracture (b) and a vertical fracture (c). Results related to the receivers at the surface. The spectrum related to the model with one horizontal fracture is characterized by the highest amplitude. The spectra referred to the models with one fracture at 45° and one vertical fracture show a similar peak amplitude (which occurs at about 18 Hz for the 45°-fracture model and at about 22 Hz for the vertical-fracture model); moreover, they are characterized by a much stronger attenuation of the high-frequencies components if compared to the model with one horizontal fracture. The strongest high-frequencies attenuation occurs for the model with one vertical fracture.

The influence of the fracture length has been tested for several models with a single horizontal fracture. It results clear that it strongly affects the seismic behavior of the fracture since the 'fracture length to wavelength ratio' is crucial in determining the seismic response of a discontinuity. The incident wave interacting with the fracture undergoes an increasing attenuation as the fracture length increases, which can be indicative of the fact that scattering (and therefore the scattering attenuation) becomes more and more significant when the fracture length approach the wavelength. The fracture length influence is evident in the frequency domain. Again, this is particularly true for the reflected wavefield recorded at the surface (Fig. 8.0.4): an increase in the fracture length from one tenth of the wavelength (Fig. 8.0.4a) to half wavelength (Fig. 8.0.4c) yields an increase in the peak amplitude and a shift of the peak frequency towards lower frequencies. Indeed, the higher the length of the fractures is, the higher the amount of energy that is back-scattered towards the surface, which explains the increase in the peak amplitude; moreover, a decrease of the peak frequency occurs, which could mean that the higher frequencies are preferentially attenuated when scattering is predominant. As the fractures approach the wavelength, a significant increase in the peak amplitude and a shift of the peak frequency towards higher values (Fig. 8.0.4d) is visible; maybe this is due to the higher amount of energy that is back-scattered towards the suface or to the reflection contribution that starts to be more relevant. To prove this, the output from the model with one horizontal fracture, 500m long (2λ), has been added in Fig. 8.0.4:

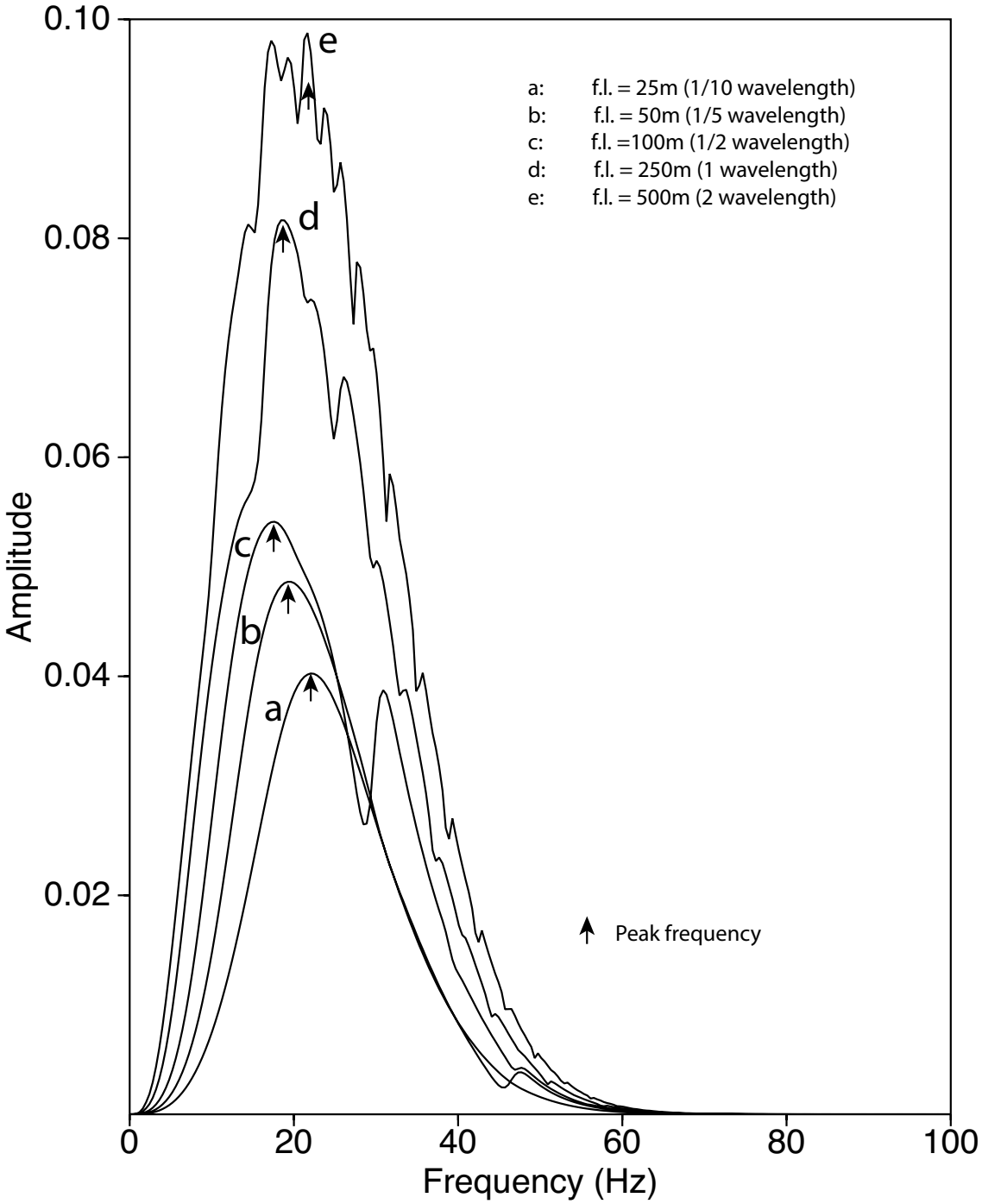

FIGURE 8.0.4. Amplitude spectra for the models with one horizontal fracture that differ because of the fracture lengths: f.l. = 25m (a); f.l.=50m (b); f.l.=100m (c); f.l.=250m (d); f.l.=500m (d). Results related to the receivers at the surface. An increase in the fracture length from one tenth of the wavelength to half wavelength yields an increase in the peak amplitude and a shift of the peak frequency towards lower frequencies. As the fractures approach the wavelength, a significant increase in the peak amplitude and a shift of the peak frequency towards higher values occur.

On the basis of the previous figure, a plot of the peak frequency versus the fracture length has been derived (Fig. 8.0.5): as the fracture length increases, initially there is a decrease of the peak frequency; when the fracture length reaches 100m (half wavelength), there is a strong increase in the peak frequency.

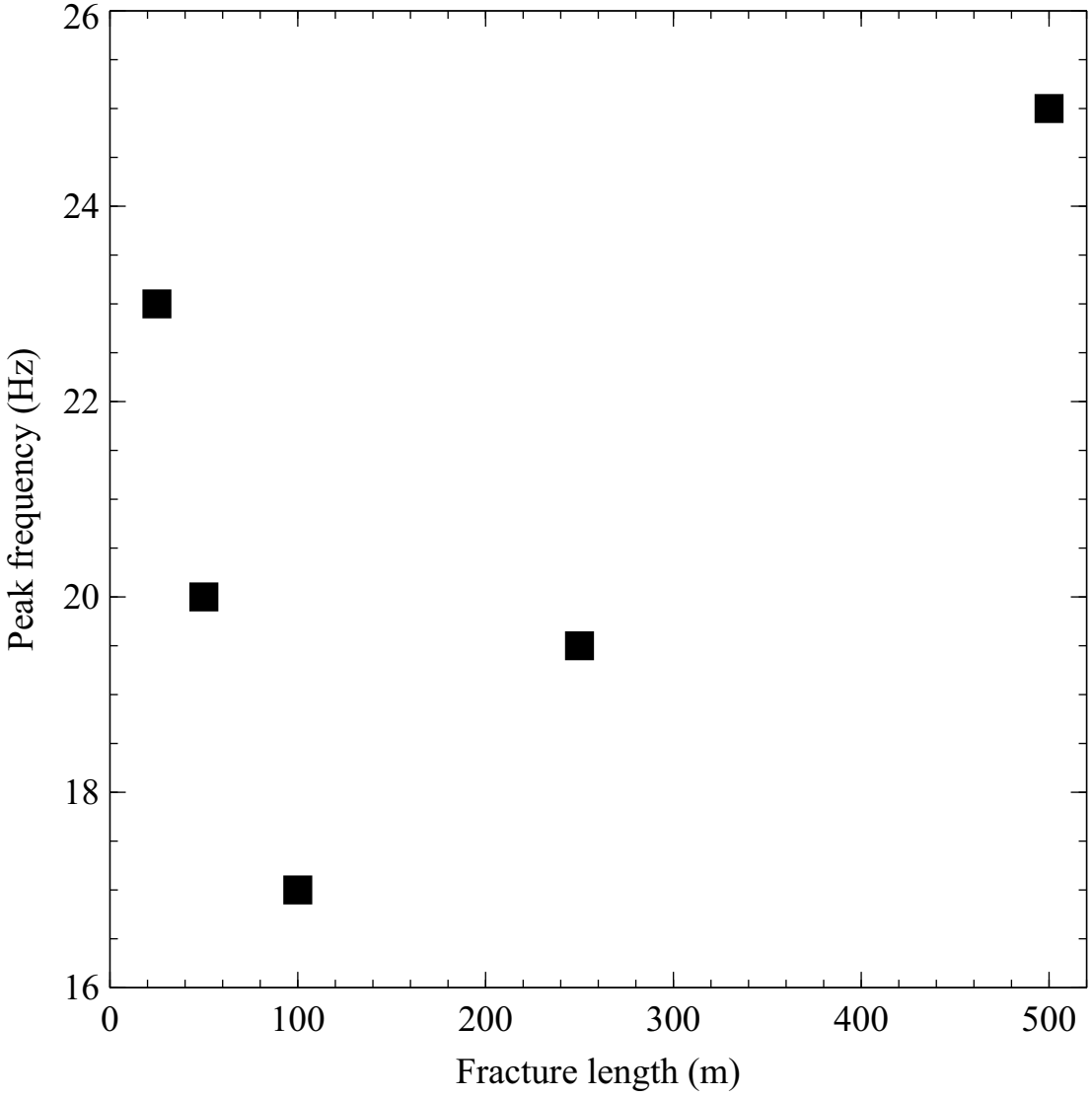

FIGURE 8.0.5. Plot of the peak frequency vs the fracture length based on the previous figure (for models with one horizontal fracture). As the fracture length increases, initially there is a decrease of the peak frequency; when the fracture length reaches 100m (1/2 wavelength), there is a strong increase in the peak frequency.

It seems that when scattering is predominant, fractures act more as low-pass filters for the wavefield that is back-scattered towards the surface, yielding a stronger attenuation of the higher frequencies; when it starts to be less predominant (because, for example, reflection starts to play a role), higher frequencies are less attenuated.

By doing the same analysis for the model with one vertical fracture, it results in a much less clear difference among the several models (Fig. 8.0.6), meaning that the fracture length weakly affects the model with a vertical fracture. The reason could be that, despite of the length, a vertical fracture always produces a diffracted wavefield (no reflected wavefield occurs).

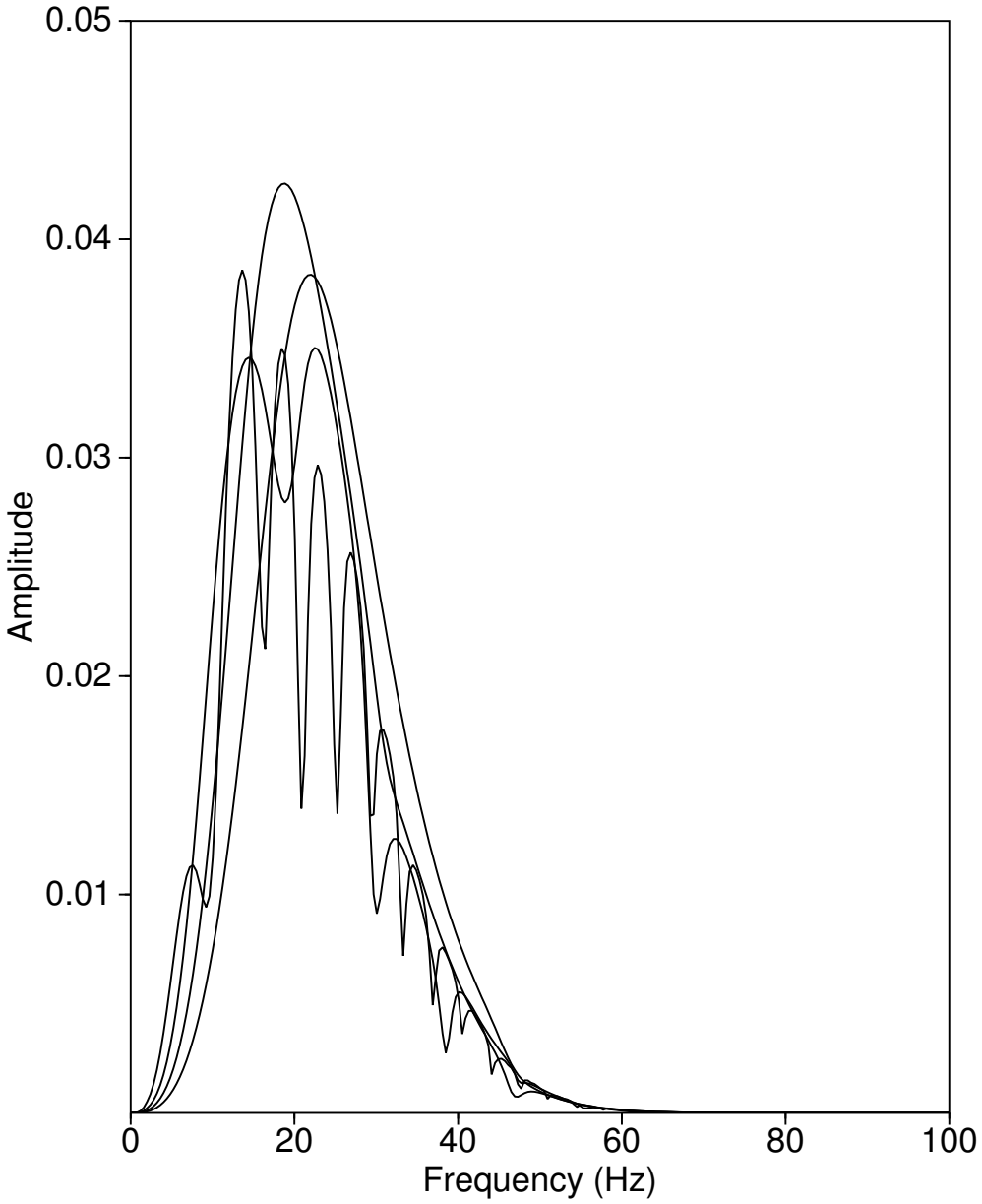

FIGURE 8.0.6. Amplitude spectra for the models with one vertical fracture that differ because of the fracture lengths: f.l. = 25m (a); f.l.=50m (b); f.l.=100m (c); f.l.=250m (d). Results related to the receivers at the surface.

For the models with a discrete distribution of fractures the effect of the fractures orientation was analyzed for the case of one hundred fractures with a length of 100m. It was not possible to get useful information based either on the wiggle traces nor on the amplitude spectra for the wavefield recorded at the surface. For this reason,

it has been performed a qualitative analysis in the frequency-wavenumber domain. Indeed f-k plots can be implemented to examine the direction and apparent velocity of seismic waves. The signature of the fractures orientation is represented by the different energy density distributions: when inclined fractures are present, the overall energy density diminishes but local peaks are present that indicate a preferential direction of approach of the reflected waves (due to the fracture orientation). This result is valid for the wavefield recorded at the surface; much less satisfying were the results for the receivers at 4000m. Surprisingly, the influence of the fractures orientation on the transmitted wavefield has yielded the most significant effects in the frequency domain (Fig. 8.0.7): the horizontal fractures network has the strongest effect on the transmitted wavefield attenuation, especially for what concerns the high-frequencies range (the relative spectrum has the lowest peak amplitude and the lowest peak frequency, Fig. 8.0.7a); on the other hand, a network of vertical fractures or fractures close to the vertical have the weakest effect on the attenuation of the wavefield, preserving the highest peak amplitudes and peak frequencies (Fig. 8.0.7b-e). A network of fractures at 45° or 70° produce an intermediate effect (Fig. 8.0.7c-d):

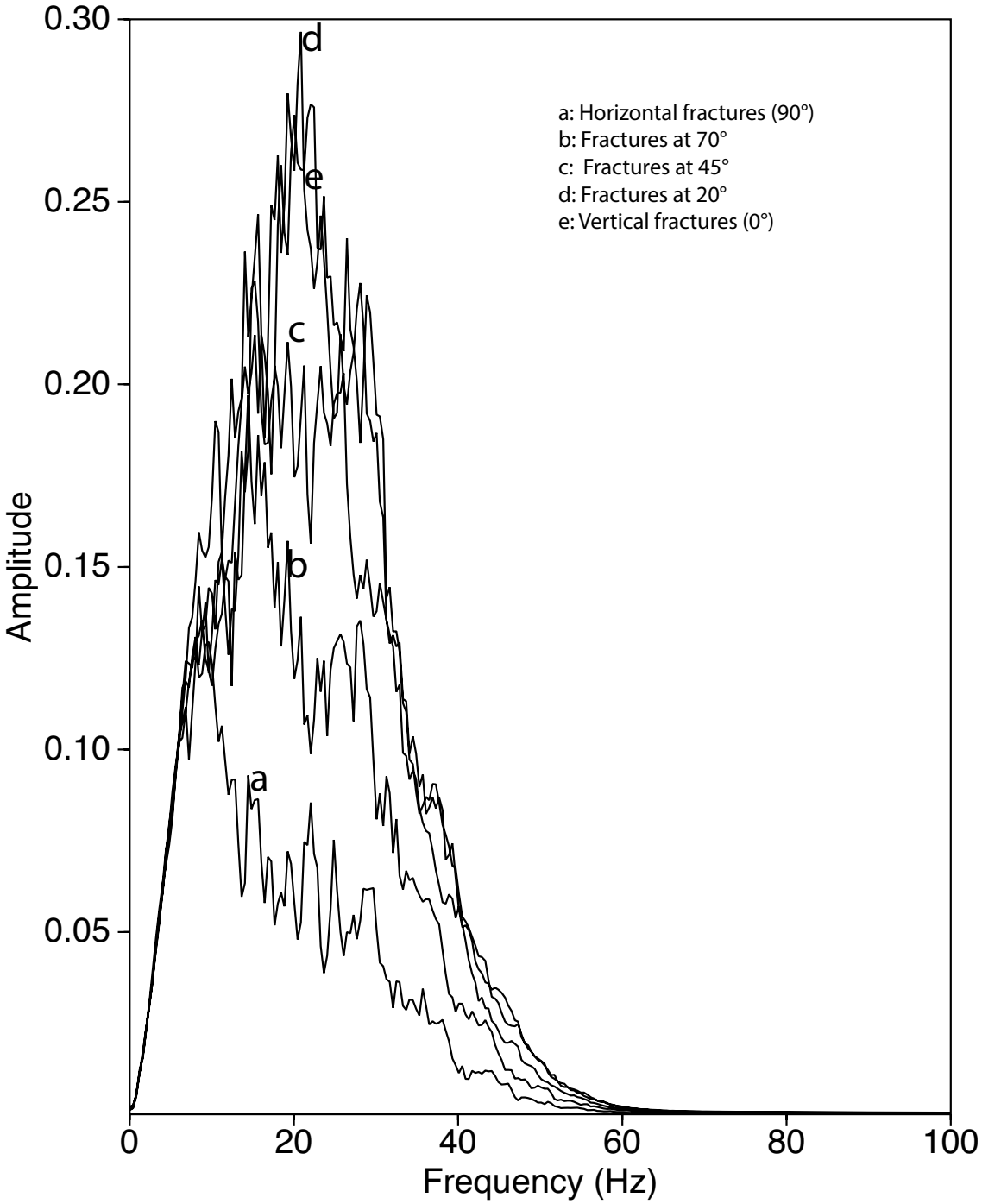

FIGURE 8.0.7. Amplitude spectra for the models with one hundred 100m-long fractures that differ because of the fractures orientation: horizontal fractures (a); 20° inclined fractures (b); 45° inclined fractures (c); 70° inclined fractures (d); vertical fractures (e). Results related to the receivers at the depth of 4000m. The horizontal fractures have the strongest effect on the transmitted wavefield attenuation, especially for what concerns the high-frequencies range (the relative spectrum has the lowest peak amplitude and the lowest peak frequency); on the other hand, vertical fractures or fractures close to the vertical have the weakest effect on the attenuation of the wavefield, preserving the highest peak amplitudes and peak frequencies.

It can be deduced that fractures oriented in the direction of propagation weakly attenuates the wavefield. This is opposite to what was found by Hall and Wang (2012), who demonstrated that the fractures oriented in the direction of propagation affect the wavefield more than those perpendicular, due to the more disruptive effect of the diffractions (Fig. 3.10). The reason of this difference could be that in their simulations they tested the influence of the fractures orientation on fractures with a length equal to the wavelength but they extended these results to all the cases where the fracture length is less than or comparable to the wavelength (that is where the fracture is acting at least in part as a reflector). Actually it seems that when the fractures have a length smaller than the wavelength, as for the results shown in Fig. 8.0.7, the effect on the transmitted wavefield is opposite. This can be due do the smaller 'fracture length to wavelength ratio', which causes the diffraction to be predominant over the reflection process: when this is the case, horizontal fractures tend to spread the diffracted waves laterally, whereas the vertical ones force part of the diffracted wavefield to down-propagate through the medium.

The effect of the fractures length for a discrete number of fractures has been tested on models with one hundred horizontal and one hundred vertical fractures. As confirmed by previous researches (Vlastos et al., 2003), scattering starts to become significant (longer coda waves) when fractures approach a certain length, that is about one fifth of the wavelength for the results of this work (horizontal fractures models); increasing the fracture length, the scattering effect become more and more evident, yielding longer coda waves. This is actually evident for the wavefield recorded at the surface, but for the transmitted wavefield the length effect is much less clear. In the frequency domain, as the fractures length approaches the wavelength (Fig. 8.0.8, left-hand side) the peak amplitude increases, maybe due to the higher amount of energy that is back-scattered and/or to the fact that fractures start to act more as reflector; moreover, as the fractures length increases, a slight shift of the peak frequency towards higher frequencies can be noticed, especially when they approach the wavelength. This confirms the results related to the model with a single fracture. The effect of the length in the frequency domain is much more effective in the transmitted wavefield (Fig. 8.0.8, right-hand side): as the fractures length increases, a significant decrease of the peak amplitude is observed, due to the higher attenuation of the wavefield as it crosses longer fractures (more energy is reflected and back-scattered towards the surface); in particular, the higher frequencies seem to be much more affected by the presence of longer fractures. In addition, it can be noticed a shift of the peak frequency towards lower frequencies as the fractures length increases.

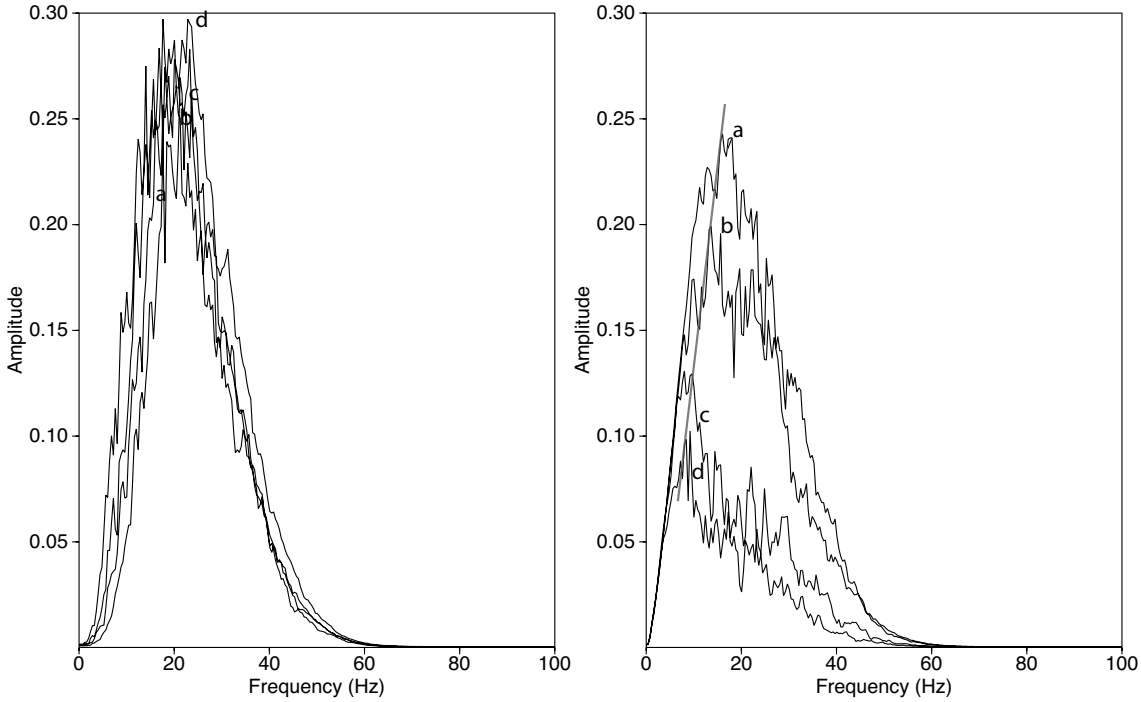

FIGURE 8.0.8. On the left-hand side: Amplitude spectra for the models with one hundred horizontal fractures that differ because of the fracture lengths: f.l. = 25m (a); f.l.=50m (b); f.l.=100m (c); f.l.=250m (d). Results related to the receivers at the surface. As the fractures length approaches the wavelength, the peak amplitude increases; moreover, as the fractures length increases, a slight shift of the peak frequency towards higher frequencies can be noticed. On the right-hand side: Amplitude spectra for the models with one hundred horizontal fractures that differ because of the fracture lengths: f.l. = 25m (a); f.l.=50m (b); f.l.=100m (c); f.l.=250m (d). Results related to the receivers at the depth of 4000m. As the fractures length increases, a significant decrease of the peak amplitude is observed. In addition, it can be noticed a shift of the peak frequency towards lower frequencies as the fractures length increases.

The same analysis has been made for the model with one hundred vertical fracture. In this case the opposite trend occurs: for the reflected wavefield there is a shift of the peak frequency towards lower frequencies as fractures length increase (Fig. 5.11), while for the transmitted wavefield there is a shift towards higher frequencies (Fig. 5.12).

The effect of the fracture density on the seismic signature has been tested for horizontal fractures that have a length of about half wavelength (100m). As the fractures number increases, the signal gets more complicated resulting in longer coda waves (Fig. 5.15 and Fig. 5.16). Analyzing the wavefield recorded at the surface in the frequency domain (8.0.9, left-hand side), it results that the amplitude of the spectra increases as the fractures number increases, since the higher number

of fractures yields more energy to be scattered back to the surface. On the contrary, for the transmitted field (Fig. 8.0.9, right-hand side) the trend is opposite: as the fractures become more numerous, the amplitude of the spectrum decreases, due to the stronger attenuation imposed by a higher number of fractures. Moreover, it seems that the higher frequencies are more attenuated than the lower ones when the fracture density increases.

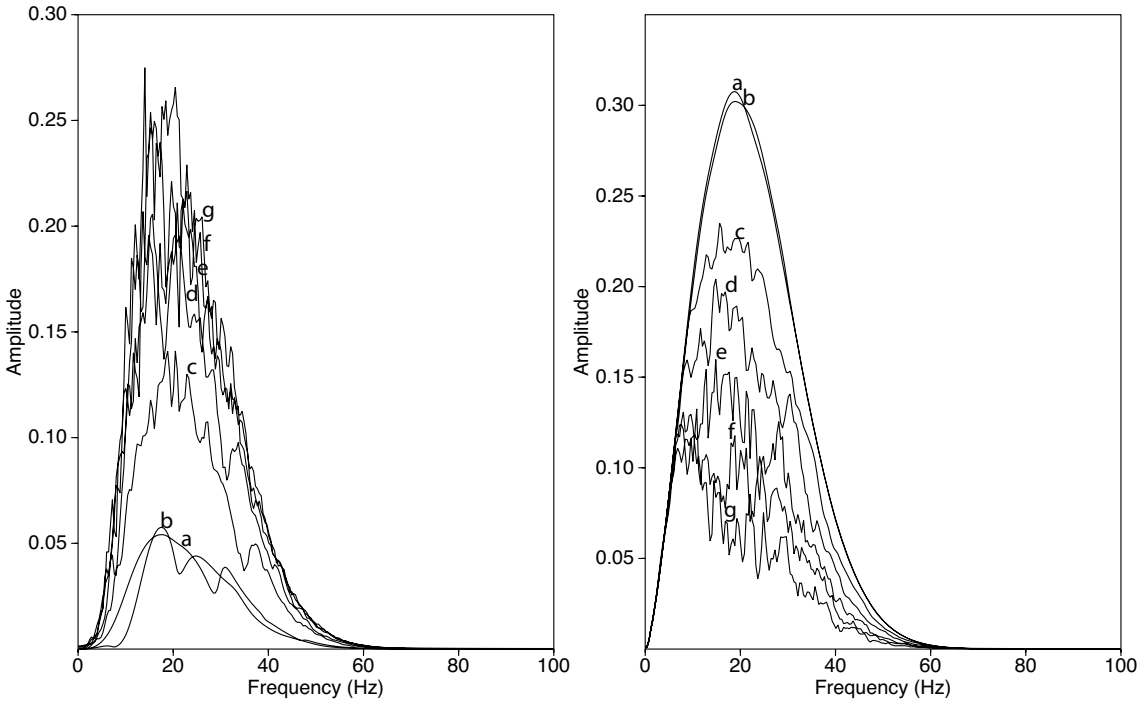

FIGURE 8.0.9. On the left-hand side: Amplitude spectra for the models with 100m long horizontal fractures but with different fracture densities: one (a), two (b), ten (c); twenty (d); fifty (e); seventy (f); one hundred (g). Results related to the receivers at the surface. The amplitude of the spectra increases as the fractures number increases. On the right-hand side: Results related to the receivers at the depth of 4000m. As the fractures become more numerous, the amplitude of the spectrum decreases; in addition, the higher frequencies are more attenuated than the lower ones.

On the basis of Fig. 7.9 (right-hand side), two plots have been derived. The first (Fig. 8.0.10) shows the peak frequency as a function of the fractures number: an increase in the fracture density yields a decrease of the peak frequency; in particular, increasing the fracture number from 2 to 10 cause the most significant decrease; when fractures increase from 10 to 50, the rate of change is much less evident; from 50 fractures on, there is again a relevant decrease of the peak frequency.

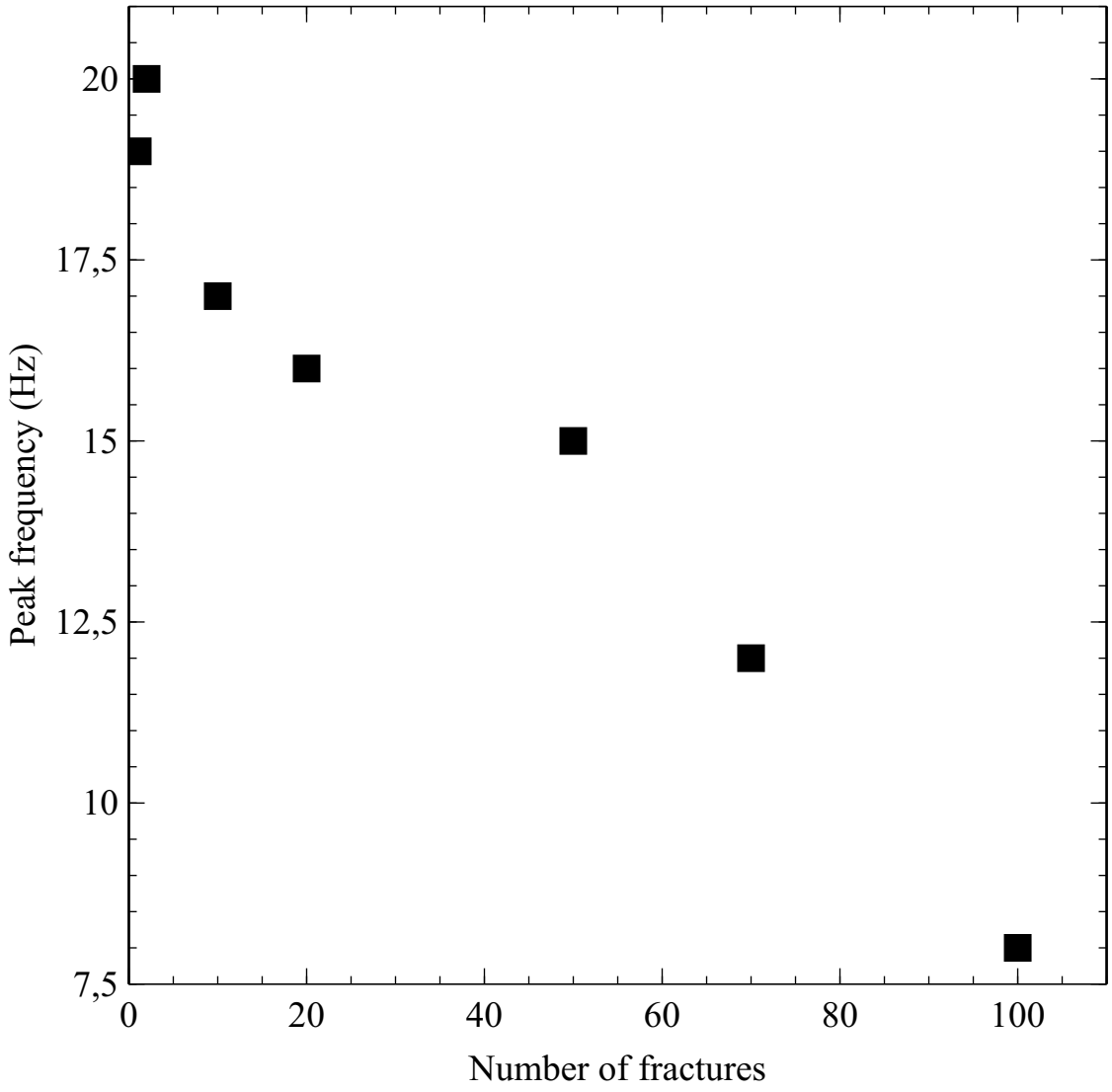

FIGURE 8.0.10. Plot of the peak frequency vs the number of fractures, based on Fig. 7.9 (right-hand side), for models with 100-m long horizontal fractures (transmitted wavefield). An increase in the fracture density yields a decrease of the peak frequency.

The second plot aims to characterize the high frequencies attenuation relatively to the low frequency: for each spectrum, the amplitude which corresponds to 30Hz (representative of the high frequency range) and the amplitude which corresponds to 5Hz (representative of the low frequency range) have been measured; their ratio (A30/A5 in Fig. 8.0.11) is indicative of the different frequency ranges attenuation. Looking at Fig. 8.0.11, it is possible to see that an increasing number of fractures yields a strong decrease in the A30/A5 ratio, which means that the high frequencies are more attenuated with respect to the lower frequencies as the fracture densities increases:

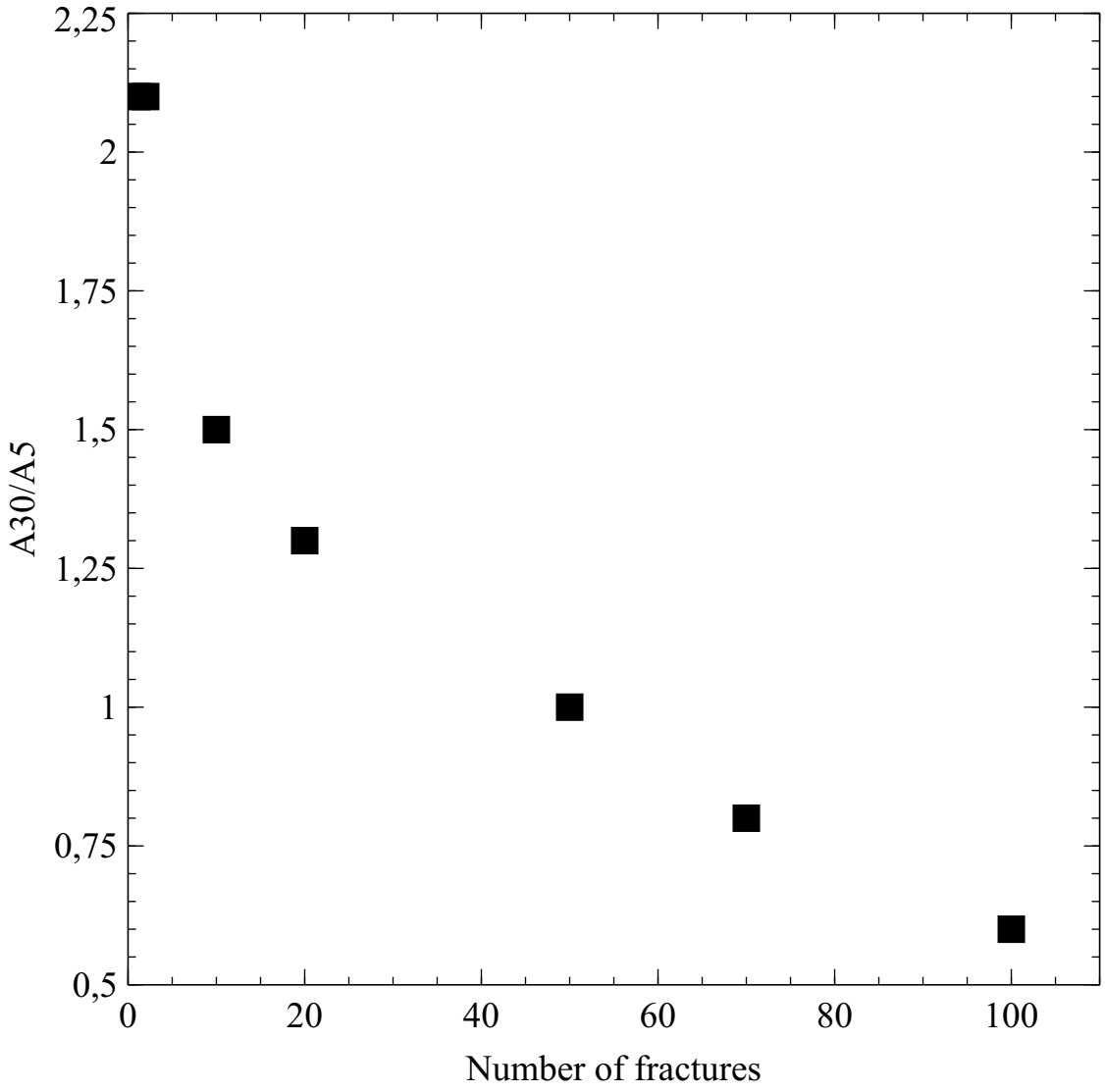

FIGURE 8.0.11. For each spectrum in Fig. 7.9 (right-hand side), the amplitude which corresponds to 30Hz (representative of the high frequency range) and the amplitude which corresponds to 5Hz (representative of the low frequency range) have been measured; their ratio (A30/A5) is indicative of the different frequency ranges attenuation: the high frequencies are more attenuated with respect to the lower frequencies as the fracture densities increases.

It could be concluded that an increasing fracture density yields the effects of a low-pass filter for the transmitted wavefield.

The effect of the layering has been tested first by comparing the outputs from the layered model with the fractured layer with those from the layered model which does not contain any fractures. The wavefield that is reflected back from the top of the layer is completely disrupted by the presence of the fractures inside the layer: the diffraction hyperbolae destructively interfere with the reflected wavefield which

is strongly attenuated. On the other hand, the reflection from the bottom of the layer is still visible and it seems not to be affected by the presence of fractures. Looking at the transmitted wavefield, the field which reaches the top of the fractured layer is severely disrupted by the presence of the fractures but it is somehow "reconstructed" by the diffraction hyperbolae produced by the fractures. On the contrary, the wavefield transmitted across the bottom of the layer is not visible at all. In the frequency domain, for what concerns the wavefield recorded at the surface, the amplitude spectrum does not show a significant decrease in the peak amplitude if compared to the spectrum of the incident wavefield, maybe because the field reflected from the layer boundaries is much more predominant over the diffractions caused by the fractures. More significant is the difference in the peak amplitude between the spectrum of the wavefield transmitted across the fractured layer and across the unfractured layer: in this case, the fractures encountered by the transmitted wavefield affects its frequency content.

The outputs from the layered model have also been compared to those referred to the model which contains one hundred horizontal fractures as well, but randomly distributed in a otherwise homogeneous model. In the frequency domain, regarding the wavefield recorded at the surface, the effect of the fractured layer consists in a strong decrease of the peak amplitude compared to the unfractured medium (Fig. 8.0.12); maybe the reason is the higher distance of the fractures from the array and to the destructive interference of the diffractions in the layer which has a high fracture density. For what concerns the results for the receivers at 4000m, the spectrum referred to the fractured medium is more homogeneous if compared to that of the unfractured one; moreover, it presents a higher peak frequency. It could be deduced that, for a fixed number of fractures, high frequencies are more attenuated if those are widespread in the medium instead of being concentrated in a layer.

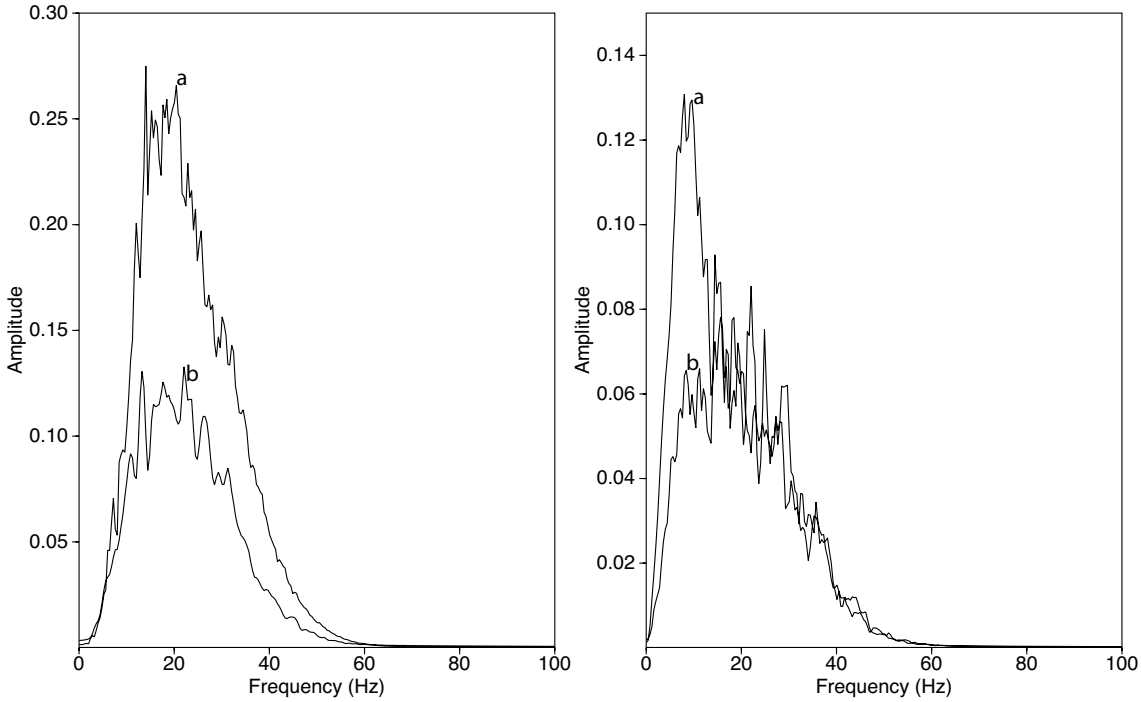

FIGURE 8.0.12. Amplitude spectra for the no layered medium (a) and the layered medium (b). Results related to the receivers at the surface (on the left-hand side) and at 4000m (on the right-hand side). The presence of a fractured layer yields a strong decrease of the peak amplitude in the spectrum of the reflected wavefield if compared to the unfractured medium case. On the other hand, the transmitted wavefield spectrum referred to the fractured medium is more homogeneous if compared to that of the unfractured one; moreover, it shows a higher peak frequency.

Summing up, fractures strongly affect the seismic response, yielding wave diffraction, reflection, transmission and scattering; moreover, they generally attenuate the incident signal, reducing the amplitude of the wavefield. In most of the cases, their presence has an effect in the frequency domain, introducing a shift in the peak frequency and a change in the peak amplitude; sometimes, the maximum frequency varies as well. All these signatures are strongly dependent on the considered fracture parameters (length, orientation, density), that cannot be considered separately: for example, the effect of the fracture length has opposite effect in the frequency domain, depending on the orientation of the fractures. Moreover, it results difficult to correlate a specific trend with a specific parameter: for example, considering the transmitted wavefield, a stronger frequencies attenuation and a lower peak frequency can be attributed to a higher number of fractures, but also to longer fractures or to the presence of fractures oriented in the direction perpendicular to the wave propagation (horizontal fracture in this case). This shows that additional information are

required in order to characterize the fracture networks in term of orientation, length or density.

Tab.2 sums up the effects of the fracture features on the seismic signal:

	Reflected wavefield	**Transmitted wavefield**
	Single fracture models	
Fracture orientation	Significant effect in the time and frequency domain	Weak effect in the time and frequency domain
Fracture length	Strong effect in the time and frequency domain (horizontal fracture model)	Significant effect in the time and frequency domain (horizontal fracture model)
	Multiple fractures models	
Fracture orientation	Very weak effect in the time and frequency domain. Significant effect in the f-k domain	Very weak effect in the time and f-k domain. Strong effect in the frequency domain
Fracture length	Significant effect in the time domain, less in the frequency domain	Weak effect in the time domain. Strong effect in the frequency domain
Fractures density	Significant effect in the time and frequency domain	Significant effect in the time domain. Strong effect in the frequency domain
Layering	Strong effect in the time and frequency domain	Significant effect in the time and frequency domain

Tab.2 : Overview of the effects of the single fracture features on the seismic signal

Concluding, it should be said that the described approach is based on strong assumptions: the subsurface models are quite simple and the only element of disturbance is represented by the fractures. Obviously in reality there are others elements that leave an imprint on the seismic signature (fine layering, local heterogeneities, fluids etc.) and this makes the identification of the fractures signatures much more difficult. Moreover, for all the models it has been assumed a constant density and a constant velocity over a depth of 5 Km (except the layered model), which is not the case in reality. The velocity and density contrast between the fractures and the surrounding rocks has been kept really high in order to maximize the fractures effect, but this is not always the case. A strong limitation of the described approach is that it only considers the acoustic wave propagation (P-waves); shear waves have a high potential in revealing fractures features and they should be included for a more completed analysis.

CHAPTER 9

Conclusions

Fractures have been included in finite-difference modeling in order to test how they affect seismic wave propagation. In particular, the signature of the fracture length, orientation and density has been analyzed; moreover, a fractured layer embedded between two unfractured media has been modeled in order to implement a more realistic case. The results discussed in this work have clearly shown:

- A significant attenuation effect (in the time and frequency domain) which interests a wavefield propagating in a fractured medium; on the contrary, no significant velocity change has been described, proving that P-waves are not good in revealing possible time delays due to the presence of fractures;
- The imprint of the presence of fractures on a seismic signal is basically revealed by the creation of diffracted/scattered and transmitted waves. Coda waves have been recognized as well. All this contributes to make the seismic response much more complex;
- Fracture orientation influences the amplitude of the signal and the length of the coda waves in the time domain and affects the peak amplitude and the peak frequency in the frequency domain; the imprint of the fracture orientation is peculiar in the frequency-wavenumber domain;
- Fracture length affects the amplitude of the signal and the length of the coda waves in the time domain and affects the peak amplitude and the peak frequency in the frequency domain;
- Fracture density yields significant effects in the frequency domain, by affecting the peak amplitude and the peak frequency;
- The introduction of a fractured layer yields strong change in the incident signal, which is highly attenuated and disrupted;
- All the identified signatures are strongly dependent on the considered fracture parameters (length, orientation, density), that cannot be considered separately: the effect of a specific parameter on the seismic signal can be opposite depending on the other fracture features;
- The correlation of a specific trend with a specific parameter is not straightforward: the same seismic signature can be attributed to different fracture parameters. Additional information are required in order to characterize the fracture networks in term of orientation, length or density;

- Despite of the complexity of fractured systems, some recurrent trends and characteristic responses have been determined.

CHAPTER 10

Recommendations for future researches

Further researches on this topic are highly recommended. In particular, it would be more interesting to test the response of randomly oriented fractures and fractures with random lengths; this would make the modeling outputs more reliable. Moreover, additional layers could contribute to a more realistic scenario. An additional parameter that should be tested is the fracture spacing, which is involved in the scattering phenomenon and in the possible formation of channel waves. The simulation of S-waves propagation is strongly suggested, as they have already proved to carry more information about the fracture networks (especially for what concerns the velocity). The implementation of data from laboratory tests and/or tests in wells could help in checking the reliability of the modeling outputs and could supply additional information. Eventually, a 3D simulation represents the natural follow-up of this work.

11

References

- Aki, K., 1969, "Analysis of the seismic coda of local earthquakes as scattered waves", J. Geophys. Res. 74, 615–631
- Aki, K. and Wu, R.-S., 1988, "Scattering and Attenuation of Seismic Waves", V. 1-3
- Boadu, F. K. and Long, L. T., 1996, "Effects of fractures on seismic-wave velocity and attenuation", Geophys. J. Int., vol. 127, no. 22, pp. 86-110, pp. L11309
- Coates, R.T. & Schoenberg, M., 1995 "Finite-difference modeling of faults and fractures", Geophysics, 60, 1514-1526
- Gu, B.L., Suarez-Rivera, R., Nihei, K.T. & Myer, L.R. 1996, "Incidence of plane waves upon a fracture", J. Geophys. Res., 101, 25337-25346
- Hall F., Wang Y., 2012, "Seismic response of fractures by numerical simulation", Geophys. J. Int., Vol. 189, Issue 1, pages 591–601
- Hardage B., June, 2011, "S-Waves on Crack? Not So Much", (AAPG Explorer)
- Haugen, G. U. & Schoenberg, M., 2000, "The echo of a fault or fracture", Geophysics, 65, 176–189
- Hudson, J.A., 1981, "Wave speeds and attenuation of elastic waves in materials containing cracks", Geophys. J. R. astr. Soc. v. 64 p. 133–150
- Kurt T. Nihei, Weidong Yi, Larry R. Myer, and Neville G. W. Cook, 1999, "Fracture channel waves", J. Geophys. Res, Vol. 104, No. B3, pp. 4769–4781
- Pyrak-Nolte, L.J., Myer, L.R. & Cook, N.G.W., 1990, "Anisotropy in seismic velocities and amplitudes from multiple parallel fractures", J. geophys. Res., B7, 95, 11345-11358
- Schoenberg, M., 1980, "Elastic wave behaviour across linear slip interfaces", J. acoust. Soc. Am., 68, no. 5, 1516–1521
- Schoenberg M. & Protazio J., 1992. "'Zoeppritz' rationalized and generalized to anisotropy", J. Seis. Expl., 1, 125-144
- Sheriff R., 1981, "Encyclopedic Dictionary of Exploration Geophysics", SEG

- Vlastos, S., Liu, E., Main, I. G. & Li, X. Y., 2003, "Numerical simulation of wave propagation in media with discrete distributions of fractures: effects of fracture sizes and spatial distributions", Geophys. J. Int., 152, 649-668
- Wapenaar and Berkhout, 1989, "Elastic Wave Field Extrapolation - Redatuming of Single and Multi-component Seismic Data"
- Weidong Yi , Seiji Nakagawa , Kurt T. Nihei , James W. Rector , Larry R. Myer , Neville G. W. Cook, 1998, "Numerical Investigation of Fracture Channel Waves", 1998 SEG Annual Meeting
- Willis, M.E., Burns, D.R., Rao, R., Minsley, B., Toksoz, M.N. & Vetri, L., 2004, "Spatial orientation and distribution of reservoir fractures from scattered seismic energy", Geophysics, v.71, no.5, O43-O51, 2006
- Xu, S., and M.S. King, 1989, "Shear-wave birefringence and directional permeability in fractured rock: Scientific Drilling", v. 1/1, p. 27-33
- Zhang J. and Gao H., 2009, "Elastic wave modelling in 3-D fractured media: an explicit approach", Geophys. J. Int., vol. 177, no. 3, pp. 1233-1241